Band 71

Schriftenreihe des Lehrstuhls für
Wasserchemie und Wassertechnologie
und der DVGW-Forschungsstelle am Engler-Bunte-Institut
des Karlsruher Instituts für Technologie (KIT)

Investigation of the fouling driving factors
in drip irrigation systems

Jueying Qian

Herausgeber
Harald Horn

Karlsruhe 2017

Jueying Qian
Investigation of the fouling driving factors in drip irrigation systems

Titelbild: Biofilm formation in the microfluidic devices mimicking real dripper geometry

Investigation of the fouling driving factors in drip irrigation systems

zur Erlangung des akademischen Grades eines
DOKTORS DER INGENIEURWISSENSCHAFTEN (Dr.-Ing.)

der Fakultät für Chemieingenieurwesen und Verfahrenstechnik des
Karlsruher Instituts für Technologie (KIT)

genehmigte
DISSERTATION

von
M. Sc. Jueying Qian
aus Shanghai, China

Referent: Prof. Dr. rer. nat. Harald Horn
Korreferent: Prof. Dr.-Ing. Eberhard Morgenroth
Tag der mündlichen Prüfung: 03.02.2017

Acknowledgement

Firstly, I would like to express my sincere gratitude to my supervisor Prof. Dr. Harald Horn for his continuous support during my PhD study. I really appreciate your open talks with all the PhD students about our needs and provide us the best support and professional working environment. I am lucky to be your PhD student. I would like to thank Prof. Eberhard Morgenroth for taking over the second referee and your careful review of my thesis.

I am deeply grateful to Dr. Michael Wagner, who gave me the access to work in this group at the beginning. I appreciate your all-round assistance in experiment design, data processing and writing reports (project reports, thesis, manuscripts, etc.). I really appreciate that you are direct (seems to be a German stereotype), e.g. pointing out my time management problem. This helps me to improve myself constantly. I will keep all your help and guidance in my heart. A special thanks goes out to Dr. Gudrun Abbt-Braun for her warm and kind support in my research. She takes care of our administration processes as well as research problems. For me she is kind of mother of all the PhD students in the institute.

My sincere thanks goes to all Colleagues, all Technicians and all former Colleagues of the Chair of Water Chemistry and Water Technology at Engler-Bunte-Institut. The group has been a source of friendships as well as good advice and collaboration.

I would like to thank my passionate office mate Stephanie West, for a good companion during my PhD. I don't talk a lot but in heart I like you and your personality a lot. I would like to thank Dr. Chunyan Li, my friend and my sincere sister. Our friendship already began since master study. I was also lucky to have Dr. Di Peng and Dr. Meijie Ren in the group. It was such a pleasure to have someone to share the same culture and speak Chinese from time to time. I would like to thank Dr. Elham Fatoorehchi, which is also a good cooking chef, with whom I tried my first Iranian food. Fabian Brunner, who is always there when I have problems and questions. Marc Tuczinski, you are funny, talkative and I must thank you again for correcting all the protocols of our practical courses for three years. Shelesh Agrawal, genius and superman, who doesn't know the word "rest". Samuel Welker, marvelous ginger beard, lives far away from city center, pursues nature and inner harmony. I miss the time when you and Shelesh were in the institute. Dr. Eva Gilbert, I admire you so much, especially your personality. We had so many summer barbecue parties when you were there. I would like to express my thanks to Dominic Breitkopf. You are courageous and we understand well with each other. I am grateful to work with Laure Cuny, Oliver Jung, Isa Remdt, Alexander

The discussion with Mr. Steiner was always pleasant. I like all the people there and thank you again.

I would like to thank all my friends, especially Dr. Zhanyun Wang, Quan Niu, Chenlin Liu, Yiting Wang and Boyu Liu. Research is one part of my life. But I won't walk through my PhD without the companion of you.

Last but not least I would like to thank my partner Florian Blauert. Thank you for taking good care of me and being on my side. Thank you for your countless advices (which are mostly right), discussions and encouragement. It has been a great journey with you and will be, too. At the end, I would like to thank my parents, Jianfa Qian and Meizhen Lu. Thank you for giving me so much freedom and supporting me without borders. I am sorry that I didn't stay with you a lot and took good care of you. I love you so much and I will spend more time with you.

I appreciate all the people I met. I won't be me without you. I am really thankful.

Jueying Qian

Abstract

Drip irrigation is a water efficient technology which is used worldwide in agriculture. Water and nutrients are transported directly to the root zone of the plants at a uniform and designed discharge rate. This is achieved due to the design of drippers which are integrated in the drip pipes. Drippers are devices of a few centimeters in length consisting of a labyrinth and basin compartment. Constant discharge rate within a certain water pressure range is assured by the labyrinth compartment, in which the hydraulic energy dissipates along the zigzag-like flow path. In water scarce regions, treated wastewater (TWW) is used for drip irrigation. As consequences of nutrients and particles in the TWW, drippers are progressively blocked by fouling process. Although the first drip irrigation systems have been established since 1959 in Israel, there is still a significant knowledge gap surrounding the fouling mechanisms inside the drippers. This is due to the reason that drippers are made from non-transparent plastics, and integrated in the drip pipes. In this work, non-invasive visualization of biofilm formation inside the drippers, fouling potential of TWW and the influence of inorganic particles on biofilm formation in dripper geometry are specially targeted in this work.

A lab-scale and pilot-scale drip irrigation experiments were conducted using synthetic wastewater (SynWW) and real tertiary treated wastewater (T-TWW), respectively. The mean discharge rate was only 35 % of the nominal discharge rate, when there was $0.04 - 1$ g/m² dry matter in the pipe of the lab-scale experiment using SynWW. Although there was more deposition ($4 - 14$ g/m²) in the pipe of pilot-scale system using T-TWW, the mean discharge rate was the nominal value (100 %). The high inorganic fraction in the fouling material of pilot-scale system implies that the inorganic particles from T-TWW helped to mitigate the dripper blockage. Addition of phosphate in pilot-scale experiment increased the portion of organic fouling in the pipe and aggravated the blockage problem, which suggests that organic fouling material causes more severe blockage than inorganic fouling material.

With the aim of visualizing the biofilm formation and assessing the fouling conditions inside the drippers, 3D printed microfluidic devices (MFDs) mimicking dripper structures were used to monitor the biofilm formation *in-situ* and non-invasively by means of optical coherence tomography (OCT). To mimic the temperature conditions in (semi-) arid areas, experiments were conducted in a temperature box simulating a daily temperature cycle between $20 - 50$ °C for 30 days. MFDs were either fed with T-TWW, secondary treated wastewater (S-TWW) or T-TWW doped with nutrients. OCT data sets (3D) illustrated that biofilm establishment and development was influenced by fluid dynamics. MFDs consist of

a labyrinth and a basin compartment. Total biofilm volumetric coverage (in both labyrinth and basin compartment) showed the formation rate is highest with T-TWW doped with nutrients containing 18 mg/L COD (1.4 % MFD volume/d), and lowest with T-TWW containing 6 mg/L BOD_5 (0.1 % MFD volume/d). The malfunction of drippers is mainly due to the biofouling in the labyrinth compartment, although a labyrinth coverage with biofilm of up to 60 % did not reduce the drip rate, whereas further increasing coverage to 80 % reduced the discharge rate by 50 % in this study. Moreover, there was a clear effect of the daily temperature cycle on biofilm accumulation. Biofilm accumulation rate was inhibited to 0.1 – 0.2 % MFD volume/d in daily temperature cycle for all three cultivation media.

Finally, the influence of inorganic particles on biofilm formation was investigated. Biofilms were cultivated in either MFDs or flow cells, using SynWW doped with diatomaceous earth (DE) and/or montmorillonite (MMT). The biofilm development was again monitored over time by means of OCT. Results showed that incorporation of inorganic particles into the biofilm structure with total suspended solids (TSS) of 30 and 60 mg/L caused more detachment events during normal biofilm cultivation in the MFDs than without particles. Biofilm compressibility was determined and a positive correlation between the DE concentration and biofilm compressibility was observed. This is one of the most important findings from this work. Biofilms become more compressible when cultivated with 30 and 60 mg/L DE. The biofilm structure is supposed to be stabilized when it gets compressed at increasing shear stresses. Therefore, detachment at high shear stresses was the lowest when biofilms were cultivated with 60 mg/L DE, compared to biofilms cultivated with less or no inorganic particles.

Zusammenfassung

Zur Verringerung des Wasserverbrauchs wird Tröpfchenbewässerung in der Landwirtschaft weltweit eingesetzt. Wasser und Nährstoffe werden durch Rohre mit konstanter und definierter Ausflussrate direkt zu der Wurzelzone der Pflanzen transportiert. Dies geschieht durch die Einarbeitung von sogenannten Tropfern in die Rohre. Die Tropfer bestehen aus einer Labyrinthstruktur gefolgt von einer Beckenstruktur. Dadurch wird der Wasserdruck reguliert und eine gleichmäßige Ausflussrate sicherstellt. In wasserarmen Regionen wird teilweise behandeltes Abwasser zur Tröpfchenbewässerung verwendet. Aufgrund der im Abwasser vorhanden gelösten Nährstoffe und Partikel tritt in den Tropfern Fouling auf, was zu Verstopfungen und damit einer Reduktion der Ausflussrate führt. Obwohl die Tröpfchenbewässerungssysteme seit 1959 in Israel in Betrieb sind, ist das Verständnis der Foulingmechanismen innerhalb der Tropfer begrenzt. Dies liegt daran, dass Tropfer aus nicht transparenten Kunststoffen hergestellt werden und in die Tropfrohre integriert sind. Dadurch kann Fouling nicht zerstörungsfrei verfolgt werden. Ziel dieser Arbeit war es daher mit Hilfe nicht invasiver Visualisierung der Biofilmbildung innerhalb der Tropfergeometrie, das Foulingpotential von behandeltem Abwasser und den Einfluss von anorganischen Partikeln auf die Biofilmbildung zu untersuchen.

Dazu wurde neben einem Laborsystem auch eine Pilotanlage mit künstlichem bzw. tertiär behandeltem Abwasser betrieben. Im Laborsystem lag die mittlere Ausflussrate bei nur 35 % des Zielwertes, wenn sich im Rohr 0,04 - 1 g/m² Trockenmasse befand. Obwohl in den Rohren der Pilotanlage mit tertiär behandeltem Abwasser mehr Foulingmaterial stattfand (4 - 14 g / m²), war die mittlere Ausflussrate der gewünschte Wert (100 % des Zielwertes). Der hohe anorganische Anteil in dem Foulingmaterial der Pilotanlage deutet darauf hin, dass die anorganischen Partikel im tertiär behandelten Abwasser dazu beitrugen, die Blockade der Tropfer zu verringern. Die Zugabe von Phosphat in der Pilotanlage förderte den Anteil des organischen Foulingmaterials im Rohr und verstärkte das Fouling, was darauf hindeutet, dass organisches Foulingmaterial eine stärkere Blockade als anorganisches Foulingmaterial verursacht hat.

Mikrofluidische Kanäle (microfluidic devices, MFDs), die die Strukturen der Tropfer nachahmen, wurden verwendet um die Biofilmbildung innerhalb der Tropfergeometrie zu visualisieren und bewerten. Die Biofilmbildung wurde *in-situ* und nicht invasiv mittels optischer Kohärenztomographie (optical coherence tomography, OCT) 3-dimensional beobachtet. Um die Temperaturbedingungen in (halb-) ariden Bereichen nachzustellen

wurden Versuche in einer Temperaturbox durchgeführt, die einen täglichen Temperaturzyklus von 20 - 50 °C über 30 Tage simulierte. In den MFDs wurde die Biomasse entweder mit tertiär behandeltem Abwasser, sekundär behandeltem Abwasser oder mit Nährstoffen zugeführtem tertiär behandelten Abwasser kultiviert. OCT-Datensätze zeigen, dass die Etablierung und Entwicklung von Biofilmen durch die Fluiddynamik beeinflusst wurde. MFDs bestehen aus einer Labyrinth- und einer Beckenstruktur. Die gesamte volumetrische Bedeckung (Labyrinth- und Beckenstruktur) mit Biofilm zeigte, dass die Bildungsrate des Biofilms am höchsten war (1,4 %/d), wenn tertiär behandelndes Abwasser mit Nährstoffen (CSB = 18 mg/L) als Medium eingesetzt wurde. Am niedrigsten war die Bedeckung bei tertiär behandeltem Abwasser mit 6 mg/L BSB_5 (0,1 %/d). Die Blockade der Tropfer ist vor allem auf die Biofilmbildung in der Labyrinthstruktur zurückzuführen. Eine Bedeckung in der Labyrinthstruktur mit Biofilmen von bis zu 60% verringerte die Ausflussrate nicht, wohingegen eine weitere Zunahme der Bedeckung auf 80%, die Ausflussrate in dieser Studie um 50 % verringerte. Darüber hinaus gab es eine deutliche Auswirkung des täglichen Temperaturzyklus auf die Biofilmbildung. Die Bildungsrate wurde auf 0,1 - 0,2 %/d im täglichen Temperaturzyklus für alle drei Kultivierungsmedien reduziert.

Zuletzt wurde der Einfluss von anorganischen Partikeln auf die Biofilmbildung untersucht. Biofilme wurden entweder in MFDs oder in Fließzellen mit künstlichem Abwasser kultiviert. Diatomeenerde (DE) und/oder Montmorillonit (MMT) wurden zu künstlichem Abwasser zugegeben. Die Biofilmbildung wurde erneut mittels OCT über 30 Tage beobachtet. Die Ergebnisse zeigen, dass der Einbau von anorganischen Partikeln in die Biofilm-Struktur, mit Feststoffkonzentrationen von 30 und 60 mg/L im Zulauf, mehr Ablöseereignisse verursachte als Biofilme, die ohne Partikeln kultiviert wurden. Zusätzlich wurde die Biofilmkompressibilität bestimmt und eine positive Korrelation zwischen DE-Konzentration und Biofilmkompressibilität beobachtet. Biofilme werden kompressibler, wenn sie mit 30 und 60 mg/L DE kultiviert werden. Die Biofilmstruktur soll stabilisiert werden, wenn sie bei zunehmenden Schubspannungen komprimiert wird. Daher war die Ablösung bei hoher Schubspannungen am niedrigsten, wenn die Biofilme mit 60 mg/L DE kultiviert wurde, im Vergleich zu Biofilmen, die mit weniger oder keinen anorganischen Partikeln kultiviert wurden.

Table of Contents

List of Tables

List of Figures

Nomenclature

Abbreviations

BOD$_5$	biochemical oxygen demand in 5 days	(mg/L)
CFD	computational fluid dynamics	
CLSM	confocal laser scanning microscopy	
COD	chemical oxygen demand	(mg/L)
CV	coefficient of variation	(%)
DE	diatomaceous earth	
DM	dry matter	(g/m²)
EPS	extracellular polymeric substance	
MFD	microfluidic device	
MMT	montmorillonite	
OCT	optical coherence tomography	
oDM	organic dry matter	(g/m²)
PPCPs	pharmaceutical and personal care products	
SEM	scanning electron microscopy	
S-TWW	secondary treated wastewater	
TSS	total suspended solids	(mg/L)
TWW	treated wastewater	
T-TWW	tertiary treated wastewater	

Greek symbols

β	biofilm compressibility	(1/Pa)
τ_w	wall shear stress	(Pa)
η	dynamic viscosity of water	(Pa·s)
μ	specific growth rate of the microorganisms	
μ_{max}	maximum specific growth rate	
Φ	biofilm porosity	(%)

Mathematical symbols

Cov_{after}	biofilm volumetric coverages after treatment	(%)
Cov_{before}	biofilm volumetric coverages before treatment	(%)
Cov	biofilm volumetric coverages in whole flow channel	(%)
Cov_{basin}	biofilm volumetric coverages in labyrinth	(%)
$Cov_{laby.}$	biofilm volumetric coverages in basin	(%)
D_h	hydraulic diameter	(m)
K_s	half-velocity constant in Monod equation	(mg/L)
$\bar{L}_f$	mean biofilm thickness	(µm)
L_f	biofilm thickness	(µm)
s	standard deviation of discharge rates	(L/h)
S	concentration of the limiting substrate for growth in Monod equation	(mg/L)
u_{max}	maximum flow velocity in the flow cell	(m/s)
u_c	biofilm formation rate	(%/d)
V_{basin}	volume of the basin compartment	(mm³)
$V_{biofilm}$	volume of biofilm (including pores)	(mm³)
$V_{biofilm,basin}$	volume of biofilm in the basin compartment	(mm³)
$V_{biofilm,laby.}$	volume of biofilm in the labyrinth compartment	(mm³)
$V_{flow\ channel}$	volume of the whole flow channel	(mm³)
$V_{laby.}$	volume of the labyrinth compartment	(mm³)
V_{voids}	volume of voids in the biofilm	(mm³)
$\bar{x}$	mean discharge rate	(L/h)

Chapter 1

Introduction

Water scarcity is one of the biggest challenges in 21st century. Almost one-fifth of the world's population now live in areas of physical water scarcity (UNDP, 2006). Exacerbated by population growth, rapid urbanization, and climate change, 52 % of the global population in the world is estimated to live under stressed water-resource conditions by 2050 (Schlosser et al., 2014). Water availability and accessibility is tightly related to crop production. Among all the water usage, 69 % of the world's fresh water use is refer to agriculture (FAO, 2016). Therefore, efficient irrigation methods are crucial to cope with the worldwide water scarcity problem.

Drip irrigation is one of the most efficient methods for irrigation. While sprinkler systems have an average water efficiency of 75 %, drip irrigation can increase the water efficiency to 90 – 95 %. Since population growth and urbanization increases the demand for fresh water, treated wastewater (TWW) appears to be a valuable water resources to supplement agricultural irrigation. In arid countries such as Israel, Jordan, Peru, and Saudi Arabia, TWW has long been used for crop irrigation (WHO, 1989; Wu et al., 2014). However, the use of TWW causes the formation of a fouling layer inside the drip irrigation pipes and drippers, which leads to gradual blockage of the drip irrigation system. To overcome the fouling problem and promote the water saving drip irrigation technology, the knowledge gap surrounding fouling driving factors as well as suitable anti-fouling strategies need to be filled.

1.1　What is drip irrigation?

Drip irrigation is a worldwide used technology. In drip irrigation, water is delivered in pipes and drips through drippers at defined discharge rate under a certain pressure range. Drippers are integrated in the drip pipe at designed distance. Each dripper incorporates a labyrinth flow channel which dissipates the water kinetic energy and reduces the inlet water pressure.

There are pressure-compensating and non-pressure-compensating drippers. The pressure-compensating technology can deliver a uniform flowrate even in areas with difficult topographical conditions. For pressure-compensating drippers, a diaphragm is integrated in the dripper to regulate and maintain the same flowrate even if pressure/elevation changes. Figure 1-1 shows the application of a small drip irrigation and the design of a Netafim™ dripper (Netafim[TM] Ltd., Israel). A small-scale drip irrigation systems usually is comprised of a water tank, a pump (if necessary), a filter (pore size between $75 - 150\ \mu m$) and drip pipe.
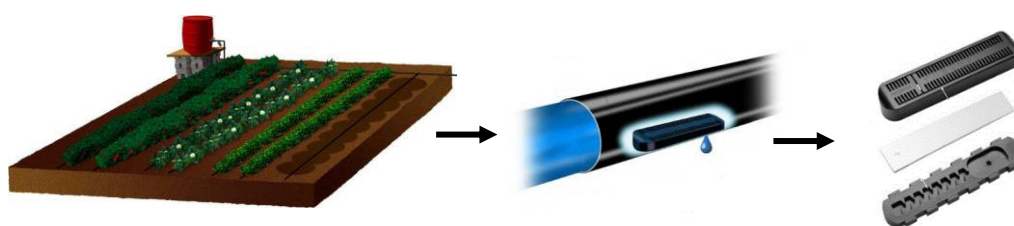
Figure 1-1. An example of a small-scale drip irrigation system from Netafim[TM], Israel.

1.2　Water reuse with drip irrigation: advantages and disadvantages

In arid and semi-arid regions, TWW is often used in agriculture. For example, in Israel 85 % of domestic TWW is reused in agriculture, which is more than 45 % of the water used for irrigation purposes (MFA, 2016). In Spain, about 10 % of TWW is reused and 80 % of the reused water is for irrigation (Esteban, 2009; Raso, 2013). Similarly, about 37 % of the reused municipal TWW in California was used for irrigation in 2009 (SWRCB and DWR, 2009; Wu et al., 2014).

The use of TWW for irrigation is an economic way to reduce costs and save resources. TWW contains many essential nutrients for plant growth and its application may reduce fertilizer application rates (Neilsen et al., 1989). It is reported that crops and vegetables grown with secondary and tertiary TWW were comparable or even better, in respect of dry weight

and yield, compared to irrigation with groundwater and fertilizer (Lubello et al., 2004; Mohammad and Ayadi, 2004). Al-Nakshabandi et al. (1997) reported that the eggplant yield under TWW was twice the average eggplant production under fresh water irrigation using conventional fertilizer application in Jordan.

Moreover, drip irrigation reduces the contact of plants and farmers to pathogens from the TWW compared to sprinklers and flood irrigation (Armon et al., 2002; Forslund et al., 2012; Song et al., 2006). Furthermore, drip irrigation can reduce the soil salinization when irrigated with TWW. Sousa et al. (2011) observed increase of some soil parameters (pH, electrical conductivity, organic matter, Ca^{2+}, Na^+, K^+, Mg^{2+} and NH_4^+) after application of TWW, indicating that irrigation with TWW can cause a soil sodization. By application of drip irrigation, TWW is transported directly to the root zone of the plants. Thus the amount of TWW applied is reduced and only the wet zones of the soil were accumulated with salt which can be diluted with rain water. Moreover, water reuse in irrigation further decreases pollution of surface waters and provides groundwater recharge (Maurer et al., 1995).

Except for pathogens, using TWW may increase the heavy metal and micro-pollutants concentrations in the plant. It is reported that the heavy metal concentrations in the leaves and fruits of eggplant when cultivated with TWW was comparable to that with drinking water (Al-Nakshabandi et al., 1997). Wu et al. (2014) measured the levels of 19 commonly occurring pharmaceutical and personal care products (PPCPs) in 8 vegetables irrigated with TWW under field conditions. They used tertiary treated wastewater (T-TWW) without or with a fortification of each PPCP at 250 ng/L until harvest. Analysis of edible tissues showed a detection frequency of 64 % and 91 % in all vegetables from the TWW and fortified water treatments, respectively. And the total concentrations of PPCPs detected in edible tissues were in the range of 0.01 − 3.87 and 0.15 − 7.3 ng/g (dry weight), respectively. They concluded that the accumulation of PPCPs in vegetables irrigated with TWW was likely limited under field conditions.

The main problem concerning the performance of drip-irrigation systems is that utilizing wastewater effluents is clogging the drippers (Adin and Sacks, 1991). Clogging in the drippers leads to reduced mean discharge rate as well as reduced uniformity of discharge rates along the pipe. In consequence, the crop yield reduces. Depending on the water quality and controlling procedures, drip irrigation systems can be used for more than 10 years or need to be changed every season. As discussed above, drip irrigation using TWW is a water efficient technology and one of the best choices in the deteriorating water stress condition. Thus preventing and reducing fouling formation in the drip pipe is an important issue.

1.3   Fouling driving factors in drip irrigation

There are four interlinked mechanisms of dripper blockage: (1) physical clogging due to interception and deposition of particulate matter; (2) scaling due to chemical precipitation; (3) adsorption due to hydrophobic interaction of soluble or colloidal organic macromolecules; and (4) bacteria and algae growth (Dosoretz et al., 2011; Tarchitzky et al., 2013). All these four mechanisms lead to formation of fouling layers in the drippers.

Fouling is directly related to water quality in drip irrigation systems. Capra and Scicolone (2005) studied the drip performance with six different treated municipal wastewater (primary and secondary TWW). They reported that high total suspended solids (TSS, between $3 - 376$ mg/L in the six TWW), biochemical oxygen demand in 5 days (BOD_5) (between $15 - 200$ mg/L), and pH (between $7.1 - 7.8$) were the water characteristics best correlated with dripper blockage. Biofilm formation is a major factor for blockage. Tarchitzky et al. (2013) quantified the organic fouling material in the drip pipe irrigated with eleven different water sources. They found that total phosphorus concentration (between $5 - 20$ mg/L), the sum of calcium and magnesium concentration (between $5 - 10$ meq/L) and the pH (between $7.6 - 8.5$) of the TWW were best correlated to the portion of organic carbon in the fouling material.

Drip irrigation technology also spreads in the US, especially in California, Florida and Texas. Regarding the water quality, US EPA (2012) defined that secondary treated wastewater (S-TWW, BOD_5 and TSS < 30 mg/L) can be used for irrigation of food crops if further steps including filtration and disinfection were applied. For irrigation of processed food crops and non-food crops in the US, the S-TWW only need to be disinfected before use. In Israel, TWW is required to the level of 20 mg/L BOD_5 and 30 mg/L TSS, due to a demand of better wastewater quality for irrigation (Becker, 2013; Brenner et al., 2000). However fouling still occurs with the above mentioned water quality, especially when fertigation is applied. In fertigation, fertilizers are added in the irrigation water and transported to the plants with drip irrigation systems. The additional nutrients in the fertilizer together with the carbon source and other nutrients in the TWW provide bacteria a food feast which leads to severe blockage problem.

Moreover, the suspended particles in the water contribute to the fouling process in the drip irrigation system. TWW is stored in reservoirs during the rainy season, and then used as a water source for irrigation during the dry summer (Adin and Sacks, 1991). The quality of the irrigation water thus depends on the undergone treatment as well as the physical and biological processes occurring in the reservoir. The suspended particles in the stored TWW have a complex composition, including various microorganisms, such as bacteria, protozoa

and phytoflagellata. Organic and mineralized flocs, as well as clay particles and other inorganic colloidal matter, are also present (Feigin et al., 1991). Previous studies have reported that the blockage of irrigation system happened when the algae (sizes ranged from $3-50\,\mu m$) concentration in the water source increased by a factor of 10 in July compared to May in Israel (Adin and Sacks, 1991). But there is still no study showing the effect of inorganic particles on dripper blockage.

Furthermore, drip irrigation is widely used in arid and semi-arid areas where the air temperature is high. To the author's knowledge, no study has been performed to investigate the fouling formation inside drippers at a controlled daily temperature cycle up to 50 °C. High temperature can hinder the growth of microorganisms, but also promote inorganic scaling. Therefore the impact of high temperature on fouling layer formation when cultivated with TWW is of research interest.

Although the main approach to control dripper blockage is proper water treatment (Nakayama and Bucks, 1991), dripper features such as dripper types (pressure-compensating or non-pressure-compensating) and flow path geometrical parameters also influence the dripper blockage (Li et al., 2006; Qingsong et al., 2008; Yan et al., 2009; Zhou et al., 2014). Duran-Ros et al. (2009) and Ravina et al. (1992) found that the drippers with the highest flow/discharge rate and largest flow channel were less sensitive to clogging. Liu and Huang (2009) report that pressure-compensating drippers performed better compared to non-pressure-compensating drippers when TWW was used. Moreover, the operational parameters, such as irrigation frequency, also influence the dripper blockage process (Zhou et al., 2016, 2015).

1.4 Fouling control

The current studies of fouling control in drip irrigation systems focus on using different water filtration methods. Generally speaking, sand filters are more efficient than screen filter and disk filters (Adin and Elimelech, 1989; Capra and Scicolone, 2005). Puig-Bargués et al. (2005) studied the filtration efficiency of screen filters (98 µm, 115 µm and 178 µm), disk filters (115 µm, 130 µm and 200 µm) and sand filter (effective diameter for filtration = 0.65 mm). Results first showed that sand filter was more efficient at removing particles in the range of $10-80\,\mu m$ in diameter. By analyzing the particle volume distribution it was found that particles larger than the disk and screen filter pores appeared in the filtrates. This is probably due to the fact that flocs can break during the filtration process (Adin and

Elimelech, 1989). However, because of the economic reason, screen and disk filters are more often used to pretreat the TWW compared to sand filters with a common recommendation of $100 - 200$ mesh ($75 - 150\,\mu\text{m}$) (Bucks et al., 1979).

Disinfection and acidification are most common procedures to reduce the fouling material in the irrigation systems and recover the drip performance. Katz et al. (2014) studied acidification and chlorination procedures of field trials when TWW is used. Their study recommended daily chlorination and acidification every 6 weeks. While the drip performance is maintained, the acidic cleaning agent and disinfection by-products are discharged to the soil, plants, and environment, which are potential health risks. Therefore, a balance between drip performance and amount of cleaning agents applied should be studied.

Another important procedure to maintain the drip performance is flushing. The fouling layer in the irrigation system is a mixture of microorganisms, extracellular polymeric substance (EPS), chemical precipitation and particulate matters. Regarding the flushing velocity, it is reported that a flushing velocity of $0.5 - 0.6$ m/s is necessary to remove not only small particles, but also larger particles from drip irrigation pipes (Hills and Brenes, 2001; Nakayama et al., 2007). Moreover, the flushing velocity is also correlated to the operation velocity. Stoodley et al. (2002) reported that biofilms grown under higher shears were cohesively stronger than those grown under lower shears and higher flowrate was needed to initiate biofilm detachment.

1.5 Detection and monitoring of biofilm formation in drip irrigation systems

Currently, the major methods to evaluate the performance of drip irrigation systems are to measure discharge rates of the drippers and count total number of clogged drippers (Duran-Ros et al., 2009; Li et al., 2009; Puig-Bargués et al., 2010). Additionally, the amount of dry matter and organic dry matter in the pipe are quantified (Katz et al., 2014; Tarchitzky et al., 2013), and the characteristics of the organic deposition was studied (Tarchitzky et al., 2013).

However, blockage occurs inside the drippers, which are integrated into the drip pipes. Fouling accumulation inside drippers can only be accessed after being opened and examined. In former studies, the biofilm inside the dripper was scratched out and the amount of phospholipid fatty acids of the fouling material was quantified (Oliver et al., 2014; Yan et al.,

2010; Zhou et al., 2015). However, the width and height of the inner flow path is often less than 1 mm, which makes an exact quantification of biofilm/fouling deposits challenging and less accurate.

To observe the fouling condition inside the drippers, scanning electron microscopy (SEM) and optical camera were used. For example, Oliver et al. (2014) showed that biofilms in the dripper structure contained bacteria, fungi, EPS and particles by means of SEM. Katz et al. (2014) showed the deposit distribution in the labyrinth of the drippers at the mesoscale (mm range) with an optical camera (Figure 1-2). To date, researchers were not able to monitor the biofilm structure and formation non-invasively at the mesoscale in the drippers. This is mainly due to the reason that the biofilm structure is destroyed after cutting and opening the drippers. Furthermore, the technologies which have been investigated do not support three-dimensional imaging with high resolution.
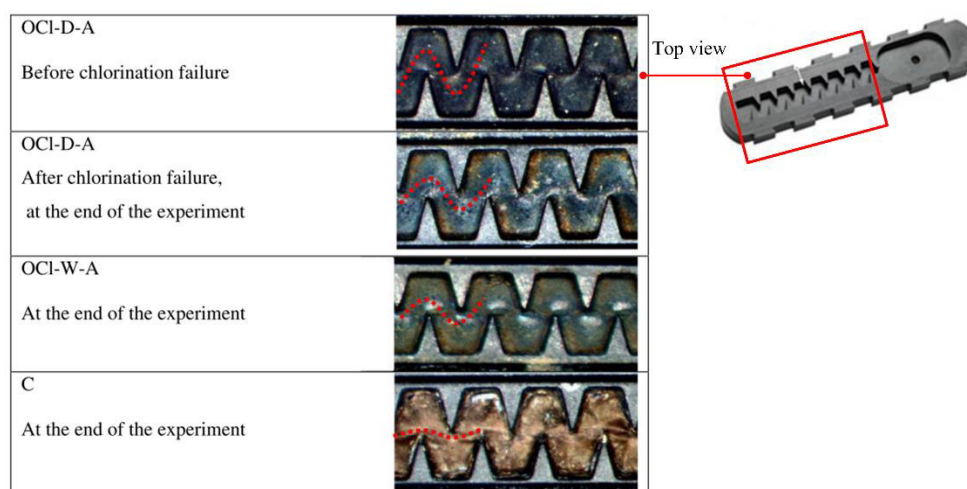
Figure 1-2. Binocular photos of water flow path in the drippers. This figure is adapted from Katz et al. (2014). The red dotted lines indicate the water flow paths, and the brown area is the fouling material accumulated in the dripper. "OCl-D-A" means daily chlorination plus acidification every six weeks. "OCl-W-A" means weekly chlorination and acidification every six weeks. "C" means control (no chlorination and no acidification).

Optical coherence tomography (OCT) is a high-resolution, non-invasive, *in-situ* biological imaging technology (Boppart et al., 1998, 1997; Bouma and Tearney, 2001; Huang et al., 1991; Tearney et al., 1997). As one of the tomographic imaging methods, such as ultrasound imaging and X-ray computed tomography, OCT scans by sections. By using wavelength typically in the near inferred range, OCT is able to penetrate a few mm into the biological sample and acquire a resolution at μm range.

During the imaging process, white light (light with broad bandwidths) is split into a sample arm and a reference arm. The sample is placed in the sample arm and there is usually a mirror in the reference arm. Combining the light reflected from both arms generates an interference pattern, which records the optical path length information, or in another way, time of flight information. The time of flight information in turn yields spatial information about the microstructure of the biological sample (Huang et al., 1991). Figure 1-3 depicts the setup of a generic OCT system.
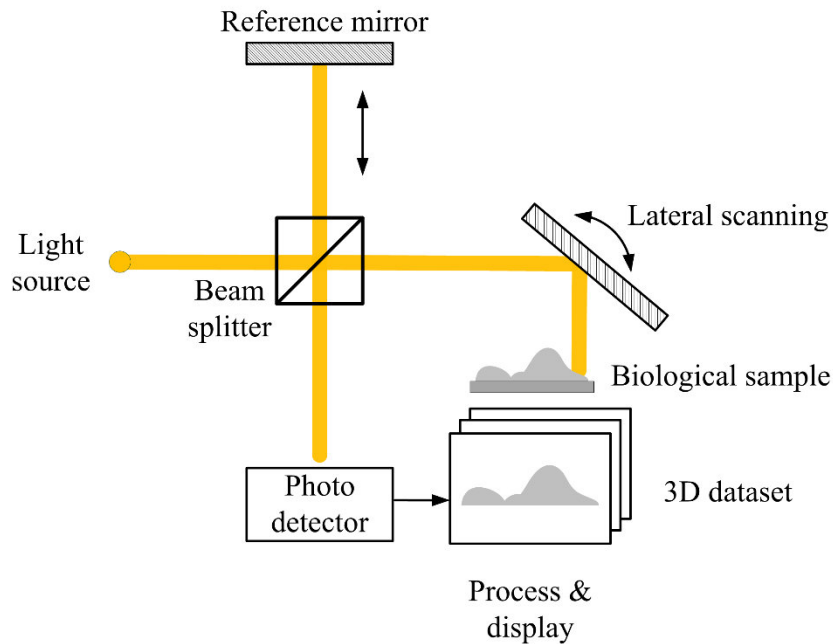
Figure 1-3. Schematic drawing of a generic OCT system.

Using OCT for biofilm investigation was first performed by Xi et al. (2006) and Haisch and Niessner (2007). They compared the biofilm images obtained by OCT and confocal laser scanning microscopy (CLSM), and proposed that OCT is a non-invasive, label- free, real-time, *in-situ* and/or *in-vivo* imaging modality for biofilm. Wagner et al. (2010) first quantified the biofilm structure parameters from the OCT datasets, such as biofilm thickness, porosity and density. In the last few years, OCT has been proven to be a suitable tool to quantify biofilm volume and reveal biofilm structures at the mesoscale (mm range) (Derlon et al., 2012; Dreszer et al., 2014; Li et al., 2016; West et al., 2016). Furthermore, OCT can be used as an imaging technique to investigate biofilm rheological properties such as shear modulus and Young's modulus (Blauert et al., 2015). The biofilm structure obtained by OCT was also incorporated into simulations to understand the influence of biofilm structure on mass transfer and particle attachment (Li et al., 2015; Shen et al., 2015).

1.6   Research questions and objectives of this work

Although fouling problem in drip irrigation has been studied since 1990s, there is still a significant knowledge gap. In this work, extensive work has been done to characterize the fouling behavior in the drip irrigation systems and to monitor biofilm formation under different cultivation conditions. The objectives were to understand the fouling mechanisms and fouling driving factors for drip irrigation systems.

In Chapter 2, a lab-scale drip irrigation system fed with synthetic wastewater (SynWW) was built up and biofouling behavior under controlled operation parameters was obtained. Afterwards, a pilot-scale drip irrigation system was operated directly in the wastewater treatment plant, Karlsruhe (Germany) to study the biofilm formation in real field conditions. The results from both lab-scale and pilot-scale experiments were compared and the fouling mechanisms were characterized.

Experiments with drip pipes (Chapter 2) do not allow a comprehensive understanding of the fouling development inside drippers. In Chapter 3, biofilms were cultivated in 3D printed microfluidic devices resembling the internal dripper geometry. Optical coherence tomography (OCT) was incorporated to monitor the biofilm formation overtime. In this Chapter, an insulated temperature controlled box was constructed to simulate a daily temperature cycle from ambient temperature (20 °C) up to 50 °C. The focus of this section was to (1) observe the biofilm structure and development inside drippers *in-situ* over time; (2) determine the biofilm formation rate in dependence on different cultivation/irrigation media and temperature conditions; and (3) derive a correlation between the detected biofilm volume and the dripper discharge rate.

The role of the inorganic particles in TWW on biofilm formation and mechanical properties is still not well investigated. In Chapter 4, diatomaceous earth (DE) and montmorillonite (MMT) particles were added to the SynWW to create TSS concentrations of 10, 30, and 60 mg/L. The objectives of this section were to (1) observe the biofilm structure and development in MFDs at different TSS concentrations; (2) study the biofilm stability by flushing and chlorine treatment; and (3) determine the compressibility and mechanical stability of biofilms cultivated at different TSS concentrations.

In summary, the intention of this Ph.D. thesis is to examine fouling driving factors in drip irrigation systems, to characterize the fouling material, and to investigate the biofilm formation in the dripper geometry. Specially, biofilms were cultivated in 3D printed MFDs representing the dripper structure and monitored *in-situ* by OCT. It is the first time that the biofilm structure in the dripper structure was revealed non-invasively and at mesoscale.

Moreover, the influence of daily temperature mimicking the real climate condition in (semi-)arid regions on biofilm formation in the MFDs was investigated. Finally the role of inorganic particles on the biofilm structure, compressibility, and biofilm stability was studied.

1.7   Overview of the experiments performed

In order to assist the reader, an overview of all experiments conducted is provided in Table 1-1.

Table 1-1. Overview of all experiments conducted in this work.

Experiment series		Experiment name	Cultivation media	Remarks	
Drip irrigation system	lab-scale	Exp. A	SynWW[1]	Comparison behavior in lab-scale and pilot-scale drip irrigation systems	Chapter 2
	pilot-scale	Exp. B	T-TWW[2]		
Microfluidic devices (MFD)	MFD operated with temperature control box	Exp. CI	T-TWW	Influence of water quality and daily temperature cycle on biofilm formation	Chapter 3
		Exp. CII	S-TWW[3]		
		Exp. CIII	T-TWW doped with nutrients		
	MFD operated with addition of particles	Exp. DI	SynWW + DE / MMT[4]	Pre-experiment, influence of inorganic particles on biofilm formation in MFDs	Chapter 4
		Exp. DII	SynWW + DE	Influence of different particle concentrations on biofilm formation in MFDs	
Flow cell	Flow cell operated with addition of particles	Exp. E	SynWW + DE	Influence of inorganic particles on biofilm mechanical stability and compressibility	

1: SynWW means synthetic wastewater.

2: T-TWW means tertiary treated wastewater.

3. S-TWW means secondary treated wastewater.

4. DE and MMT are diatomaceous earth and montmorillonite, respectively.

Chapter 2

Fouling mechanisms in drip irrigation systems

2.1   Introduction

Drip irrigation is an efficient irrigation technology used worldwide. Water and nutrients are delivered in pipes and drip through embedded emitters (drippers) directly to the root zone of plants. Drippers are devices of a few centimeters in length consisting of a labyrinth and basin compartment (region). Constant discharge rate within a certain water pressure range is achieved by the labyrinth region, in which the hydraulic energy dissipates along the zigzag-like flow path (Dasberg and Or, 1999).

As the worldwide demand for fresh water keeps increasing, more and more attention is paid on water reuse (Schacht et al., 2016). The use of treated wastewater (TWW) in agriculture has been propagated in water-scarce regions, e.g. in Middle East, the south of Europe, America (Arizona, California) and Australia. In Israel 85 % of domestic TWW is reused in agriculture (MFA, 2016). In California, about 37 % of the reused municipal TWW was used for agricultural irrigation in 2009 (SWRCB and DWR, 2009; Wu et al., 2014). One advantage of combining drip irrigation with TWW over sprinkler or surface irrigation is that drip irrigation reduces the risk of exposing agricultural goods and farm workers to pathogens (Armon et al., 2002; Forslund et al., 2012; Song et al., 2006).

However, fouling occurs in the pipes and drippers of the drip irrigation systems, especially when TWW is used. Li et al. (2009) showed that by using treated municipal wastewater (TWW) for irrigation (high five day biochemical oxygen demand, BOD_5),

drippers were clogged much more severely compared to ground water (low BOD_5) resulting in a 26 % lower mean discharge rate. The biofilm formation in the flow channel of the inner dripper structure causes gradual drop of the discharge rate until it is totally blocked. Since drippers are blocked non-uniformly alone the drip pipe, crop yield reduces due to less and uneven water distribution in the field.

In order to maintain the drip performance, irrigation systems need to be cleaned regularly (Christensen et al., 1990; Saravanan et al., 2006). The most common procedurals are using disinfectants (e.g. chlorine, H_2O_2) and acids (e.g. HCl). Katz et al. (2014) investigated acidification (with HCl) and chlorine treatment of field trials when TWW was used. Their study recommended regular chlorine treatment (daily) and acidification (every 6 weeks) in order to maintain the system performance. Since the acidic cleaning agent and disinfection by-products increase the ecological and human health risks, the amount of cleaning agent should be controlled.

Till now, researchers often used real TWW to study the fouling behavior of drip irrigation systems in order to mimic the real conditions in the field (Oliver et al., 2014; Ravina et al., 1997; Yan et al., 2010). However, the composition of TWW is complicated which includes numerous organic and inorganic pollutants and varies from day to day according to the performance of the treatment plant. Studies under controlled lab conditions using synthetic wastewater (SynWW) are of research interest to have a concrete evaluation of the fouling mechanisms.

In this work, a lab-scale drip irrigation system (Exp. A) was built in the experimental hall of Engler-Bunte-Institut (EBI), KIT in 2014. SynWW mimicking the wastewater quality in Israel was used to feed the lab-scale system. In 2015, a pilot-scale drip irrigation system (Exp. B) was constructed directly at the wastewater treatment plant, Karlsruhe (Germany). Fresh TWW was used in the irrigation system. The objectives are to compare the drip performance of the two experiments and evaluate the fouling mechanisms behind.

2.2   Materials and methods

2.2.1 Experimental setup

Lab-scale drip irrigation system (Exp. A)

Figure 2-1 depicts the schematic drawing of the lab-scale irrigation system. The experimental setup mainly consisted of a substrate tank, a pump and approximately 14 m drip pipe. The

drip pipe contained 15 Netafim DripNet™ drippers and the initial discharge rate was 1 L/h per dripper. In total 6 hours irrigation were applied per day (1 h irrigation + 1 h rest) at 0.5 bar water pressure at the beginning of the pipe. The mean retention time of water during irrigation was 8.6 min.

The system was inoculated with activated sludge bacteria from wastewater treatment plant, Karlsruhe (Germany) for 24 hours. The experiment was then performed for 236 days with synthetic wastewater (SynWW, see Table 2-1).
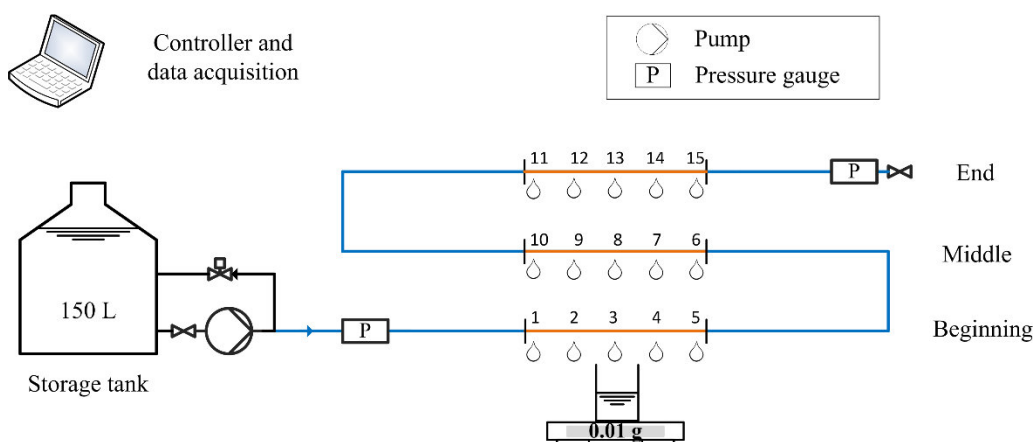
Figure 2-1. Lab-scale drip irrigation system (Exp. A).

Chlorine treatment in the Exp. A

At days 149 and 186, shock chlorine treatment employing sodium hypochlorite (NaOCl) were performed (duration = 1.5 h). For shock chlorine treatment, 30 min chlorine treatment with high concentration of free chlorine (60 mg/L) was followed by 60 min chlorine treatment with low concentration of free chlorine (15 mg/L). Continuous chlorine treatment was performed from day 219 to 236 by injecting concentrated sodium hypochlorite solution ($\approx$ 80 mg/L) for the last 10 min of each irrigation cycle. The resulting free chlorine concentration in the pipe near the injection point was $\leq$ 23 mg/L.

Pilot-scale drip irrigation system (Exp. B)

A pilot-scale drip irrigation system was set-up at the effluent channel of wastewater treatment plant, Karlsruhe (Germany). Due to the installation at the wastewater treatment plant, the drip irrigation system was operated under more realistic conditions with respect to the water quality, pipe length (e.g. number of drippers) and daily temperature cycle compared to the

lab-scale experiment. Total length of the system was 26 m with 130 Netafim DripNet™ drippers at a nominal drip rate of 1 L/h. Fresh tertiary treated wastewater (T-TWW) from the treatment plant was pumped to the system totally 6 hours per day (1 h irrigation + 1 h rest) at 0.8 bar water pressure at the beginning of the pipe. During irrigation, the mean water retention time was 1.8 min. The experiment was performed from 05. Jun. 2015 to 19. Nov. 2015 for 168 days. The average monthly temperature between June and November 2015 was 14.3 °C – 29.8 °C, which was higher than the 30-year average monthly temperature (5.4 °C – 20.1 °C). The detailed temperature conditions were provided in S 2-1 (Supplementary information to Chapter 2).
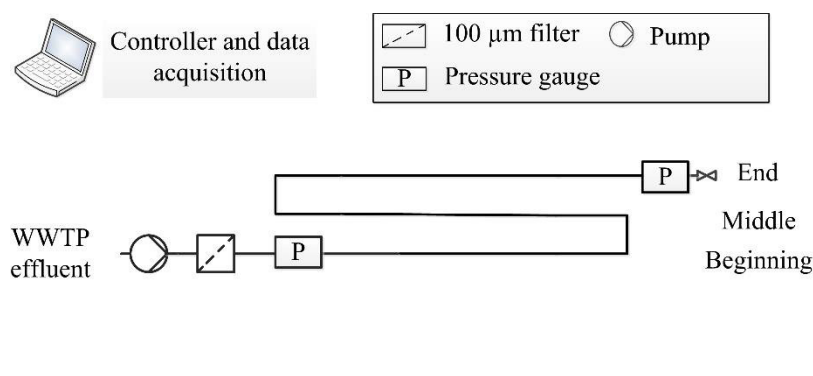
Figure 2-2. Pilot-scale drip irrigation system installed at the local wastewater treatment (Exp. B).

2.2.2 Cultivation medium

Synthetic wastewater (SynWW) for Exp. A

SynWW used in the lab-scale drip irrigation system was made of chemicals and drinking water from Karlsruhe (Germany) as listed in Table 2-1. In order to have comparable experiments as the Israeli project partner which used TWW in their experiment, the amount of COD, NH_4^+, NO_3^-, PO_4^{3-}, SO_4^{2-}, Cl^-, Na^+, and K^+ in the SynWW was formulated according to the water quality of the TWW in Israel. The comparison of the SynWW and the wastewater quality in Israel is shown in S 2-2 (Supplementary information to Chapter 2).

Table 2-1. Composition of the synthetic wastewater.

Substance	mg/L
$NaCH_3COO$	20.5
$(NH_4)_2SO_4$	14.3
NH_4Cl	5.8
$NaNO_3$	28.9
KH_2PO_4	1.2
$K_2HPO_4 \times 3H_2O$	10.6
NaCl	381.3
KCl	46.9

Treated wastewater (TWW) for Exp. B

TWW was used in the pilot-scale drip irrigation system (Exp. B). All the TWW was from the Karlsruhe municipal wastewater treatment plant (Germany). The treatment plant has now a three-stage treatment process: mechanical treatment, activated sludge and trickling filter.

Table 2-2. Characteristics of the tertiary treated wastewater in Exp. B.

Parameter	mg/L
COD	25.5
NH_4^+-N	0.3
NO_3^--N	10.1
PO_4^{3-}-P	0.4
BOD_5	6.2

Starting from day 109, concentrated solution containing K_2HPO_4 and KH_2PO_4 was dosed into the pilot-scale system. The end concentration of ortho-phosphate in the pipe was 1 mg/L. The molar ratio between K_2HPO_4 and KH_2PO_4 was 7:1.

2.2.3 Quantification of discharge rate

To compare the performance of both Exp. A (lab-scale) and Exp. B (pilot-scale), the discharge rates of both systems were monitored. In Exp. A, the discharge rate of all the 15 drippers were measured twice per week. For the Exp. B, 13 drippers at the beginning of the pipe, 11 drippers in the middle of the pipe and 11 drippers at the end of the pipe were chosen

to be monitored. The discharge rate of Exp. B was measured three times per week. Each measurement was double-determination. Mean discharge rate and coefficient of variation (CV) were calculated. CV is defined as the ratio of standard deviation s to the mean discharge rate $\bar{x}$ (Everitt, 1988):

$$Coefficient\ of\ variation\ (CV) = \frac{s}{\bar{x}} \times 100\%$$

(2-2)

2.2.4 Quantification of fouling material in the drip pipe

Sampling

In both experiments, a piece of pipe was cut at the beginning, in the middle and at the end of the irrigation pipe on different sampling days for biofilm sampling. A piece of new pipe was replaced at these positions so that the length of the irrigation system remained unchanged. The biomass was scratched off for analysis of dry matter and organic dry matter. Sampling day for Exp. A was on day 87, 148, 149, 181, 186, 213, and 236. Sampling day for Exp. B was on day 96, 161, and 165.

Dry matter and organic dry matter

The dry matter (DM) and organic dry matter (oDM) was measured according to the standard method (DIN 38414, 1985). The scraped biofilm samples were first dried at 105 °C till the weight was constant. Then the dry biomass was subjected to ignition at 550 °C for 3 h. Both DM and oDM were expressed in g/m^2 after considering the total surfaces of the substratum to quantify the amount of biofilm in the irrigation pipes.

2.3 Results and discussion

Exp. A was performed in the experiment hall using SynWW, which is a combination of Karlsruhe drinking water and nutrients containing 13 mg/L COD. Exp. B was performed in the wastewater treatment plant Karlsruhe with direct access to fresh tertiary treated wastewater (T-TWW) which had an average BOD$_5$ of 6 mg/L and total suspended solids (TSS) of less than 10 mg/L. Both systems used the same DripNet™ drip pipe produced by Netafim™ (Netafim™, Ltd., Israel, with a nominal discharge rate of 1 L/h.

2.3.1 Discharge rate of drip irrigation systems

Figures 2-3 and 2-4 show the relationship between the mean discharge rate and the coefficient of variation (CV) in Exp. A and B. CV is calculated as the standard deviation of the discharge rate over the mean discharge rate. It indicates the uniformity of the drip irrigation system. According to ISO 9621 (2014), drip irrigation systems are considered malfunctioning when CV of discharge rates exceeds 7 %. High drip uniformity is important for the farmers to automate irrigation and have comparable and expected harvest in the whole field.
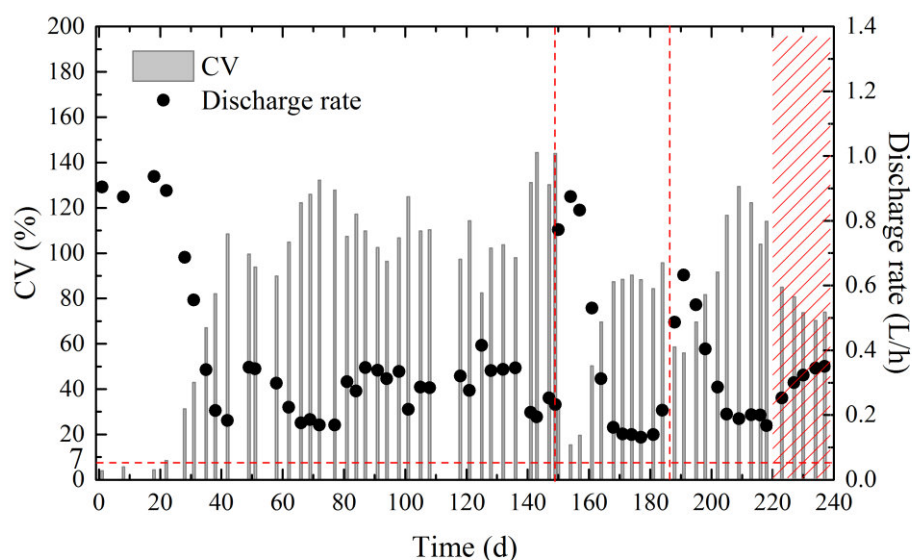
Figure 2-3. Coefficient of variation (CV) and mean discharge rate in Exp. A (lab-scale experiment). The vertical dotted lines indicate the two shock chlorine treatments performed on day 149 and day 186. The hatched bar highlights a long-term chlorine treatment starting from day 219. The horizontal dotted line indicates a CV of 7 %. The drip irrigation systems are supposed to be malfunction when CV exceeds 7 % (ISO, 2014).

Figure 2-3 depicts that with progressing operation of the lab-scale system (Exp. A), the mean discharge rate decreased steadily and the CV rose gradually. Already after 40 days of operation, the mean discharge rate dropped to 10% − 40% of the initial/nominal discharge rate. Figure 2-3 also reveals the recovery of the discharge rate after shock chlorine treatments on day 149 and 186 and CV dropped simultaneously. It was observed that the mean discharge rate kept increasing for the next 3 − 5 days after shock chlorine treatments. It implies that the structure of biofilm might be weaken by chlorine treatment and further detachment occurred until all the weakened biomass was flushed away. However, within 20 days after the two

shock chlorine treatments, the mean discharge rate reached low points again. The detached biomass might become food for the surviving microorganism in the biofilm and the thickness reduction may decrease substrate transport limitations into the biofilm layer, therefore, a faster re-growth of biofilm can be observed after short chlorine treatments. It is thus suggested that flushing treatment should be combined with chlorine treatment to remove all the detached biomass from the system. On day 219, continuous chlorine treatment started. Consequently, the dripper discharge rate recovered and CV decreased again.

Figure 2-4 displays the mean discharge rate and CV in the pilot-scale experiment (Exp. B). The mean discharge rate remained 1 L/h for 100 days with pure T-TWW before the addition of ortho-phosphate on day 109. The CV also maintained to be lower or slightly higher than 7 %. After the addition of phosphate, the mean discharge rate remained at 1 L/h for two weeks before it gradually went down to 0.6 L/h and kept relative constant between 0.5 – 0.6 L/h till the end of the experiment. To be mentioned, The PO_4^{3-}-P concentration of T-TWW was 0.4 mg/L. After addition of ortho-phosphate, the end concentration of PO_4^{3-}-P in the pipe was 1 mg/L.
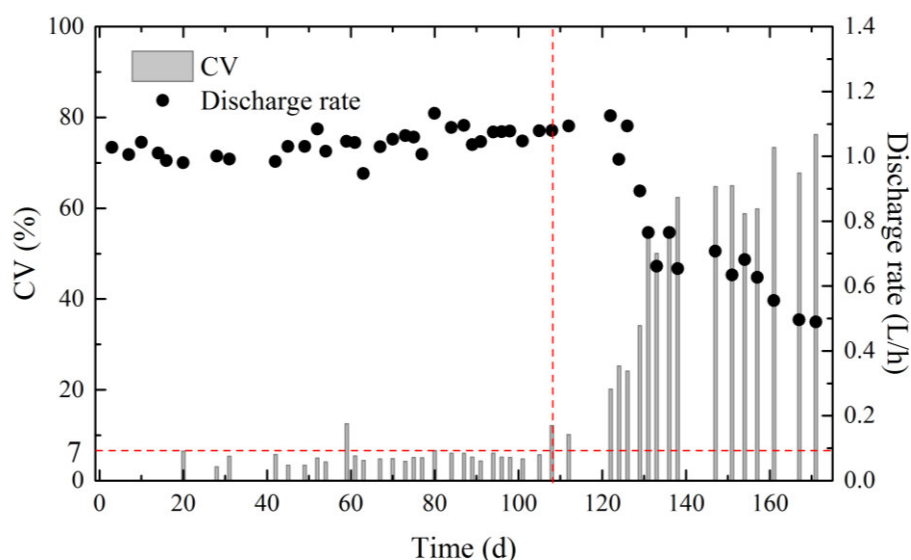
Figure 2-4. Average coefficient of variation (CV) and mean discharge rate in Exp.B (pilot-scale experiment). The vertical dotted line indicates the beginning of ortho-phosphate dosage. The horizontal dotted line indicates a CV of 7 %.

The total nitrogen and PO_4^{3-}-P in the T-TWW was around 10 and 0.4 mg/L, respectively. It was supposed that P was a lacking nutrient element for bacteria growing in Exp. B (pilot-

scale). In Israel, it is common in the field to add fertilizers, e.g. N and P, to the drip irrigation water and this process is called "fertigation" (Bar-Yosef, 1999). Data gathered in Exp. B showed that the mean discharge rate decreased to 50% in two weeks only with the phosphate dosage. Although the wastewater quality and climate are different between Germany and Israel, it implies that fertigation, which incorporates a combination of different nutrients, will definitely accelerate the blockage problem due to rapid biofilm growth and inorganic precipitation. Fertigation is an efficient and environment-friendly method, for instance, it reduces fertilizer leaching into groundwater (Gärdenäs et al., 2005; Hebbar et al., 2004; Malik et al., 1994). Better fertigation procedurals, such as applying different nutrients separately should be studied in future.

Comparing the lab- and pilot-scale experiments, it suggests that using SynWW caused an earlier and more severe biofouling problem. Fouling is the undesired deposition of material on surfaces (Epstein, 1982). Biofouling refers to the undesirable accumulation of a biotic deposit on a surface (Characklis, 1990). Fouling occurring in drip irrigation using TWW is mainly due to bacteria growth, accumulation of particles, and inorganic precipitation (Dosoretz et al., 2011; Tarchitzky et al., 2013). SynWW contains sufficient nutrients for bacteria. COD, N (both NH_4^+-N and NO_3^--N) and P of the cultivation medium was 13, 9, and 2 mg/L. No substrate limitation was assumed except for biofilm formed at the end of the pipe which was 15 meter long. On the other hand, the COD and BOD_5 of the T-TWW was 28 and 6 mg/L, respectively. The T-TWW used in this study was treated with a high load activated sludge system followed by nitrification in a trickling filter. Therefore, the residual substrate in the T-TWW was supposed to be slowly biodegradable compared to raw wastewater and acetate. The biofilm formation with T-TWW was thus slower compared to SynWW.

2.3.2 Discharge rate at different positions of the drip irrigation systems

In both experiments, the irrigation pipes were three times folded and therefore the pipes were divided into three sections: "beginning", "middle" and "end". CV was calculated separately for these three sections and is illustrated in Figure 2-5(a) for Exp. A and (b) for Exp. B. It clearly shows that CV was higher at the beginning and in the middle of the pipe in Exp. A before the chlorine treatment on day 149. Biofilm grew slower at the end of pipe probably due to less access to nutrients which caused less fouling problem.
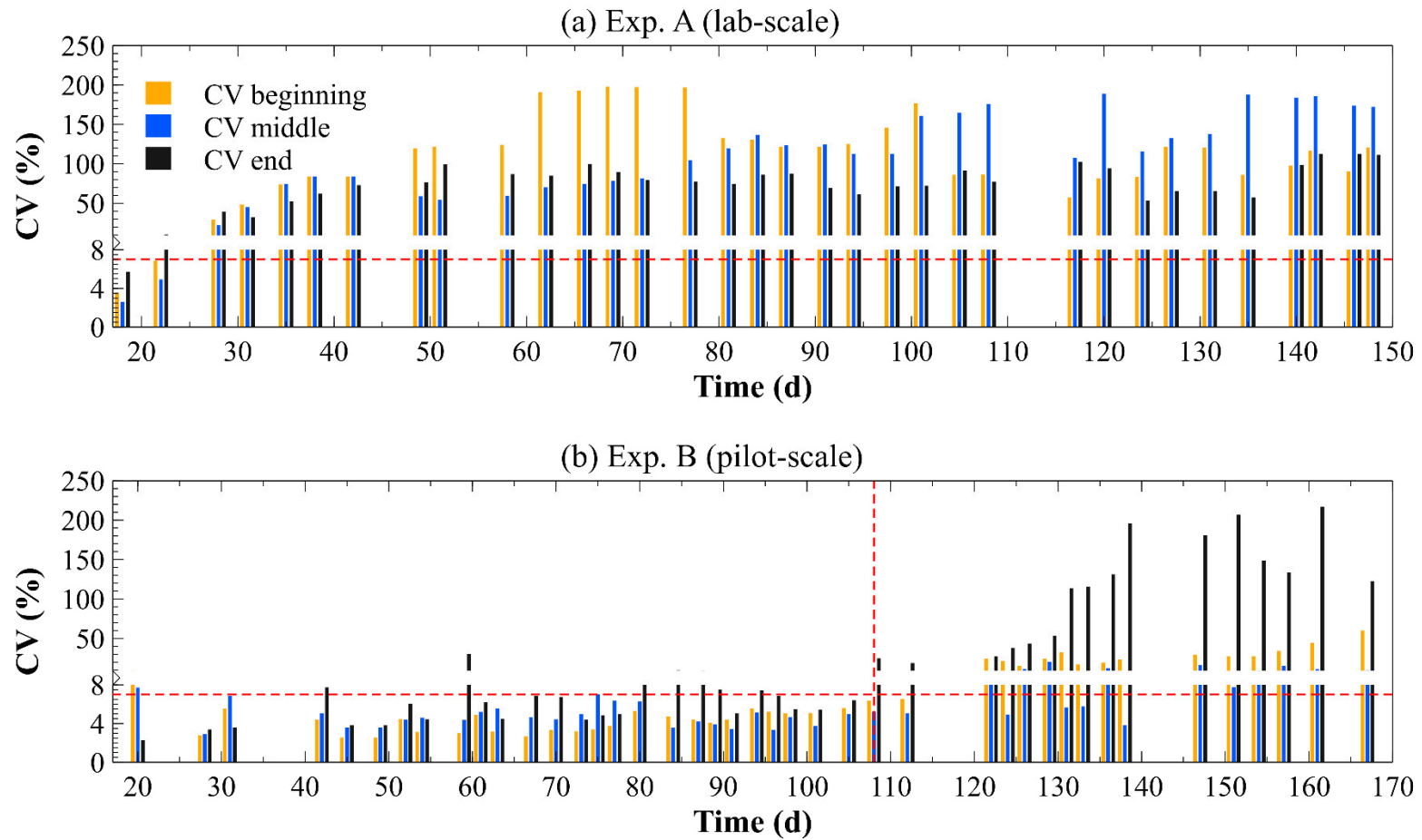
Figure 2-5. Coefficient of variation (CV) at different sections of the drip pipe in (a) Exp. A and (b) Exp. B. The horizontal dotted lines indicate a CV of 7 %. The vertical dotted line in Figure 2-5(b) indicates the beginning of ortho-phosphate dosage.

The distribution of CV in Exp. B was different compared to Exp. A. CV at the end of the pipe was most of the time the highest in Exp. B. Only after addition of phosphate, CV at the beginning of the pipe increased to above 7 %. This results may be explained by the following reasons. First, the T-TWW contains slowly biodegradable nutrients and thus the nutrients availability was low in the whole system (also at the beginning of the pipe). Second, there were suspended particles in the T-TWW which were flushed to the end of the pipe and accumulated there. It thus caused a higher blockage problem there together with a lower shear stress at the end of the pope. Duran-Ros et al. (2009) and Ravina et al. (1992) also observed a greater blockage of drippers located at the end of the pipes when wastewater was used for irrigation.

The high CV at the end of the pipe before phosphate addition also suggests that accumulation of suspended particles played an important role in fouling with TWW. After phosphate addition, CV at the beginning and in the middle of the pipe also increased indicating a rising problem of biofilm formation in the whole pipe.

2.3.3   Quantification of fouling material

Dry matter (DM) and organic dry matter (oDM) were measured from the fouling material formed inside the drip pipe and are listed in Table 2-3. In lab-scale experiment, the analyses of the DM revealed that there was more fouling material at the beginning of the pipe (DM = 1.1 g/m²) than at the end of the pipe (DM = 0.04 g/m²) after three months (87 days). The amount of DM at the beginning of the pipe tripled after another 2 months on day 148 in Exp. A. Simultaneously the DM at the end of the pipe was still only 0.03 g/m². The reason for more fouling material at the beginning of the pipe in Exp. A was due to the higher nutrient availability at the inlet. There were also no particles in the cultivation medium in Exp. A, therefore the fouling layer formed in the pipe was bacteria, extracellular polymeric substance (EPS) and inorganic precipitations. This complied with the results that there was a high organic fraction (oDM/DM > 70 %) in the fouling material at the beginning of the pipe. Moreover, the amount of DM at the end of the pipe was very low, therefore the quantification of the DM and oDM might lack a certain precision.

While irrigation with pure T-TWW for 96 days, the DM in Exp. B was around 4 g/m² at the beginning and 14.3 g/m² at the end of the pipe, respectively. Biofilm formation was faster after continuous addition of phosphate from day 109. Simultaneously, DM increased by 500 – 800 % after day 109 in two months. Especially at the beginning of the pipe, where

phosphate was dosed, DM rose by 8-times. This result is also reflected by the faster increment of CV at the beginning of the pipe in Figure 2-5(b) after phosphate addition.

The percentage of oDM varied between 40 – 50 % along the pipe in Exp. B (Table 2-3). Again, addition of phosphate supported biofilm formation and increased the amount of organic matter (biomass) – expressed by the oDM – at the beginning of the pipe by up to 10 % (from 40 % to 51 %). These findings allow to accept the proposed hypothesis: phosphate was the limiting nutrient in the T-TWW produced by wastewater treatment plant, Karlsruhe. The high amount of inorganic dry matter in the fouling material also suggests accumulation of inorganic particles.

Table 2-3. Dry matter and organic dry matter in the lab-scale Exp. A and pilot-scale Exp. B.

	DM (g/m^2) beginning	DM (g/m^2) end	oDM (%) beginning	oDM (%) end
Exp. A, SynWW (day 87, discharge rate:0.35 L/h)	1.1	0.04	74 %	(29 %)*
Exp. A, SynWW (day 148, discharge rate:0.23 L/h)	3.6	0.03	89 %	(71 %)*
Exp. B, T-TWW (day 96, discharge rate:1.07 L/h)	4.1	14.3	40 %	47 %
Exp. B, T-TWW (day 161, discharge rate:0.55 L/h)	31.7	73.6	51 %	47 %

* Low amount of mass which might lack a certain precision.

Comparing the amount of DM and the mean discharge rate in both Exp. A and B, it is observed that higher deposit at the beginning of the pipe in Exp. A and at the end of the pipe in Exp. B also resulted in server blockage there. This implies a correlation between the amount of fouling material in the pipe and dripper blockage. Higher amount of deposition in the pipe indicated higher nutrients availability or particle concentrations at that section, which also positively influenced biofilm formation in the near-by drippers. Secondly, the results above demonstrates that more biomass in the pipe doesn't necessarily equal to severe

blockage in the dripper. It shows that the discharge rate was only 35 % of the nominal discharge rate when there was around 0.04 – 1 g/m² biomass in Exp. A (day 87). However, the irrigation pipe in Exp. B performed well even with DM that was 1 – 2 orders of magnitude higher than that in Exp. A. This result is interesting. Li et al. (2011) reported that one of the mechanisms for dripper blockage was accumulation of detached biofilm (from pipe) in the drippers. Higher amount of deposition in Exp. B probably caused higher biofilm detachment in the pipe, but the drippers were not clogged before the addition of phosphate. This may be explained by the composition of the fouling material. The fouling material in Exp. B had a higher inorganic fraction (50 – 60 %) compared to Exp. A (20 – 30 %). This suggests that the mechanical property of the fouling material in Exp. A and B might be different, which had an impact on the degree of dripper blockage. Tarchitzky et al. (2013) also reported that the drip performance was better when the fouling material deposited in the drip pipe had higher inorganic fraction, which is probably due to the accumulation of inorganic particles.

However, what happened in the dripper cannot be observed directly, since drippers are made of non-transparent material and integrated inside the pipe. Exact quantification of dry weight in the dripper is challenging because the width and height of the inner flow path is often less than 1 mm. Therefore it was of high interest to find a way to visualize and quantify the biofilm accumulation in the dripper structure, as well as to study the influence of inorganic particles on biofilm development.

2.4　Summary

Drip irrigation utilizing TWW is a practical irrigation method in (semi-) arid regions. From this group of experiments, the following is concluded:

- The fouling behavior and mechanisms in the drip irrigation system using real T-TWW were different compared to that using SynWW. Due to the organic and inorganic particles in the T-TWW in Exp. B (pilot-scale), severe fouling occurred at the end of the pipe and the drip performance was the worst there. On the other hand, severe blockage of the drippers first occurred at the beginning of the pipe in Exp. A (lab-scale) utilizing SynWW.
- The amount of fouling material in the pilot-scale system (Exp. B) was 1 – 2 orders of magnitude higher compared to that in Exp. A. However, the average discharge rate in Exp. B remained the initial value (1 L/h) before addition of phosphate, which was higher than that in Exp. A (0.35 L/h). This observation suggests that the high inorganic deposition in

Exp. B (50 – 60%), which was probably from the inorganic particles in T-TWW, helped to mitigate the dripper blockage.

- Addition of phosphate in Exp. B increased the organic fouling material in the pipe and aggravated the blockage. The discharge rate decreased to 0.5 – 0.6 L/h after phosphate addition. This implies that organic fouling material causes more severe blockage than inorganic fouling material.

Chapter 3

Influence of water quality and daily temperature cycle on biofilm formation

3.1   Introduction

The main methods to evaluate the fouling condition in drip irrigation systems rely on measuring discharge rates of the drippers and quantifying the amount of fouling material in the pipe. Till now, how biofilms form inside the drippers remains unknown. Li et al. (2009) and Yan et al. (2010) found that the mean discharge rate of irrigation systems using TWW did not change at the beginning of the experiments before it dropped rapidly. However, they were not sure what exactly happens in the drippers. Fouling accumulation inside drippers can only be accessed after being opened and examined since drippers are integrated inside the drip pipes. Moreover, the width and height of the inner flow path is often less than 1 mm, which makes an exact quantification of biofilm/fouling deposits challenging and less accurate.

By applying imaging techniques, the biofilm formed in the dripper could be revealed. Former studies using scanning electron microscopy (SEM) showed that the deposit was a mixture of bacteria, extracellular polymeric substances (EPS) as well as inorganic particles accumulating in the flow path of the dripper (Yan et al., 2009). As a microscopic method, SEM detects the local rather than global deposit structure (Wagner et al., 2010). Morgenroth and Milferstedt (2009) addressed the importance of biofilm structural properties of the mesoscale (millimeter range), especially, when biofilm systems need to be understood more in detail, for instance, in aspects of biofilm structure, biofilm function, and mechanisms for biofilm development. To date, researchers were not able to monitor the biofilm formation

non-invasively at the mesoscale in drip irrigation systems, mainly due to the reason that the biofilm structure is destroyed after cutting and opening the dripper.

To allow for a comprehensive understanding of the fouling development inside drippers, 3D printed microfluidic devices (MFDs) resembling the internal dripper geometry were used. Optical coherence tomography (OCT) was applied to investigate biofilm formation non-invasively and *in-situ* over time. Compared to confocal laser scanning microscopy (CLSM), which is a conventional technology when it comes to 3D analysis of biofilms, OCT has a higher penetration depth (millimeter range), a large imaging area and there is no need for staining (Staudt et al., 2004; Wagner et al., 2010). OCT has been proven to be a suitable tool to quantify biofilm volume, reveal biofilm structure and access biofilm material properties at the mesoscale (Blauert et al., 2015; Derlon et al., 2012; Dreszer et al., 2014; Li et al., 2016; West et al., 2016).

Biofilm formation is directly related to water quality. Capra and Scicolone (2005) studied the drip performance with six different treated municipal wastewater (primary and secondary treated wastewater). They reported that high TSS, BOD_5, and pH are the water characteristics best correlated with dripper blockage. In the US and Israel, secondary treated wastewater (S-TWW) is allowed to be applied as irrigation water. With the spread of tertiary treatment of wastewater, the tertiary treated wastewater (T-TWW) is also used in the agriculture (Pollice et al., 2004; UNEP, 2005). The influence of T-TWW on dripper blockage need more attention.

Temperature also has an effect on the growth of microorganisms and biofilm formation (Ingraham, 1958; Pirt, 1985; Watanabe and Okada, 1967). Drip irrigation is widely used in arid and semi-arid areas where the air temperature is generally high and shows large variations between day and night. At air temperatures of 35 – 45 °C, soil or rock surface temperatures may reach 50 – 60 °C in arid areas (Qin et al., 2005; Verheye, 2007). Till now, studies about drip irrigation were usually conducted in experimental halls at ambient temperatures, or directly in the field without temperature control (Li et al., 2009; Liu and Huang, 2009; Yan et al., 2010, 2009). Oliver et al. (2014) conducted a drip irrigation experiment with controlled water temperature starting from 17 °C and increasing by 1 °C every 21 days till 23 °C was reached. Their objective was to mimic medium soil thermal variation. Till now, no study has been performed to investigate the fouling formation inside drippers at a controlled daily temperature cycle up to 50 °C.

In Chapter 3, an insulated temperature controlled box was constructed to simulate a daily temperature cycle from ambient temperature (20 °C) up to 50 °C. The objectives of the study in this Chapter are to (1) observe the biofilm structure and development inside drippers over

time; (2) determine the biofilm formation rate in dependence on different cultivation/irrigation media and temperature conditions; and (3) derive a correlation between the detected biofilm volume and the dripper discharge rate.

3.2   Materials and methods

3.2.1 Microfluidic device

The 3D printed (RCP30 photopolymer, ENVISIONTEC GmbH, Germany) microfluidic devices (MFDs) mimic the geometry of Netafim DripNet™ drippers with a nominal discharge rate of 1 L/h (Netafim™ Ltd., Israel). The dripper geometry is divided into a labyrinth and a basin compartment with a total volume of 44.45 mm³ (Figure 3-1(a)). Water from the inlet passes through the zigzag-like labyrinth and emits through the basin compartment. Transparent coverslips allowed for the *in-situ* and non-invasive OCT imaging.
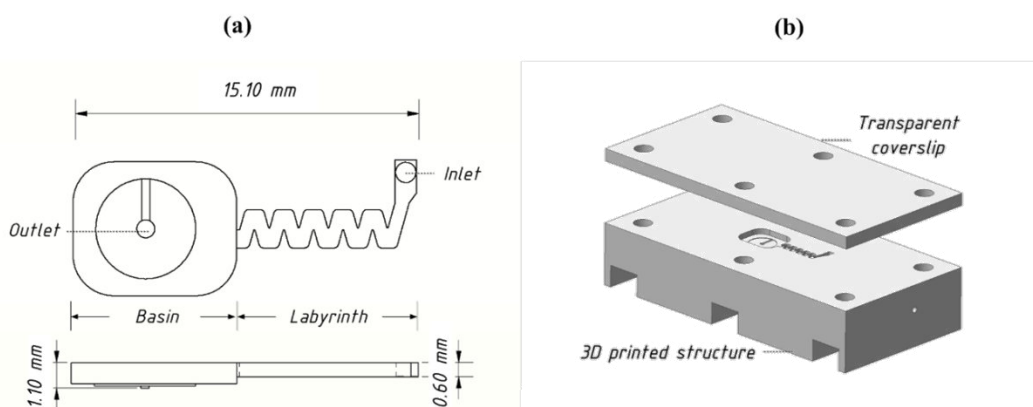
Figure 3-1. (a) Schematic drawing of the dripper composed of a labyrinth and basin compartment; (b) 3D rendering of the designed microfluidic device.

3.2.2 Cultivation medium

In this study secondary and tertiary treated wastewater (TWW) from the local wastewater treatment plant (Karlsruhe, Germany) was used as cultivation medium. Secondary treated wastewater (S-TWW) was collected from clarifiers following the activated sludge process. Tertiary treated wastewater (T-TWW) was sampled from the effluent channel after the trickling filters and the last stage clarifiers. Both S-TWW and T-TWW were filtered (100 µm pore size).

Three experiments were conducted. In Experiments CI and CII, T-TWW and S-TWW was used, respectively. In Experiment CIII, T-TWW with addition of 12 mg/L COD (sodium acetate) and 3 mg/L NH_4^+-N (NH_4Cl) was used to mimic higher loaded wastewaters. Exp. CI, CII, and CIII are named in such a sequence that Exp. CI has the best water quality (T-TWW, lowest COD) and Exp. CIII has the worst water quality (T-TWW + nutrients, highest COD). Detailed water quality parameters are listed in Table 3-1.

Table 3-1. Characteristics of the cultivation media.

Parameter (mg/L)	Exp. CI (T-TWW)	Exp. CII (S-TWW)	Exp. CIII (T-TWW + nutrients)
COD	25.5	34.6	37.8
NH_4^+-N	0.3	9.7	3.4
NO_3^--N	10.1	0.1	10.1
PO_4^{3-}-P	0.4	0.7	0.4
BOD_5	6.2	18.5	18.5
Dissolved oxygen	> 3.8	> 2.2	> 1.0

3.2.3 Cultivation condition

Cultivation medium (see Table 3-1) was pumped to the MFDs through a peristatic pump (Ecoline, Ismatec®, Wertheim, Germany) at a flowrate of 1 L/h which corresponds to a mean flow velocity of 0.77 m/s within the labyrinth (Reynolds number Re = 462) and of 0.07 m/s in the basin. The accurate value of Re and shear stress in the labyrinth and basin shall be further assessed by computational fluid dynamics (CFD) simulation. The discharge rates of the MFDs were monitored regularly during the experiments.

The MFDs were either operated at ambient temperature or placed in the custom-made temperature controlled box simulating the daily temperature cycle. According to field irrigation setups, the pump was operated six hours per day: 9:00-10:00, 11:00-12:00, 13:00-14:00, 15:00-16:00, 17:00-18:00 and 19:00-20:00.

3.2.4 Daily temperature cycle

To study the influence of high, changing temperatures on biofilm formation, an insulated temperature controlled box was developed to simulate a daily temperature cycle ranging between 20 °C (ambient temperature) at 7:00 to 50 °C at 12:00 (noon) and back to 20 °C in

late afternoon at 18:00. The temperature cycle was implemented according to field observations in Israel. MFDs were placed inside the temperature controlled box. The cultivation media were stored at ambient temperature outside the box. This represents the situation in the field where farmers irrigate with water from large reservoirs. The set temperature and actual temperature in the temperature box is shown in Figure 3-2.

In total, three cultivation media and two temperature settings (ambient temperature + daily temperature cycle) were compared, which resulted in six different cultivation conditions. Each experimental condition was performed in duplicate.
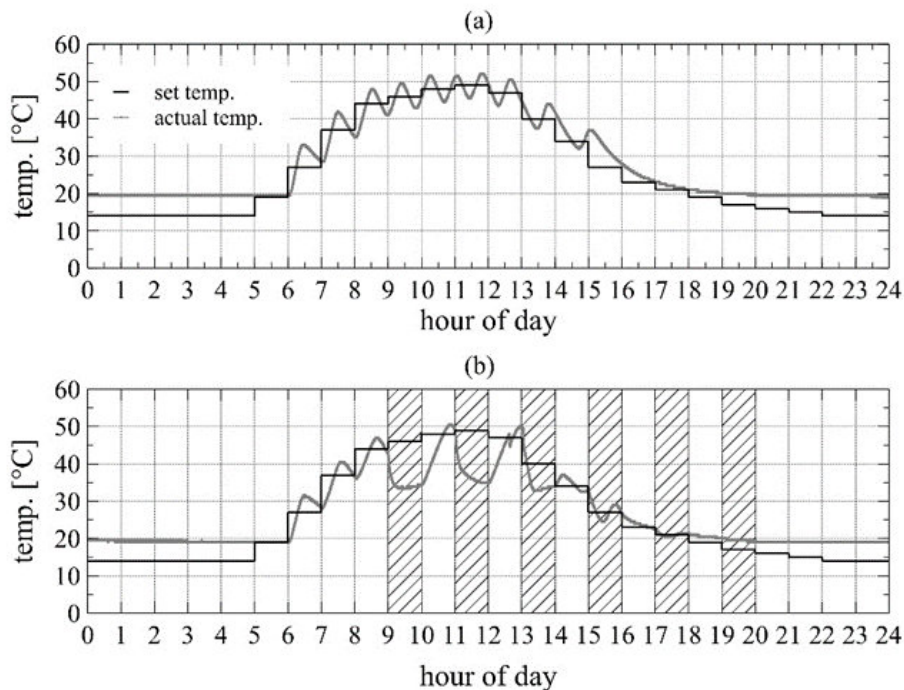
Figure 3-2. Simulated temperature profile inside the custom-made temperature controlled box (a) without MFDs and (b) with two MFDs operated in parallel. The hatched bars indicate irrigation periods. Irrigation causes a drop of the temperature. The target temperature is reached within the following irrigation break.

3.2.5 Image acquisition

Three-dimensional OCT datasets were acquired by means of a Thorlabs GANYMEDE I OCT (Exp. CII, LSM03 lens) and a GANYMEDE II OCT (Exp. CI and CIII, LSM04 lens; Thorlabs GmbH, Lübeck, Germany), respectively. The center wavelength of both OCTs is 930 nm. With both devices the voxel size in x and y was set to 10 µm. The axial resolution in air (voxel size in z direction) of the GANYMEDE I is 2.8 µm and 4.2 µm for the GANYMEDE II.

3.2.6 Image analysis

Three-dimensional OCT datasets were processed in Fiji (running on ImageJ version 1.50b, Schindelin et al. (2012)). Datasets were first converted to 8-bit grayscale images. Huang's method was used to threshold and binarize the dataset (Huang and Wang, 1995). Afterwards, the datasets were resliced from top to bottom into image stacks. Regions of interest (labyrinth and basin compartment) were selected based on the resliced image stacks. Remaining parts were allocated to the background (black). Noise and outliers were removed applying the "Find connected regions" plugin of Fiji.

In order to present a three-dimensional image stack in a two-dimensional way, depth-coded stacks were created. In those the pixel intensity equals the distance of the particular signal to the bottom substratum.

The binary dataset (three-dimensional) after removing noise and outliers was further used to quantify the biofilm volume. An in-house code was used to detect the bulk-biofilm interface. The region below the interface was quantified as biofilm. Biofilm development was characterized by calculating volumetric coverage (Cov) and biofilm formation rate (u_C).

$$Cov\,(i) = \frac{V_{biofilm}}{V_{flow\ channel}} \times 100\ [\%] \qquad (3\text{-}1)$$

$$Cov_{laby.}(i) = \frac{V_{biofilm,laby.}}{V_{laby.}} \times 100\ [\%] \qquad (3\text{-}2)$$

$$Cov_{\,basin}\,(i) = \frac{V_{biofilm,basin}}{V_{basin}} \times 100\ [\%] \qquad (3\text{-}3)$$

$Cov_{laby.}(i)$ and $Cov_{basin}(i)$ are the biofilm volumetric coverages in labyrinth and basin compartment at day i. $V_{biofilm}$, $V_{biofilm,laby}$, and $V_{biofilm,basin}$ are the volumes of biofilm inside the flow channel, in the labyrinth as well as basin compartment of the MFD, respectively. $V_{flow\ channel}$, $V_{laby.}$, and V_{basin} are the volumes of the whole flow channel, the labyrinth and the basin compartments, respectively.

The biofilm development was further described by calculating the biofilm formation rate according to Equation 3-4.

$$u_C = \frac{Cov(i + \Delta t) - Cov(i)}{\Delta t} \left[\frac{\%}{d}\right] \qquad (3\text{-}4)$$

where $Cov(i)$ and $Cov(i + \Delta t)$ are the volumetric coverages at day i and day $i + \Delta t$.

Biofilm formation rate, in other words, is the slope of the growth curve. Student's *t*-test (two-tailed) was performed to statistically evaluate the difference of the slopes/formation rates.

3.3   Results and discussion

3.3.1 Biofilm development assessed by means of OCT

The biofilm formation in real drippers cannot be monitored as the dripper is made of non-transparent plastic and integrated inside the drip pipe. Thus, the biofilm formation was observed by means of OCT over a time period of 30 days inside custom-made MFDs. S-TWW is often used in agriculture in (semi-) arid regions (UNEP, 2005). This section hence shows exemplarily the biofilm structure in one MFD fed with S-TWW at ambient temperature. Figure 3-3 reveals the biofilm development in the labyrinth from day 2 to day 28. The presented intensity equals the distance of the detected signal from the bottom of the labyrinth compartment (= 0 µm, black). This means that the lighter the color (or the higher the intensity), the thicker the biofilm. The maximal height of the labyrinth is 600 µm (Figure 3-1). For illustration purposes Figure 3-3 shows biofilm only in the lower half of the labyrinth (0 – 300 µm). Figure 3-3(a) illustrates that after two days of cultivation, the initial biofilm was sparsely distributed and more biofilm clusters were found near the inlet region. At day 6 streamers of up to 0.8 mm in length were present at the sharp edges of the labyrinth compartment reaching into the middle of the flow path. Fluid flow can induce formation of oscillating streamers (Stewart, 2012). Rusconi et al. (2011) also observed that streamers from *P. aeruginosa* biofilms formed at the edge of a similar zigzag-like microfluidic device. They further described that streamer formation is due to the secondary flows at the edges of the zigzag-like structures. Streamer formation can also be a strategy for young biofilms to access more nutrients from the bulk phase. Taherzadeh et al. (2012) found that oscillating filamentous structures enhance mass transfer from substrates and nutrients in the bulk phase into the biofilm. Within the present study streamers successively disappeared after day 28 (Figure 3-3(b)-(d)). Biofilm formed flat structures covering the bottom and walls of the

labyrinth as well as under the lid. The changing of the biofilm structure from streamer to less/no streamers was also observed by Besemer et al. (2009). They found that streamers, which developed in turbulent flow, disappeared as biofilm growth progressed.
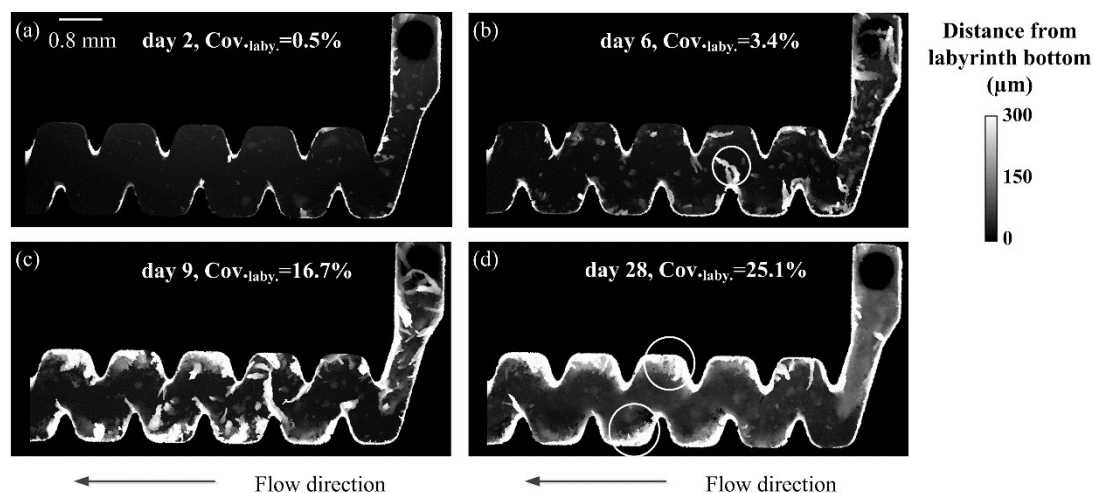
Figure 3-3. Depth-coded image showing biofilm formation in the labyrinth compartment at days 2, 6, 9 and 28 in Exp. CII (S-TWW) at ambient temperature. The calibration bar equals the distance of the detected biofilm signal from the bottom of the labyrinth compartment. The height of the labyrinth is 600 µm and this image shows only the lower half (300 µm above the labyrinth bottom). The circle in Figure 3-3(b) indicates streamers and the circles in Figure 3-3(d) shows that biofilm was more abundant at these corners.

The numbers given in Figure 3-3 are the volumetric coverage of the biofilm in the labyrinth compartment. The volumetric coverage gradually increased during the experimental period. It can be seen that approximately a quarter of the labyrinth compartment was covered with biofilm at day 28 (Figure 3-3(d)). Due to the balance between biofilm growth and detachment (as a function of cohesive strength and shear stress) a preferential flow path between the edges of the labyrinth developed.

Figure 3-3(d) also shows that biofilm was more abundant at the corners where the shear stress was lower (indicated by the circles). The shear stress and fluid dynamics in a similar labyrinth structure was simulated by Wei et al. (2006) and Al-Muhammad et al. (2016). They report that, the flow in the labyrinth-channel consisted of a main flow of high velocity and vortex zones with comparably low velocities as depicted in Figure 3-4. Boyle and Lappin-Scott (2007, 2006) found that the flow magnitude affects the initial distribution of bacterial cells on glass surfaces and the attachment rate decreases as the Reynolds number (Re) increases from 96 to 2200. These studies support results from this study (Re = 462 in the

labyrinth), that bacteria and particles from the cultivation medium had a higher chance to attach to the wall in the vortex regions compared to the section of main flow. The labyrinth compartment in the dripper is designed to reduce the water pressure from the inlet. The vortices generated at the corners of the labyrinth dissipate partly this energy and assure a constant discharge rate. However, the labyrinth structure hence increases the organic and inorganic deposition at these corners.
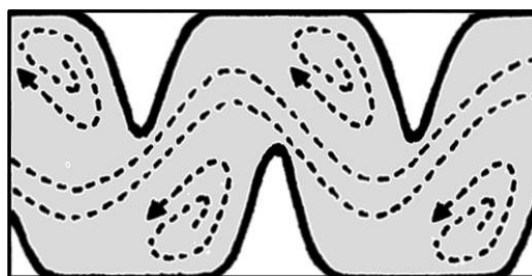
Figure 3-4. Illustration of the flow streamline in the labyrinth compartment of drippers. Flow enters from the right. Arrows indicate the vortices in the corners of the labyrinth. Adapted from Al-Muhammad et al. (2016).

Figure 3-5 shows how biofilm accumulated in the whole MFD until day 9 (Exp. CII, ambient temperature). The circle shows that more biofilm was formed at the region where shear stress is supposed to be low in the basin compartment. Compared to the labyrinth compartment, the biofilm had a lower volumetric coverage in the basin compartment (see numbers in Figure 3-5). A lower volumetric coverage in the basin compartment was also detected for other MFDs at different days (images not shown). This suggests that the basin compartment is less prone to blockage and the biofilm formation in the labyrinth compartment is more crucial to the drip performance.
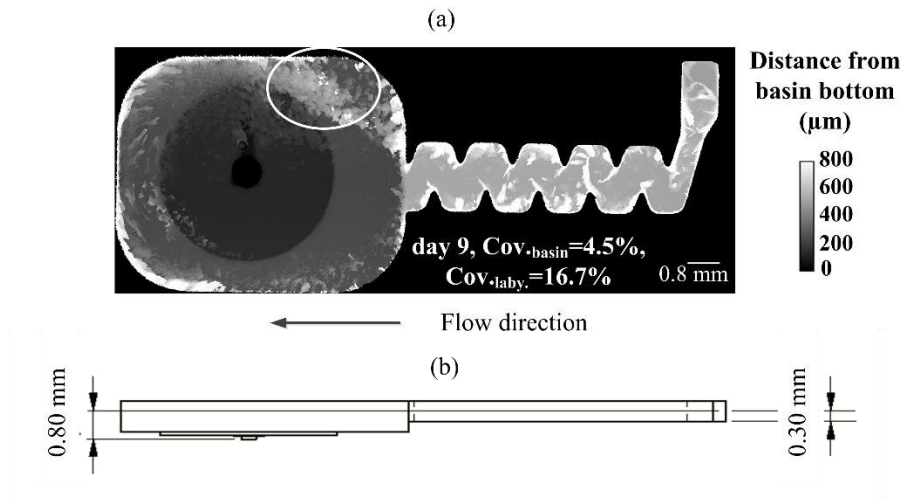
Figure 3-5. (a) Biofilm accumulation in the whole dripper geometry at day 9 of Exp. CII at ambient temperature; and (b) cross section of the MFD. The calibration bar shows the distance from the substratum of the basin compartment. The circle marks where biofilm was more abundant.

3.3.2 Influence of water quality and temperature regime on biofilm formation

Here the biofilm development in the whole MFD under T-TWW (Exp. CI), S-TWW (Exp. CII), and T-TWW doped with nutrients (Exp. CIII) (Table 3-1) was compared at ambient (const.) and varying temperatures (Figure 3-2). Results are summarized in Figure 3-6. Except for Exp. CIII (Figure 3-6(a)), biofilm formation was slow and showed a linear increase. Therefore, for simplification purposes, each experiment was linearly fitted to interpret the slope as biofilm formation rate (u_C) in %/d biofilm. The linear fits were forced to pass through the origin, because at day 0 the coverage was zero.

Ambient temperature

Figure 3-6(a) shows that the biofilm formation rate was the highest in Exp. CIII (1.37 %/d) when additional easily degradable organic carbon sources and ammonium were added to the T-TWW. As expected biofilm grew slower on treated wastewater in Exp. CI (T-TWW) and CII (S-TWW). The biofilm formation rate using S-TWW (Exp. CII) was 0.46 %/d, namely only one third of that from T-TWW doped with nutrients (Exp. CIII). Although the BOD_5 in Exp. CII and CIII was similar, it seems that the BOD_5 from S-TWW was not completely comparable to sodium acetate. The Monod equation is typically used to describe biomass formation (Monod, 1949).

$$\mu = \mu_{max} \frac{S}{K_s + S} \qquad (3\text{-}5)$$

where μ is the specific growth rate of the microorganisms. μ_{max} is the maximum specific growth rate. S is the concentration of the limiting substrate for growth. K_s is the half-velocity constant in the Monod equation and describes the substrate concentration at which the specific growth rate of the microorganisms is half of the maximum growth rate. The K_s value for the growth of biomass with (untreated) wastewater is between 10 to 40 mg biodegradable soluble COD/L (Metcalf & Eddy Inc., 2003). K_s values of less than 1 mg/L have been measured for easily degradable substances (Bielefeldt and Stensel, 1999). Thus, microorganisms can grow at the same rate if they are fed either with low COD concentrations of easily degradable substances or high COD concentrations of less easily degradable substances. The K_s value of TWW in this study was assumed to be higher than untreated wastewater, and therefore the biofilm formation rate with S-TWW (Exp. CII) was lower compared to that of T-TWW + nutrients (Exp. CIII). Although the formation rate was only one third when cultivated with S-TWW compared to with T-TWW + nutrients at ambient temperature, there is no significant difference ($p > 0.05$) between these two cultivation media probably due to the low number of replicates (n = 2) and high standard deviation for the cultivation with T-TWW + nutrients (Figure 3-6(a)).
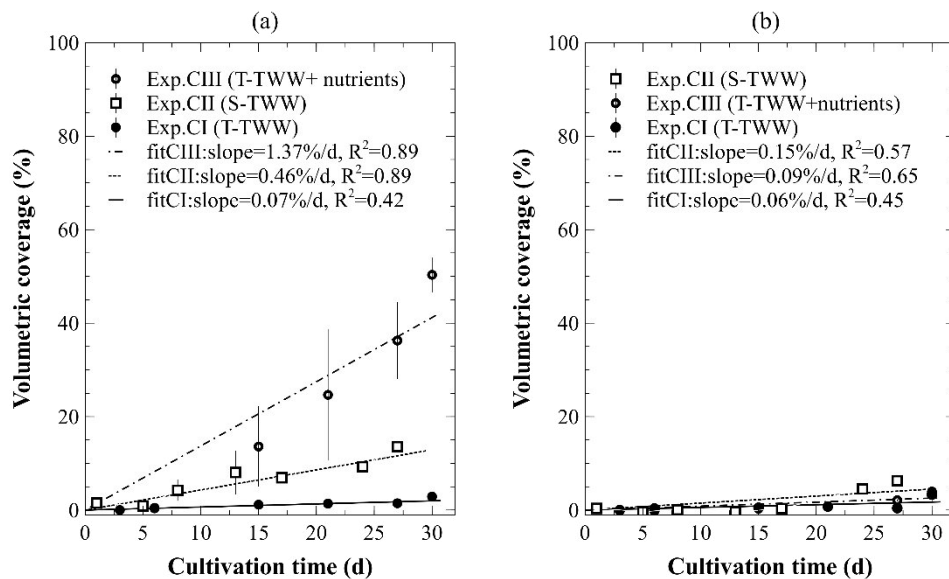
Figure 3-6. Biofilm volumetric coverage in the whole MFD at (a) ambient temperature (20 °C) and (b) when the MFDs were exposed to the daily temperature cycle of 20 – 50 °C. Error bars represent standard error of the mean (n = 2).

The biofilm formation rate of pure T-TWW (Exp. CI) was evaluated to be 0.07 %/d. It is significantly different from the other two cultivation media at ambient temperature ($p < 0.05$). The low formation rate here is mainly due to the assumed high K_S and low BOD_5 value of T-TWW (Table 3-1). Furthermore, 97 % of the nitrogen source in the T-TWW was nitrate. The bacteria in Exp. CI (T-TWW) had to use nitrate as nitrogen source, which has to be reduced before incorporation and thus might not be the preferential nitrogen source for bacteria (Gerardi, 2006).

Daily temperature cycle

Figure 3-6(b) quantifies the biofilm development in the temperature controlled box. Compared to biofilm cultivated at ambient temperature, the biofilm grew significantly slower when exposed to the daily temperature cycle up to 50 °C when fed with S-TWW and T-TWW + nutrients ($p < 0.05$). Formation rates for T-TWW at both temperature conditions were low and cannot be statistically distinguished ($p > 0.05$). Unlike biofilm formation at ambient temperature, different cultivation media (S-TWW, T-TWW, and T-TWW + nutrients) did not cause significant differences in the determined biofilm formation rates under the daily temperature cycle ($p > 0.05$). The biofilm formation rate was only 0.06-0.15 %/d independent of the cultivation medium used. Even in Exp. CIII, biofilm did not grow faster with addition of acetate and ammonium.

As reported by various groups, growth of bacteria is inhibited above a certain (optimum) temperature range (Ingraham, 1958; Pirt, 1985; Trinci, 1969). Microorganisms in wastewater treatment plants in Germany are usually adapted to temperatures around 20 to 30 °C. When the temperature exceeds 45 °C, enzymes can be deactivated which has a detrimental effect on bacterial growth. Rogers et al. (1994) studied the biofilm formation at 20 °C, 40 °C, 50 °C and 60 °C using sludge from the bottom of a calorifier. They found that at 20 °C, the biofilm was comprised of a diverse mixture of gram-negative bacteria, actinomycetes, fungi, and protozoa, but the diversity of the biofilm community was greatly reduced at 50 °C with only a few pseudomonads and *Aspergillus fumigate* left. The diversity was even lower at 60 °C. In comparison with the studies focusing on biofilm formation at constant temperatures (Farhat et al., 2016; Rogers et al., 1994), this study investigated the influence of daily temperature cycle ranging between 20 °C and 50 °C (Figure 3-2). The results indicate that such changing temperatures negatively influenced biofilm growth.

In the field, the treated wastewater used for irrigation in (semi-)arid areas is stored in large reservoirs. Due to the high heat capacity of water, the temperature of water in the

reservoir is lower than the air temperature. It is assumed that the bacteria from the stored treated wastewater are not adapted to high temperatures. Our results thus suggest that high temperatures in the field under real operation conditions might reduce or delay the biofilm formation in the drippers.

Furthermore, there are other mechanisms causing fouling in real drip irrigation systems except for biofilm formation, such as particle settlement due to high TSS concentration in the TWW and inorganic precipitation (Tarchitzky et al., 2013). Further experiments are needed to test the influence of daily temperature cycle on fouling in more complex systems.

3.3.3   Biofilm formation in the labyrinth and basin compartments

Section 3.3.2 discussed biofilm formation in the whole MFD at two different temperature conditions. In 3.3.3, the biofilm development in the labyrinth and basin compartments of the MFD was compared between Exp. CI, CII and CIII. Since the biofilm grew slowly when exposed to the daily temperature cycle, only results from ambient temperature experiments are shown. Figure 3-7 presents the biofilm formation rate determined for biofilm growing in the labyrinth and the basin, respectively. Table 3-2 summarizes the biofilm formation rates (u_C). With respect to the two different parts of the dripper, the labyrinth compartment was fouled more rapidly compared to the basin compartment in all the experiments. In Exp. CIII approximately 80 % of the labyrinth was covered with biofilm after 30 days of biofilm cultivation, whereas only around 50 % of the basin compartment was covered.

The higher biofilm formation rate in the labyrinth compared to the basin compartment is firstly due to the surface-to-volume ratio. The surface-to-volume ratio in the zigzag-like labyrinth compartment is 2.2 times higher than that of the basin compartment. Since biofilm starts to grow from the substratum towards the bulk phase, the volumetric coverage in the labyrinth increased faster. Results of Exp. CII and CIII reveal that the biofilm formation rate in the labyrinth was also approximately 2.0 − 2.4 times higher than that in the basin compartment (Figure 3-7). This suggests that the average biofilm thickness (on the bottom, top, and side walls) increased roughly at the same rate in both labyrinth and basin compartments in Exp. CII and CIII. The largest difference between the biofilm formation rates in the labyrinth and basin compartments was observed in Exp. CI (Figure 3-7). However, the biofilm volumetric coverage in the basin compartment of Exp. CI was only around 1 % at day 30 (Figure 3-7(b)), which makes it very sensitive for the calculation of such a ratio (e.g. over-/underestimation of signals).
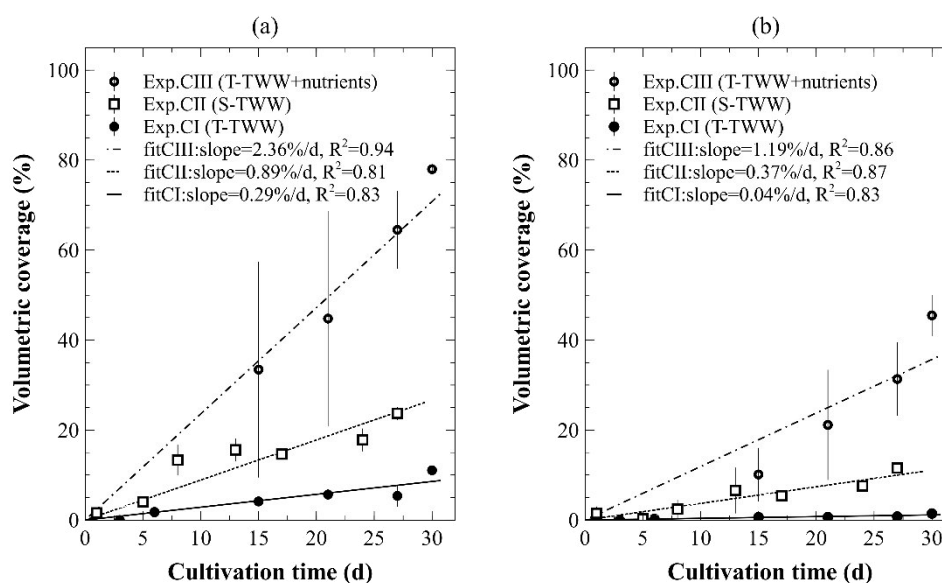
Figure 3-7. Development of the biofilm volumetric coverage in (a) the labyrinth and (b) basin compartment at ambient temperature in Exp. CI, CII, and CIII (n = 2).

Table 3-2. Summary of the biofilm formation rates (u_c).

	Whole MFD (%/d)	Labyrinth Compartment (%/d)	Basin Compartment (%/d)
Ambient temperature			
Exp. CI (T-TWW)	0.07	0.29	0.04
Exp. CII (S-TWW)	0.46	0.89	0.37
Exp. CIII (T-TWW + nutrients)	1.37	2.36	1.19
Daily temperature cycle			
Exp. CI (T-TWW)	0.06	--	--
Exp. CII (S-TWW)	0.15	--	--
Exp. CIII (T-TWW + nutrients)	0.09	--	--

Moreover, the hydrodynamic conditions are different in labyrinth and basin compartments which affects biofilm development. High shear stress in the labyrinth can provide microorganisms a thinner concentration boundary layer and thus a better substrate availability. But it doesn't assist the initial bacterial attachment and can cause more biofilm detachment (Boyle and Lappin-Scott, 2007). Further studies concerning the hydrodynamic

conditions in the MFDs covered with biofilm will help to better understand the biofilm formation in this dripper geometry.

3.3.4   Biofilm volumetric coverage and discharge rate

The amount of biofilm inside a dripper is defining its functionality. As explained in the last paragraphs, biofilms form and accumulate faster in the labyrinth compartment of a dripper. Thus, Figure 3-8 illustrates the correlation between the volumetric coverage in the labyrinth compartment and discharge rate. Results show that the discharge rate was not influenced until the volumetric coverage reached 60 % in this experimental configuration. And a further increasing coverage to 80 % reduced the discharge rate by 50 %. Thus, it is shown that the investigated dripper geometry tolerates a certain coverage by biofilm before failure of the MFD/dripper occurs, according to this experiment.

A more detailed view into the labyrinth of the MFD during Exp. CIII is presented in Figure 3-9. Exp CIII was chosen, because biofilm volumetric coverages in Exp. CI and CII were not higher than 30 % after 30 days. The MFD from Exp. CIII still allowed for a discharge rate of 1 L/h although the volumetric coverage in the labyrinth compartment was already 57 % at day 15 (Figure 3-9(a)). In Figure 3-9(a) it can be seen that the biofilm spread at the walls of the labyrinth section. It also reveals a main flow channel in the center between the edges which allowed water to flow through. At volumetric coverages higher than 60 %, the peristaltic pump was no longer able to keep the discharge rate of 1 L/h. Figure 3-9(b) shows the biofilm formation at day 30 in Exp. CIII. Within additional 15 days of cultivation, the volumetric coverage reached 77 %. Simultaneously the discharge rate dropped below 50 % of the nominal discharge rate (Figure 3-8).

The reduced discharge rate can be explained by Darcy–Weisbach equation, which describes the pressure loss in a uniform cylindrical pipe. In Darcy–Weisbach equation, the pressure loss is proportional to the square of the flow velocity. In this study, biofilm in the flow channel reduced the cross-section area and increased the flow velocity, which leaded to increasing pressure drop. If the pressure drop was higher than what the pump could deliver, the discharge rate of the MFDs decreased. More information about the hydrodynamics, for instance pressure drop and flow field, could be revealed by performing CFD simulations, which use the OCT datasets as structural templates (Li et al., 2015).
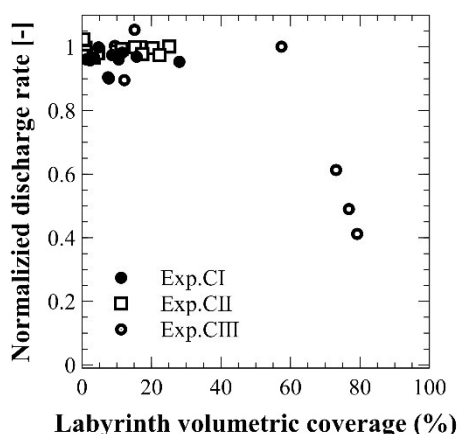
Figure 3-8. Correlation between the biofilm volumetric coverage of the labyrinth compartment of the MFDs and normalized discharge rate.
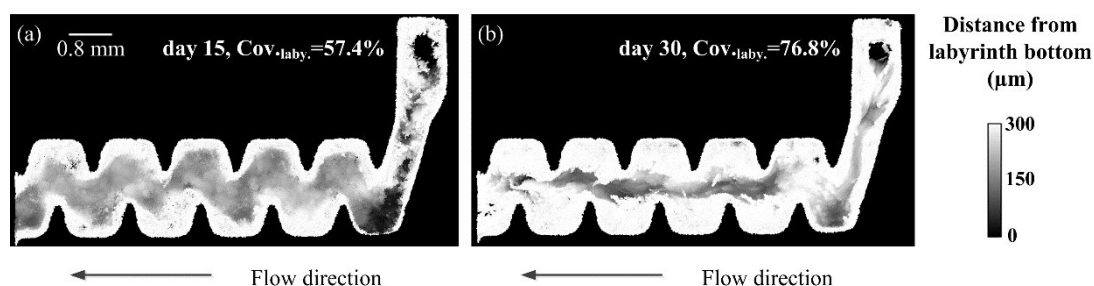
Figure 3-9. Biofilm accumulation in the labyrinth compartment on (a) day 15 and (b) day 30 during Exp. CIII.

Li et al. (2009) studied the fouling behavior of similar drip pipes (nominal discharge 1 L/h) irrigating with domestic S-TWW. It was observed that the mean discharge rate did not change for 20 days, but dropped rapidly afterwards. They suggested that the biofilm formation was quite slow at the beginning and increased quickly once a thin biofilm formed in the dripper. In this study it is shown that the biofilm formation rate is steady before the actual blockage happens. It is found that the discharge rate of 1 L/h did not change at a certain water pressure as long as the main flow path was not totally blocked. The experimental results suggest, that other methods to determine the biofilm formation/accumulation inside drippers (e.g. macroscopic discharge measurements) may underestimate the amount of biofilm. These results further imply that it is not necessarily needed to remove all biofilm in the drippers. The amount of cleaning agent(s) and number of cleaning procedures is sufficient, when a

biofilm coverage of 50% is not exceeded. Field experiments using real drip irrigation systems are required to test and reconfirm the observed results in future study.

3.4   Summary

In Chapter 3, 3D printed microfluidic devices (MFDs) were used to mimic the inner dripper geometry and OCT was applied to follow biofilm formation inside the MFDs *in-situ* and non-invasively. Three different cultivation media and two different temperature settings (ambient and daily temperature cycle) were applied to quantify the effects on the biofilm formation inside the MFDs. The achieved results justify the following conclusions:

• At ambient temperature, the biofilm formation rate inside drippers depended on nutrient availability. The biofilm formation rate was highest when acetate as an easily biodegradable substrate was added to the T-TWW used for irrigation. Second fast biofilm development was observed when S-TWW was used. Biofilm development with pure T-TWW was the slowest.

• At ambient temperature the biofilm volume in the labyrinth compartment increased more rapidly compared to the basin compartment. Blockage/Failure of the MFDs were mainly due to the blockage in the labyrinth compartment.

• In the labyrinth compartment, biofilm growth typically started at the edges of the flow channel and slowly move towards the regions with less shear. Biofilm coverage in the labyrinth of up to 60 % did not reduce the discharge rate, whereas further increasing coverage to 80 % reduced the discharge rate by 50 % in this study.

• Temperature cycles (ranging between 20 and 50 °C) have a negative impact on biofilm formation. Higher temperature keeps growth of non-adapted bacteria (mesophile) under control. Compared to experiments at ambient temperature (20 °C), the biofilm formation rate for T-TWW with additional carbon source decreased from 1.37 %/d to 0.15 %/d at daily temperature cycle. Similar behavior was observed for S-TWW.

Chapter 4

Influence of inorganic particles on biofilm development

4.1 Introduction

Treated wastewater (TWW) is often used in arid and semi-arid regions together with drip irrigation. The lab- and pilot-scale drip irrigation systems (Exp. A and B) described in Chapter 2 showed that the blockage problem of drip irrigation systems was less pronounced when cultivated with tertiary treated wastewater (T-TWW), compared to synthetic wastewater (SynWW). However, there was more biomass accumulation, especially inorganic accumulation, in the pipe when T-TWW was used. It seems that inorganic particles from the T-TWW helped to mitigate the fouling problem. Tarchitzky et al. (2013) found that the drip performance was better when the fouling material deposited in the drip pipe had higher inorganic fraction, which is probably due to the accumulation of inorganic particles. The knowledge gap of how inorganic particles influence biofilm development, limits the understanding of biofilm formation in drip irrigation systems utilizing TWW.

A lot of research has been done to study the interaction between inorganic particles and bacteria. It is reported that inorganic particles provide a better environment for the bacteria compared to bulk liquid, because particles can shield bacteria from UV and predators (Decamp and Warren, 2000; Walters et al., 2013; Wright et al., 1995). Furthermore, inorganic particles provide substantial surface areas for the adsorption of natural organic matter and soluble organic compounds, which are additional nutrients for attached bacteria. It is reported that smectite clays enhance the biofilm formation by microorganisms (Alimova et al., 2007).

Particle transportation on the biofilm surface depends on physical mechanisms such as viscous drag force, gravity, Brownian diffusion, electrostatic force, shear induced dispersion, etc. (Nywening and Zhou, 2009; Tsuda et al., 2013; Wiesner et al., 2005). de Kreuk et al. (2010) used particulate starch to feed an aerobic granule reactor and observed the attachment of particulate starch ($dp_{0.9} < 100\,\mu m$) on granules (biofilm) surface. The aerobic granules was observed to be filamentous and irregular compared to granules fed with soluble substrates, probably due to the low hydrolysis rates of particulate starch.

Most of the particles in the TWW were observed to be < 100 µm (Rickert and Hunter, 1971). However, factors which influence particle adhesion to biofilm were only evaluated for micron or sub-micron particles. The adhesion of particles on biofilm surface depends on surface properties of both biofilms and particles, as well as the solution (cultivation medium) chemistry. Paris et al. (2009) reported that biofilm age (i.e. bacterial density and biofilm properties) and convective-diffusion were found to govern particle accumulation (polystyrene particles, diameter = 0.5 µm). It was reported that older biofilms and higher wall shear stresses both increased the velocity and the amount of particle deposition on the biofilm. Shen et al. (2015) used computational fluid dynamics (CFD) to reveal the role of hydrodynamics created by surface roughness on particle adhesion (diameter = 2 µm). They found that the interception of particles with biofilm was enhanced by rough biofilm surfaces.

Application of inorganic particles on membrane surfaces has been studied and may throw light on biofilm formation with particles on solid surface, which hasn't been well investigated. Chomiak et al. (2014) reported that diatomaceous earth at a concentration of 300 mg/L increased biofilm heterogeneity and enhanced permeate flux in the ultrafiltration. In membrane bioreactors, the sludge filtration performance was improved by adding adsorbent fine particles, such as activated carbon, or colloidal particles (latex or melamine beads) (Lesage et al., 2008; Loulergue et al., 2014; Remy et al., 2010; Teychene et al., 2011). Compared to biofilm formation and particle deposition on solid substratum, the biocake formed in membrane filtration is built up additionally under permeation/viscous drag force.

In this study, biofilms were cultivated at TSS concentrations of 0, 10, 30 and 60 mg/L with synthetic wastewater (SynWW). With the *in-situ* observation by means of OCT, the biofilm formation inside the dripper geometry was monitored and quantified. The objectives of the study are to (1) investigate the impact of inorganic particles on biofilm development in MFDs mimicking dripper geometry; (2) study the influence of inorganic particles on biofilm compressibility and stability; (3) test the efficiency of cleaning strategies such as flushing and chlorine treatment + flushing.

4.2   Materials and methods

4.2.1   Cultivation medium

SynWW was used in Exp. DI, DII (MFD experiments) and Exp. E (Flow cell experiments). The composition of the SynWW was similar compared to that for the lab-scale drip irrigation system (Exp. A in Chapter 2), which mimics the wastewater quality in Israel. The difference is that all the chemical concentrations in the Exp. DI, DII, and E were 1.5 times higher than that in Exp. A. The intention was to reduce the biofilm cultivation time and enable more repetitions of experiments. The COD, NH_4^+-N and PO_4^{3-}-P in the cultivation media of Exp. DI and DII were 19.5, 6.8, and 3.3 mg/L, respectively.

Table 4-1. Composition of the synthetic wastewater.

Substance	mg/L
$NaCH_3COO$	30.8
$(NH_4)_2SO_4$	21.4
NH_4Cl	8.7
KH_2PO_4	1.8
$K_2HPO_4 \times 3H_2O$	20.9
$NaNO_3$	43.3
NaCl	591.9
KCl	70.4

Inorganic particles including montmorillonite (MMT, naturally occurring mineral, Alfa Aesar, Germany) and diatomaceous earth (DE, Celite® 22139, slightly calcined, Sigma-Aldrich, USA) were doped into the SynWW to have an end concentration of 0, 10, 30, and 60 mg/L. The particle size distribution of both particles were measured with a particle analyzer (Retsch Technology CAMSIZER XT, Haan, Germany). The median particle sizes of DE and MMT were 36.5 µm and 12.1 µm, respectively.

In Exp. DI, the effect of two different particles (DE and MMT) and particle concentrations (30 and 60 mg/L) were screened and each concentration had one replicate. Based on the results from Exp. DI, Exp. DII focused only on DE particles with concentrations of 10, 30, and 60 mg/L. In Exp. DII, the experiments with DE concentrations of 0, 10, and 30 mg/L had triplicates and there were only duplicates for DE concentration of 60 mg/L. All the experiments were listed Table 4-3 on page 55.

4.2.2 Biofilm formation with particles in microfluidic device

The MFDs used in this study were the same as in Exp. C in Chapter 3. The MFDs mimicked the geometry of Netafim DripNet™ drippers (Netafim™ Ltd., Israel) and were 3D printed (RCP30 photopolymer, ENVISIONTEC GmbH). The flow channel of the MFD is divided into a labyrinth and a basin compartment with a total volume of 44.45 mm³ (Figure 4-1 (a)). Water from the inlet passes through the zigzag-like labyrinth and emits through the basin compartment. Transparent coverslips allowed for the *in-situ* and non-invasive visualization using OCT.
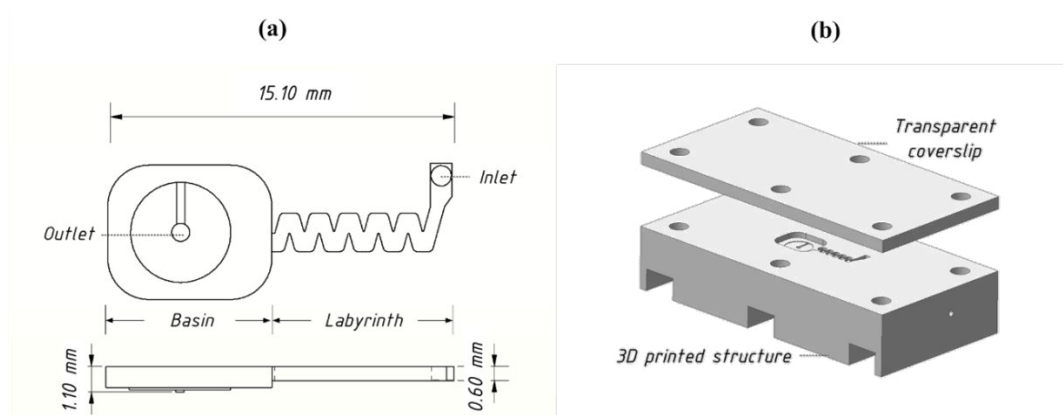
Figure 4-1. (a) Schematic drawing of the dripper composed of a labyrinth and basin compartment; (b) 3D rendering of the designed microfluidic device.

Inoculation

Activated sludge from the Karlsruhe wastewater treatment plant was used for all inoculations of the experiments using SynWW. The activated sludge was always freshly taken and filtered with paper filters (12 – 15 µm pore size). Approximately 200 mL clear and filtered sludge was added to 5 L SynWW and recirculated at 1 L/h for 24 hours, before the cultivation media was refilled.

Cultivation condition

Cultivation media was first pumped into a piece of irrigation pipe (30 cm, no drippers) and then to the MFD at a flowrate of 1 L/h via a peristaltic pump (Figure 4-2). Therefore the whole setup mimics a drip irrigation system with one dripper. To maintain a constant TSS concentration in the medium tank, the system was in flow-through mode. Every day the pump

was operated for 6 hours (1 h operation + 1 h rest). The peristaltic pump could withstand 1 bar back pressure with the pipe material used.

The biofilm development in the MFDs were monitored by means of OCT. The biofilm formed in the irrigation pipe (Figure 4-2) was observed by confocal laser scanning microscopy (CLSM) and scanning electron microscopy (SEM).
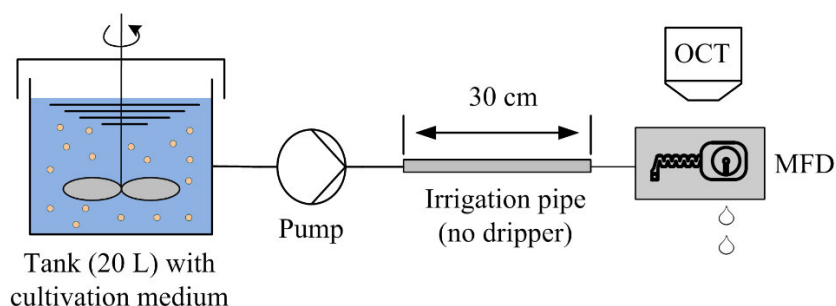
Figure 4-2. Schematic drawing of the MFDs operated with addition of inorganic particles in the cultivation medium.

Flushing experiment

In order to investigate the stability of the cultivated biofilms, flushing experiments were performed in the Exp. DII (only DE particles were added to the cultivation media). Biofilm detachment was forced by increasing the flowrate to 2.0 L/h, then to 3.0 L/h, and finally to 4 L/h. The Reynolds numbers of these three flowrates were calculated to be 924, 1386 and 1848, respectively. And the wall shear stress was calculated to be between 15.5 Pa (2 L/h) and 31 Pa (4 L/h). Each flowrate was kept constant for 15 min and each flushing experiment lasted for 45 min totally (Figure 4-3). Three-dimensional OCT datasets were taken after each step of 15 min treatment.

The flushing experiment was performed on day 13 and day 29 in MFDs cultivated with 0, 10 and 30 mg/L DE. One MFD out of the triplicates in each TSS concentration was used for this flushing experiment. These MFDs were not taken into account of the calculation of biofilm formation rates. The biofilm development in the other two MFDs (out of the triplicates, no flushing) was used to illustrate the biofilm formation over time. The flushing experiment for MFDs cultivated with 60 mg/L DE was performed on day 21 with both MFDs (duplicates). Table 4-3 in section 4-7 (page 55) summarized the experiments performed in Chapter 4.
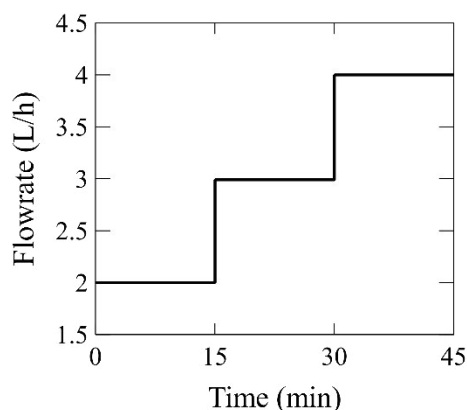
Figure 4-3. Scheme of the flushing experiment.

Chlorine treatment and flushing experiment

Additional experiments using a chlorine treatment and flushing were performed in Exp. DII. Biofilms in the MFDs were first treated with sodium hypochlorite (free chlorine = 50 mg/L) for 1 hour to investigate the effect of hypochlorite on biofilm removal. The biofilm was then treated with increasing flowrate step by step as described above in the "Flushing experiment" (Figure 4-3). Three-dimensional OCT images were acquired after 1 hour chlorine treatment and 45 min flushing experiment.

The chlorine treatment + flushing experiments were performed on day 29. For TSS concentrations of 0, 10, and 30 mg/L (triplicates), the two replicates without previous flushing experiments were used to perform the chlorine treatment + flushing experiments. For TSS concentration of 60 mg/L (duplicates), this experiment was carried out in both replicates, which were used in the flushing experiment on day 21. The overview of the experiments are listed in Table 4-3 on page 55.

4.2.3 Biofilm compressibility

Due to its complex geometry and hydrodynamic conditions within the MFDs, it is difficult to study the biofilm mechanical property. To simplify the problem, straight flow cells were used to study the mechanical properties of biofilm when cultivated with DE concentrations of 0, 10, 30, and 60 mg/L.

Biofilm cultivation

Biofilms were cultivated in straight flow cells (flow channel: 2 mm × 1 mm × 160 mm) for 20 – 27 days. The system was inoculated with activated sludge bacteria from Karlsruhe wastewater treatment plant, Germany. SynWW dosed with 0, 10, 30, or 60 mg/L DE particles was used as the cultivation medium. The experimental setup was the same as in Exp. D (Figure 4-2), except for replacing the MFDs with flow cells. The flowrate was 1 L/h and the Reynolds number was 208 in the flow cell. This Reynolds number was approximately half of that in the labyrinth of the MFDs.
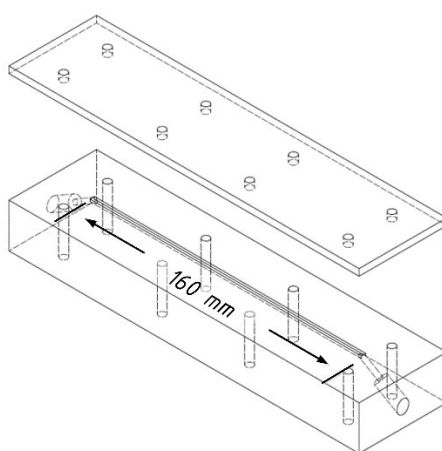
Figure 4-4. Schematic drawing of the flow cell. Channel width and height equals 2 mm and 1 mm, respectively (Blauert et al., 2015).

Shear stress induced biofilm deformation experiment

The biofilm formation in the above mentioned flow cells was monitored over time. When the mean biofilm thickness was > 100 µm, the shear stress induced experiment was performed. For each flow cell, only one stress induced experiment was carried out.

During the shear stress induced experiment, the wall shear stress of the flow cell was elevated from 0 Pa to 3.6 Pa in 9 steps and then back to 0 Pa step by step. The Reynolds number ranged from 0 (shear stress = 0 Pa) and 1066 (shear stress = 3.6 Pa). Each shear stress was held for 2 min and three-dimensional OCT images were taken in each step (Figure 4-5). To be more specific, OCT images were taken 1 min after the shear stress increased. The biofilm was supposed to be adapted to the new wall shear stress after 30 seconds (Blauert et al., 2015).

The wall shear stress was calculated according to Blauert et al. (2015):

$$\tau_w = \frac{4\eta u_{max}}{D_h} \; [Pa] \qquad\qquad (4\text{-}1)$$

where τ_w is the wall shear stress; η is the dynamic viscosity of water; u_{max} is the maximal flow velocity in the flow cell and D_h is the hydraulic diameter. It needs to be mentioned, that the wall shear stress τ_w was approximated assuming an ideal and fully developed laminar flow between two infinite parallel plates. Therefore, τ_w does not capture local disturbances of the fluid flow by the biofilm structure and movement of the biofilm itself. However, it is still the best evaluation of the stress acting on the biofilm structure which can be measured directly from the experiment (Blauert et al., 2015).
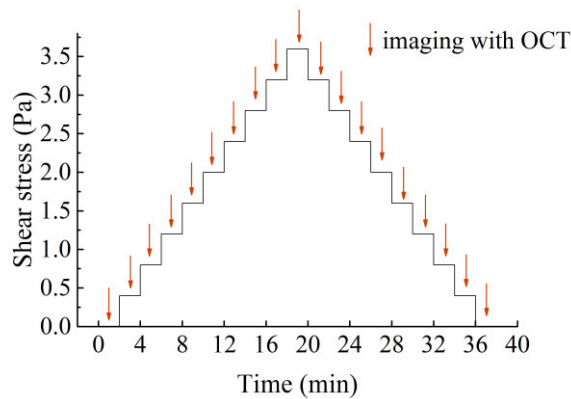
Figure 4-5. Illustration of the process of the shear stress induced deformation/detachment experiment.

4.2.4 Image acquisition (OCT)

The three-dimensional image acquisition in this chapter is similar to that in Chapter 3, section 3.2.5. In short, a Thorlabs GANYMEDE I OCT (LSM03 lens) and a GANYMEDE II OCT (LSM04 lens; Thorlabs GmbH, Lübeck, Germany) were used to acquire three-dimensional OCT datasets. The center wavelength of both OCTs is 930 nm. The axial resolution in air (voxel size in z direction) of the GANYMEDE I is 2.8 µm and 4.2 µm for the GANYMEDE II. The imaging regions and voxel sizes in x and y directions are listed in Table 4-2.

Table 4-2. Imaging settings in Exp. DI, Exp. DII, and Exp. E.

	Imaging region (width × length × height)	Voxel sizes in x and y direction
Exp. DI and DII (MFDs)	16.8 mm × 6.8 mm × 1.2mm	10 µm
Exp. E (flow cell)	2 mm × 2 mm × 1 mm	4 µm

4.2.5 Image analysis (OCT)

Quantifying biofilms in MFDs

The image analysis of the images taken from MFDs are similar compared to that in Chapter 2. All the OCT datasets were processed in Fiji (running on ImageJ version 1.50b, Schindelin et al. (2012)). The imaging process is illustrated in Figure 4-6.
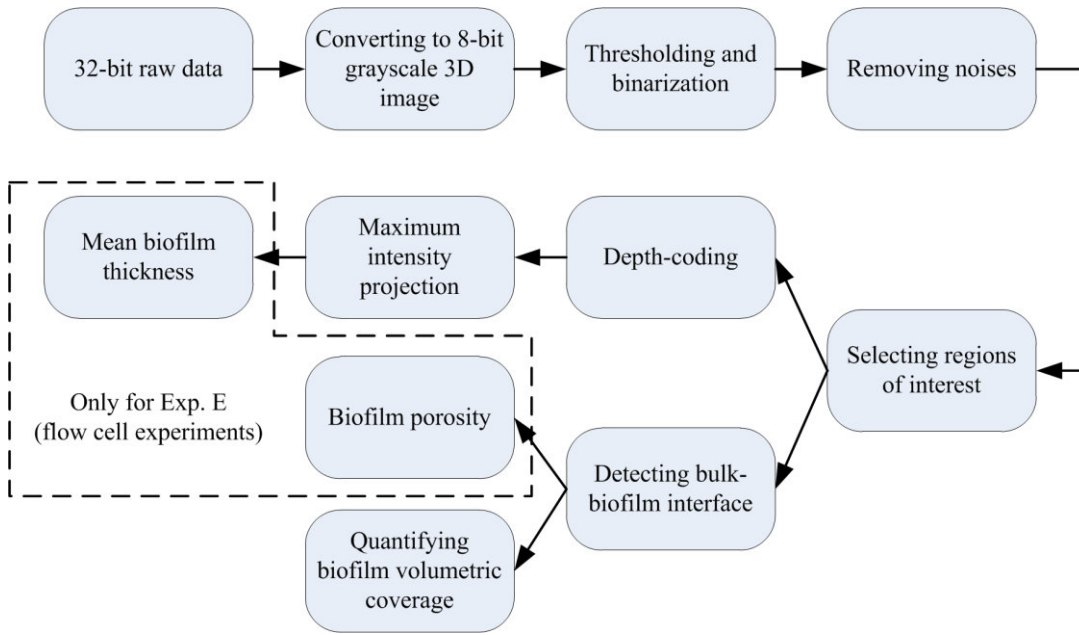
Figure 4-6. Overview of OCT data process of biofilms in MFDs and flow cells.

Quantifying biofilms in flow cells

The image analysis for biofilms in flow cells was similar compared to in MFDs, except that mean biofilm thickness and biofilm porosity were additional quantified.

Mean biofilm thickness

Calculation of mean biofilm thickness $\bar{L}_f$ was based on the 2D maximum intensity projections of the depth-coded stacks (Figure 4-6). The pixel intensity in the 2D maximum intensity projection equals the distance of the particular pixel to the bottom/substratum of the flow cell, therefore, it equals to the biofilm thickness from the bottom. Only biofilm formed in the center of the flow channel (0.8 mm × 2 mm) was accounted for thickness calculation (Figure 4-7).

$$\bar{L}_f = \frac{1}{i \times j} \sum_{j=1}^{j} \sum_{i=1}^{i} L_{f,i,j} \ [\mu m] \tag{4-2}$$

where $\bar{L}_f$ is the mean biofilm thickness. i and j are the number of pixels in x and y directions. $L_{f,i,j}$ is the biofilm thickness at position (i, j).

Biofilm porosity

The porosity used in this study was based on the image analysis of OCT datasets. As shown in Figure 4-6, the bulk/biofilm interface was detected by an in-house code. The region below the interface was quantified as biofilm (including pores), and the voids (black pixels) in the biofilm were recognized as pores in this work. Biofilm porosity (Φ) was calculated as the ratio between the total volume of voids (V_{voids}) and biofilm volume ($V_{biofilm}$).

$$\Phi = \frac{V_{voids}}{V_{biofilm}} \times 100 \ [\%] \qquad (4\text{-}3)$$
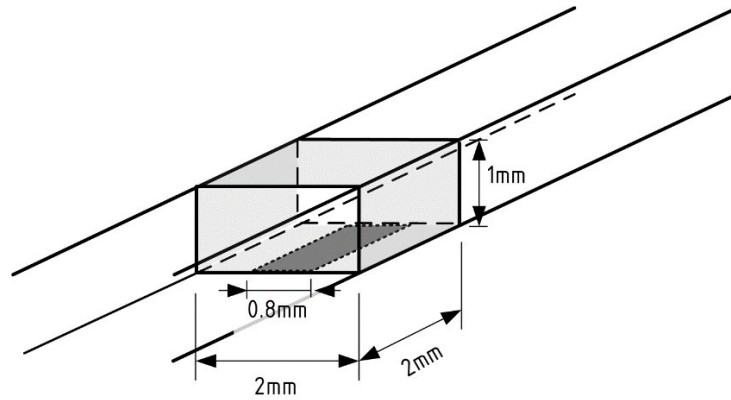
Figure 4-7. Illustration of the region used for calculation of biofilm thickness.

4.2.6 CLSM

CLSM was used to observe the biofilms formed in the inner wall of the irrigation pipes in Exp. DI. The CLSM image stacks were acquired using a Zeiss LSM700 confocal laser scanning microscope (Carl Zeiss MicroImaging GmbH, Jena, Germany). EPS glycoconjugates were stained with Aleuria aurantia lectin (AAL) Fluorescein isothiocyanate (FITC) (LINARIS Biologische Produkte GmbH, Gemany) and nucleic acids were stained with SYTO60 (ThermoFisher) according to the protocol described by (Lawrence and Neu, 1999). A water immersible lens (40× magnification, Objective W Plan-Apochromat 40×/1.0 DIC, Zeiss, Germany) was used to investigate the biofilm structure.

4.2.7   SEM

Biofilms formed at the inner wall of the irrigation pipes (Exp. DI) were visualized by SEM using a FEI model Quanta FEG 650 instrument. The irrigation pipes were cut into small pieces and freeze-dried.

4.2.8   An experimental overview in Chapter 4.

In order to assist the reader, an overview of the experiments conducted in Chapter 4 provided in Table 4-3.

Table 4-3. Experiment overview and amount of inorganic particles in the cultivation media.

Particles	Total TSS concentration	Total replicates	Flushing	Chlorine + flushing	Remarks
Exp. DI					
0 mg/L	0 mg/L	1			CLSM/ SEM
30 mg/L DE	30 mg/L	1			CLSM
30 mg/L MMT	30 mg/L	1			CLSM
15 mg/L DE + 15 mg/L MMT	30 mg/L	1			
30 mg/L DE + 30 mg/L MMT	60 mg/L	1			SEM
60 mg/L DE	60 mg/L	1			SEM
Exp. DII					
0 mg/L	0 mg/L	3	Day 13, 29[*]	Day 29[**]	
10 mg/L DE	10 mg/L	3	Day 13, 29[*]	Day 29[**]	
30 mg/L	30 mg/L	3	Day 13, 29[*]	Day 29[**]	
60 mg/L DE	60 mg/L	2	Day 21[***]	Day 29[***]	
Exp. E					
0 mg/L	0 mg/L	2			
10 mg/L DE	10 mg/L	2			
30 mg/L	30 mg/L	2			
60 mg/L DE	60 mg/L	2			

[*] The flushing experiments were performed on one MFD (one out of the triplicates).
[**] The chlorine treatment + flushing experiments were performed on the two MFDs without previous flushing experiments.
[***] The flushing experiments and chlorine treatment + flushing experiments were performed on both replicates.

4.3 Results and discussion

4.3.1 Biofilm formation with particles in microfluidic device

In the first experiment (Exp. DI) two different inorganic particles, DE ($dp_{0.5}$ = 37 µm) and MMT ($dp_{0.5}$ = 12 µm), were added to the SynWW to have TSS concentrations of 0, 30, or 60 mg/L. It was investigated, which influence the two different particles (DE and MMT) and TSS concentrations have on biofilm formation. Based on the results from Exp. DI, only DE was further used in Exp. DII, to create TSS concentrations of 0, 10, 30, and 60 mg/L. In shear stress induced deformation experiments the biofilm compressibility and stability was investigated.

4.3.1.1 Biofilm structure

Biofilm structure can be investigated at different scales. For instance, single cells and EPS in the biofilm matrix can be observed with SEM (µm range). CLSM is optimal to visualize cell clusters and microscopic structures with information about the biofilm composition in the range of a few hundred µm (Wagner et al., 2010). Along with SEM and CLSM, OCT is capable of visualizing an overall structure of biofilm in the mm range. In order to have a comprehensive understanding of the biofilm cultivated with DE and MMT, the three imaging technologies including SEM, CLSM, and OCT were used to reveal the biofilm structure from microscale to mesoscale for the biofilms formed with inorganic particles in Exp. DI.

Microscale: CLSM and SEM images

The biofilm structure at the microscale was revealed by means of CLSM (Figure 4-8(a)) and SEM (Figure 4-8(b)). Figure 4-8(a) shows that the DE particles were visualized in the biofilm matrix. DE particles have a distinguishable shape which looks like honeycomb and can be easily identified in Figure 4-8(a). MMT particles have a typical appearance of corn flakes (Keller, 1982). However, it was not possible to clearly identify them by means of CLSM. With the help of SEM, MMT particles can be observed in biofilm matrix together with DE particles (Figure 4-8(b)).

Figure 4-8 shows that the added particles were larger than bacteria and were sometimes partially submerged in the biofilm matrix. The particle part which was above the average biofilm surface can experience a high shear stress in the flow which may trigger detachment.

On the other hand, the totally submerged particles may have an influence on the biofilm mechanical properties.
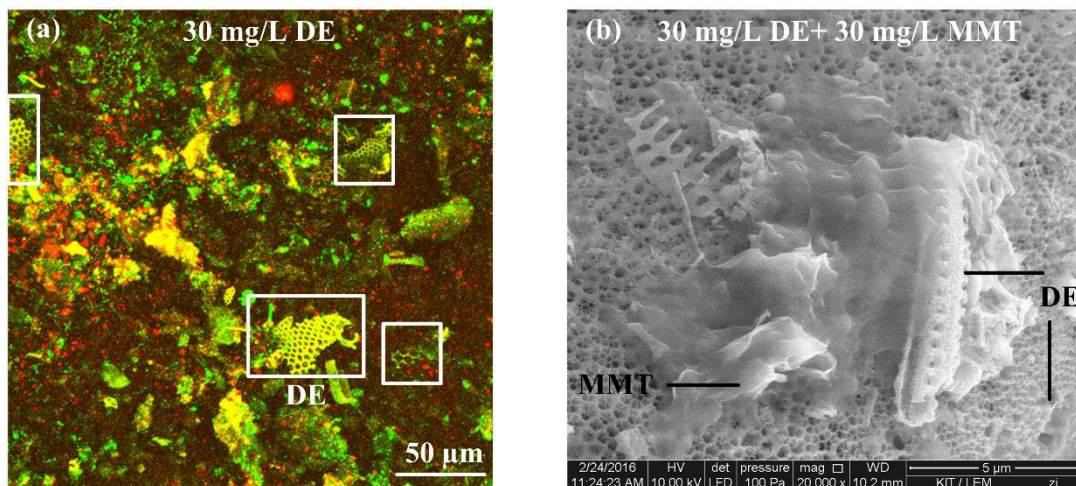
Figure 4-8. (a) CLSM image of biofilm cultivated with 30 mg/L DE at day 14 in Exp. DI; and (b) SEM image of biofilm cultivated with 30 mg/L MMT + 30 mg/L DE at day 25 in Exp. DI. The scale bars are 50 µm and 5 µm in (a) and (b), respectively. In Figure 4-8(a), the green color shows EPS glycoconjugates and the red color shows nucleic acids.

Mesoscale: OCT images

Three-dimensional OCT datasets were acquired regularly in the labyrinth and basin compartments of the MFDs during the cultivation periods. As mentioned in Chapter 3, biofilm formation in the labyrinth compartment is critical for dripper blockage compared to the basin compartment. Therefore, only OCT images of the labyrinth compartment are displayed in Figure 4-9. In order to show the bulk-biofilm interface, all the images in Figure 4-9 were depth-coded and in top-view. At day 1, small biofilm colonies were detected for all three TSS concentrations. At day 7, biofilms already covered all the surface of the labyrinth compartment and formed small, dense mound structures, roughly 100 µm in diameter. Moreover, more biofilm was formed near the wall of the labyrinth channel when particles
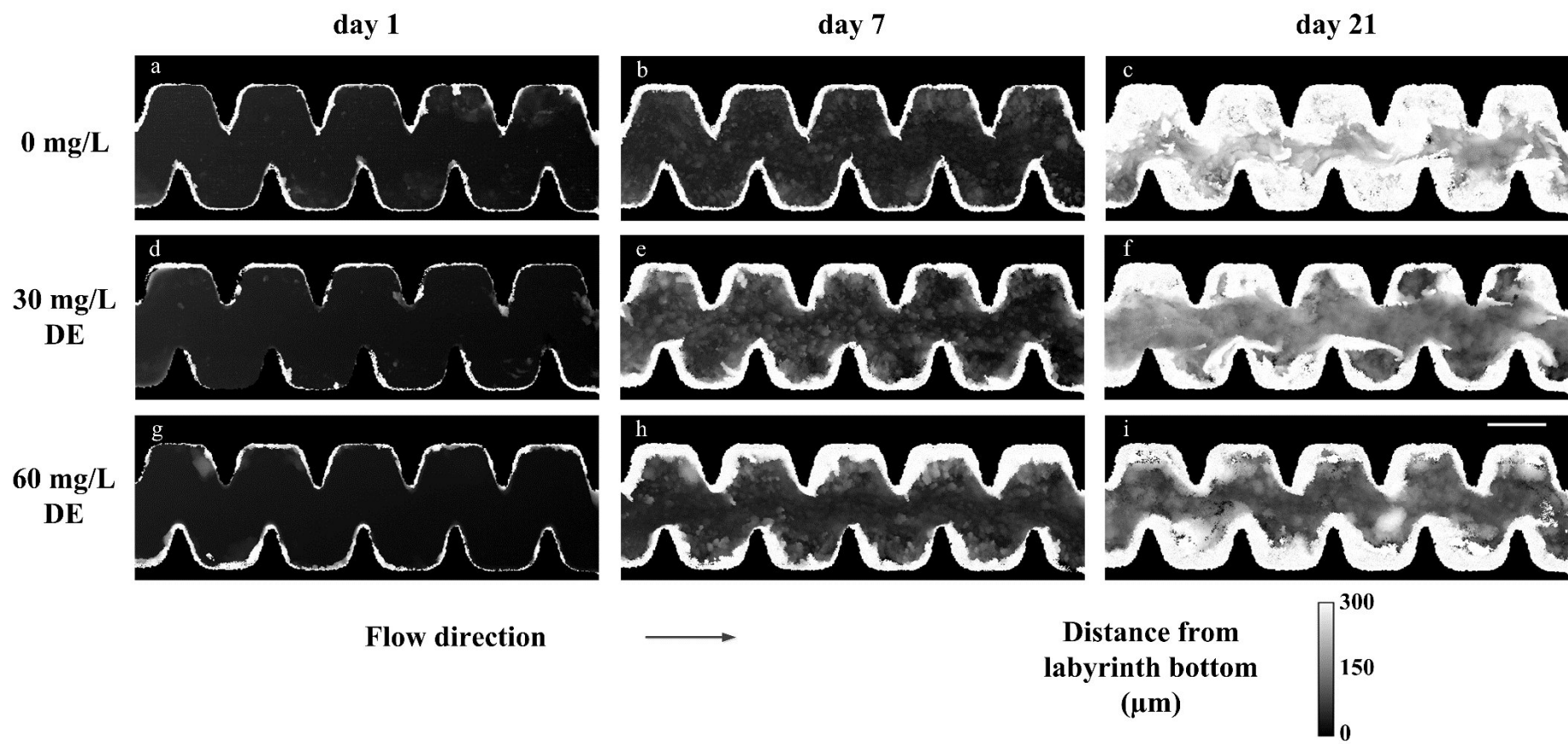
Figure 4-9. Depth-coded image showing biofilm formation in the labyrinth compartment at days 1, 7, and 21 in Exp. DI. The scale bar in 4-9(f) equals 0.8 mm. The calibration bar equals the distance of the detected biofilm signal from the bottom of the labyrinth compartment.

were present in the cultivation media (Figure 4-9(c) and (h)). Walls and corners of the labyrinth structure are regions with lower flow velocities and shear stresses compared to the center of the channel (Al-Muhammad et al., 2016; Wei et al., 2006). Inorganic particles, which have a larger diameter as well as a higher density compared to bacteria (densities of DE and MMT were $1.95 - 2.3$ g/cm^3 and $2.0 - 2.7$ g/cm^3, respectively), may collide with the walls due to higher momentum and settled down there. Inorganic particles are also reported to accumulate in biofilm matrix due to adhesion property provided by the EPS (Dreszer et al., 2013; Flemming, 2002). At day 21, it was observed that biofilm coverage was high when no inorganic particles were present in the cultivation media (Figure 4-9(c)). The formed biofilm only allowed water flow through the narrow middle channel of the labyrinth compartment in Figure 4-9(c).

Moreover, the OCT images give an overview of the biofilm formed/accumulated in the labyrinth channel and its distribution. However it was not possible to distinguish between bacteria and inorganic particles in the biofilm matrix. Although DE particles used in this study had a median size of 37 µm, and the voxel size of the OCT images was 10 µm × 10 µm in x and y directions, DE particles were not reliably identified in the biofilm by means of OCT. This is probably due to the fact that the details of the honeycomb structure of DE particles need a higher resolution than 10 µm × 10 µm. Moreover, DE particles are more reflective than bacteria, which leads to scattering of light and therefore signal loss.

4.3.1.2 Biofilm formation with DE and MMT (Exp. DI)

Three-dimensional OCT datasets were processed and biofilm volumetric coverage (Cov) in the labyrinth compartment was quantified and displayed in Figure 4-10. Biofilm formation curves were linearly fitted till the day with the first maximal volumetric coverage. The slope was described as biofilm formation rate (u_c) in %/d, describing the variation of biofilm volume over time in relation to the channel volume.
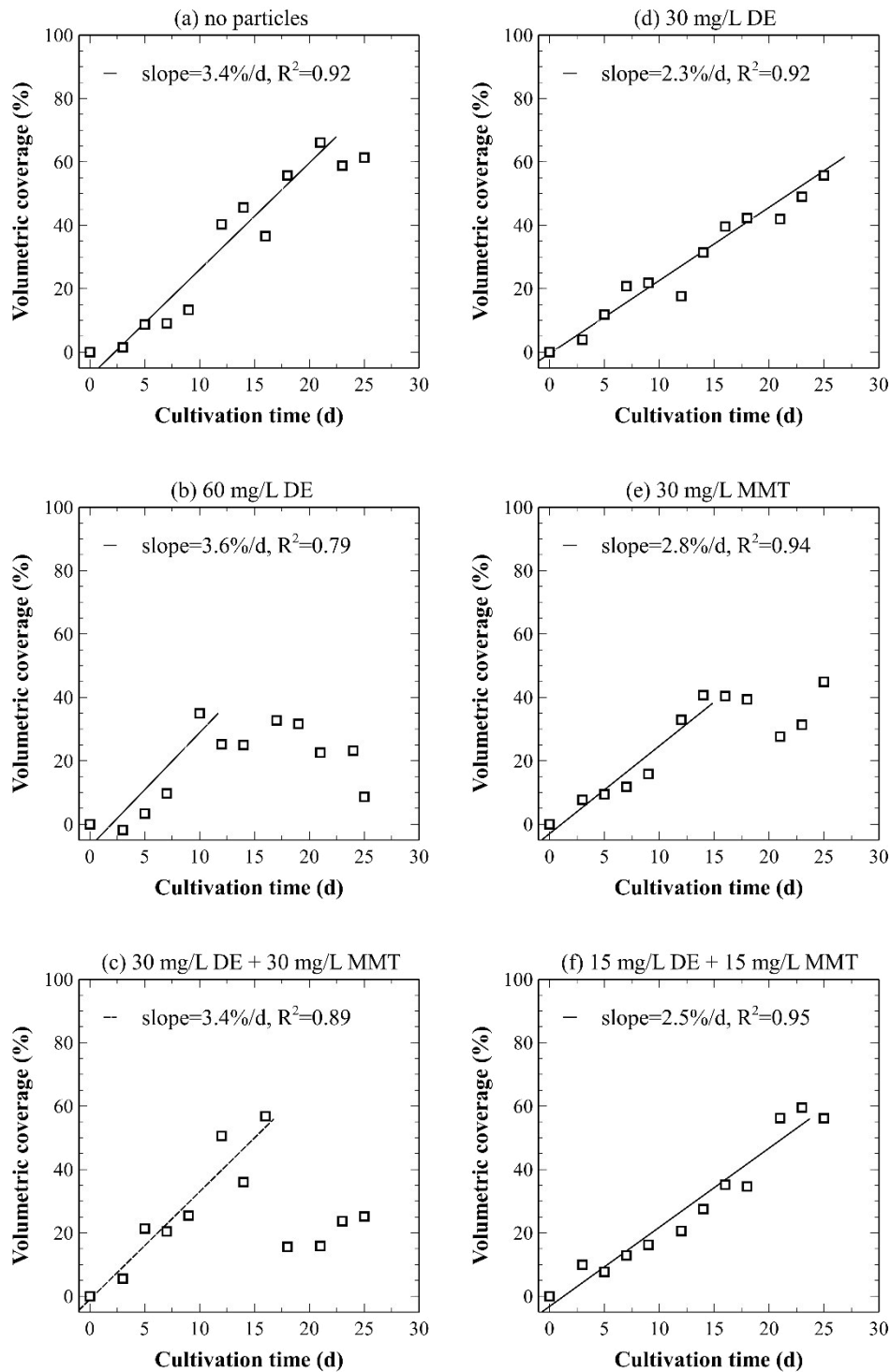
Figure 4-10. Biofilm volumetric coverage in the labyrinth compartment when cultivated with (a) no particles, (b) 60 mg/L DE, (c) 30 mg/L DE + 30 mg/L MMT, (d) 30 mg/L DE, (e) 30 mg/L MMT, and (f) 15 mg/L DE + 15 mg/L MMT (n = 1).

Figure 4-10(a) demonstrates that biofilm cultivated without particles grew steadily till the zigzag channel was filled by 66 % (day 21) with a formation rate (u_c) of 3.4 %/d. When cultivated with 60 mg/L TSS (Figure 4-10(b) and (c)), the biofilm formation rates were similar compared to without particles (u_c = 3.4 – 3.6 %/d) before the volumetric coverage reached 40 – 60 %. Afterwards, the volumetric coverages fluctuated indicating occurrence of detachment events. Due to frequent detachment, the MFDs ended up with lower volumetric coverages on day 24 when cultivated with 60 mg/L TSS (60 mg/L DE or 30 mg/L DE + 30 mg/L MMT). Moreover, biofilm cultivated with 30 mg/L DE (u_c = 2.3 %/d), 30 mg/L MMT (u_c = 2.8 %), and 15 mg/L DE + 15 mg/L MMT (u_c = 2.5 %/d) had relative lower formation rates compared to without particles or with 60 mg/L TSS (u_c = 3.4 – 3.6 %/d).

Since only one replicate was performed in each DE or MMT concentrations, Exp. DI served as a pre-experiment. The following results were observed and need to be further confirmed: (1) 60 mg/L inorganic particles caused frequent detachment during the cultivation phase, (2) 30 mg/L TSS showed a lower biofilm formation rate, before the biofilm reached the maximal coverage, and (3) it was not possible to differentiate the effect of MMT and DE based on the number of experiments performed. Based on the results from Exp. DI, only DE particles were applied in Exp. DII to confirm the first two observed phenomena.

4.3.1.3 Biofilm formation with DE (Exp. DII)

In Exp. DII, biofilm formation in the labyrinth compartment of MFDs was investigated using DE concentrations of 0, 10, 30, and 60 mg/L. Figure 4-11 demonstrates the volumetric coverage over time. It can be seen that biofilms cultivated with 0 and 10 mg/L DE grew steady until a volumetric coverage of 70 % was reached at day 15. The coverage remained stable till the end of the experiment (day 27). Biofilms cultivated with 30 and 60 mg/L DE experienced detachment events after 15 days, which can be seen from the decreasing biofilm volumetric coverage, and the large error bars in Figure 4-11(c)-(d). This suggests that 10 mg/L DE did not have a remarkable negative impact on the biofilm formation in the labyrinth of MFDs during normal cultivation conditions. Whereas DE concentrations of 30 and 60 mg/L influenced the growth by introducing detachment events.
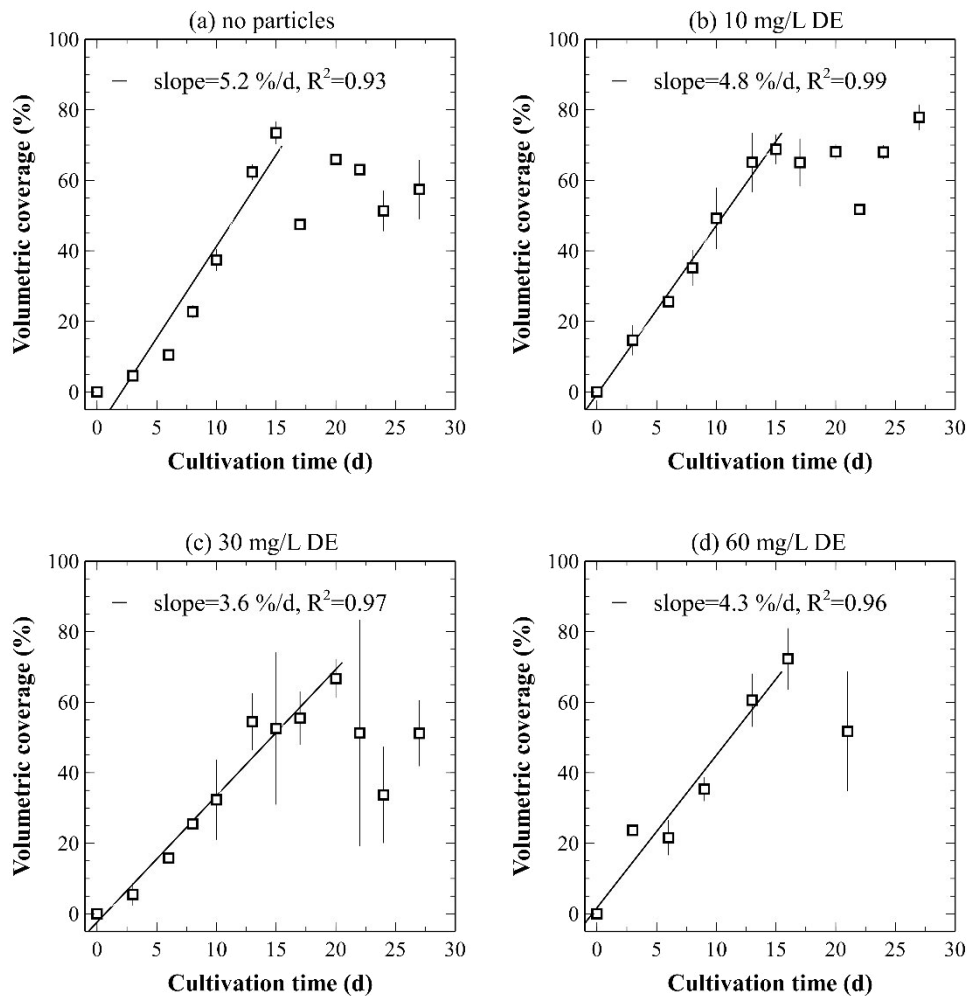
Figure 4-11. Biofilm volumetric coverage in the labyrinth compartment when cultivated with (a) no particles, (b) 10 mg/L DE, (c) 30 mg/L DE, and (d) 60 mg/L DE. Error bars represent standard error of the mean (n = 2).

Average biofilm volumetric coverage in the fluctuation phase

Figure 4-12 shows the average biofilm volumetric coverage in the fluctuation phase. The fluctuation phase was roughly assumed to start after the highest volumetric coverage and last until the end of the experiment. In general, the biofilm coverage in the fluctuation phase was the highest (69 %) with 10 mg/L DE in the cultivation medium. When the DE concentration further increased to 30 and 60 mg/L, detachment events occurred and the volumetric coverage decreased. There was 5 − 12 % less biofilm in the labyrinth when cultivated with 30 and 60 mg/L DE compared to 0 mg/L particles. Moreover, these results comply with the observations from Exp. DI.

It is also observed that the error bars in Figure 4-12 are very large, when TSS equals 30 and 60 mg/L. This implies that the two replicates were quite different and detachment happened statistically. On the other hand, the fluctuation of the volumetric coverages indicates occurrence of sloughing events in the MFDs. It seems that biofilms cultivated with 30 or 60 mg/L DE were not as cohesive as biofilms without particles. In the field, the clogged drippers were observed to recover in the pilot scale experiment (Exp. B) from this work and from Duran-Ros et al. (2009), which also used TWW for irrigation. Recovery of clogged dripper is due to biofilm detachment in the dripper geometry. In order to facilitate biofilm detachment in the drippers and maintain the performance of drip irrigation systems, it is of research interest to study the influence of inorganic particles on biofilm stability.
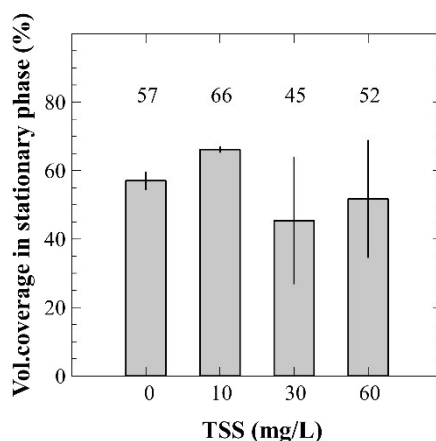
Figure 4-12. Average biofilm volumetric coverage in the fluctuation phase when cultivated with different DE concentrations. Error bars represent standard error of the mean (n = 2).

Biofilm formation rate (DE)

The average biofilm formation rates in Exp. DII in the labyrinth compartment were calculated and listed in Table 4-4. It can be seen that the biofilm formation rates slightly decreased from 5.2 %/d to 3.6 %/d when the DE concentration increased from 0 to 30 mg/L. But the formation rate increased from 3.6 %/d to 4.3 %/d when the DE concentration further set to 60 mg/L. This trend agrees with the results from Exp. DI.

Table 4-4. Biofilm formation rates (u_C) in Exp. DI and DII.

Particle concentration	Exp. DI (n=1)	Exp. DII (n=2)
0 mg/L DE	3.4 %/d	5.2 %/d
10 mg/L DE	--	4.8 %/d
30 mg/L DE	2.3 %/d	3.6 %/d
60 mg/L DE	3.6 %/d	4.3 %/d

Substrate and nutrient concentrations in Exp. DII were the same independent of particle addition. Therefore, the biofilm formation due to bacterial growth was expected to be similar. Lower biofilm formation rates (before reaching the first maximal volumetric coverage) can be explained as continuous/constant biofilm erosion (small amount of biofilm detachment), probably due to less cohesive biofilms formed with particles. Erosion refers to the continuous loss of single cells or small cell clumps due to physical forces or cell cycle mediated events (Allison et al., 1990; Walter et al., 2013). Except for biofilm erosion, it is not clear if the particles in the cultivation media had an abrasion effect on biofilm. Abrasion is the removal of biofilm due to the collision of particles with the biofilm surface. Derlon et al. (2008) investigated the erosion effect of polypropylene particles (density = 970 g/L, diameter = 3.15 – 4 mm) on biofilms. However, the abrasion effect of small inorganic particles hasn't been investigated yet. To be mentioned, that biofilms cultivated with 60 mg/L TSS (u_C = 4.3 %/d) had a higher formation rate than cultivated with 30 mg/L TSS (u_C = 3.6 %/d). Possible reason can be the settlement of the particles inside the MFDs which contributed to the biofilm formation rates.

To sum up, the possible processes contributing to the variation of biofilm volume (when cultivated with inorganic particles) are biofilm growth, detachment, and particle deposition. Particles in the cultivation media might contribute to both negative and positive effects on biofilm formation. The negative aspect was reflected by the formation of a less cohesive biofilm, which experienced sloughing or erosion. The positive effect on the increase of biofilm volume lies in the particle deposition.

The biofilm formation rates in Exp. DII were generally 1.4 times higher than Exp. DI (Table 4-4). Possible reasons can be that the tanks for the cultivation media were thoroughly washed 3 times per week in Exp. DII, and the tanks were thoroughly washed once per two weeks in Exp. DI.

4.3.1.4 Flushing experiment

To investigate the biofilm stability, biofilm flushing experiments were carried out in Exp. DII. Biofilm detachment was forced by increasing the flowrate to 2 L/h, 3 L/h and 4L/h, each with 15 min (Figure 4-3).

Figure 4-13 shows the relative biofilm volumetric coverage during the flushing experiments. The biofilm detachment was on average 18 % when the flowrate was increased from 1 to 2 L/h. When the flowrate was further increased to 3 and 4 L/h, additional 23 % and 13 % of the relative biofilm volume detached, respectively. Flushing effects have been studied before. Stoodley et al. (2002) observed an increasing biofilm detachment when the shear stress increased to 2.5 – 3 times of that during cultivation. Coufort et al., (2007) reported that approximately 50 – 60 % of the biomass detached at three-fold shear stress, and a loss of 20 % when the shear stress further rose to 20 times of the original shear stress. This study also observed highest biomass loss (23 %) when the flowrate increased to 3 L/h (1 L/h during cultivation), which complies with the results from the literature. However, on average 46 % biofilm was left after the flushing experiment. Most of the detached biomass belonged to the fragile top layer of the biofilm. It is reported that the top layer, which represents 60 % of the biofilm mass, is very fragile and can be easily detached. The basal layer, which represents 20% of the biofilm mass, is very cohesive and can resist high shear stresses. Between these two layers, a middle layer of intermediary cohesion represents 20% of the initial biofilm mass (Coufort et al., 2007; Derlon et al., 2008; Paul et al., 2012).

Surprisingly, biofilms cultivated with 60 mg/L DE experienced the least detachment (39 %), followed by 0 and 30 mg/L DE (Table 4-5). This seems to be contradictory to the results revealed by Figure 4-10 and Figure 4-11, that biofilms cultivated with 30 and 60 mg/L DE faced frequent detachment during normal cultivation. On the other hand, the results also suggests that biofilms cultivated with 10 mg/L was stable during the cultivation period, but they were not stable at a sudden rose of shear stress (two- to four-fold increase). To confirm this theory, more shear stress induces biofilm deformation and detachment experiments were conducted in flow cells. These allowed to study the biofilm deformation under changing shear stresses (section 4.3.2).
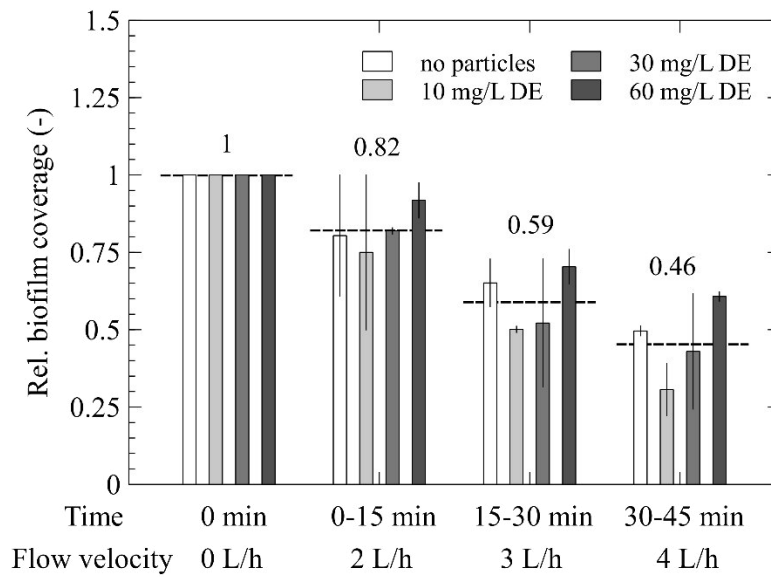
Figure 4-13. Relative biofilm detachment after the flowrate was increased from 1 L/h to 2 L/h (15 min), 3 L/h (15 min), and 4 L/h (15 min). The dotted lines and the numbers above the dotted lines indicate the average values of the four DE concentrations. Error bars represent standard error of the mean (n = 2).

Table 4-5. Relative biofilm detachment in the flushing experiments (MFD).

Rel. biofilm detachment (%)	0 mg/L DE	10 mg/L DE	30 mg/L DE	60 mg/L DE
MFD Flushing (after 45 min)	50 %	69 %	57 %	39 %

4.3.1.5 Chlorine treatment and flushing experiment

To investigate the effect of chlorine treatment, the MFDs in Exp. DII were exposed to sodium hypochlorite (free chlorine = 50 mg/L) for 1 hour. On average 24 % of the biofilm detached after 1 hour of chlorine treatment (Figure 4-14). In the field, the free chlorine concentration used in chlorine treatments is recommended to be higher than 1 mg/L at the end of the pipe. Thus the concentration used in this experiment was higher than the field recommendation. However, an average of 24 % biofilm detachment was lower than expected. This might be due to the limited chlorine penetration in the biofilm. de Beer et al. (1994) developed a chlorine microelectrode and found that chlorine concentrations measured in the biofilms (thickness $150 - 200\,\mu m$) did not reach $> 20\,\%$ of the concentration in the bulk liquid. Thicker

biofilms are reported to present a barrier to the penetration of antimicrobial agents (Cochran et al., 2000; Mah and O'Toole, 2001).

Although only one fourth of the total biofilm detached after 1 hour chlorine treatment, the biofilm structure was weakened by hypochlorite and another 50 % biofilm detached after 45 min flushing experiments. The flowrates in the flushing experiment here was 15 min at 2, 3 and 4 L/h, respectively, which was the same as in the above mentioned flushing experiment. At the end, there was only on average 25 % biofilm left in the labyrinth of MFDs. This indicates that with the help of chlorine treatment, flushing was able to remove more biofilm than flushing experiment alone (averagely 46 % biofilm was left in the labyrinth after the flushing experiment, Figure 4-13), which implies that chlorine treatment and flushing together have a better cleaning effect. Mathieu et al. (2014) also reported that the cohesiveness of drinking water biofilm was weakened under chlorination stress. This throws light on the treatment of drip irrigation systems in the fields, that chlorine treatment and flushing should be combined in order to have a better biofilm removal effect. Moreover, the amount of remaining biofilm after 45 min flushing (Figure 4-14) was lowest with no particles in the cultivation medium. It suggests that addition of DE in the cultivation media limits the susceptibility of biofilms to hypochlorite (Figure 4-14). Similarly, Srinivasan et al. (1995) reported the presence of kaolin and calcium carbonate particles in the mono- and binary population biofilms (*Pseudomonas aeruginosa* and *Klebsiella pneumoniae*) reduced disinfection efficacy.
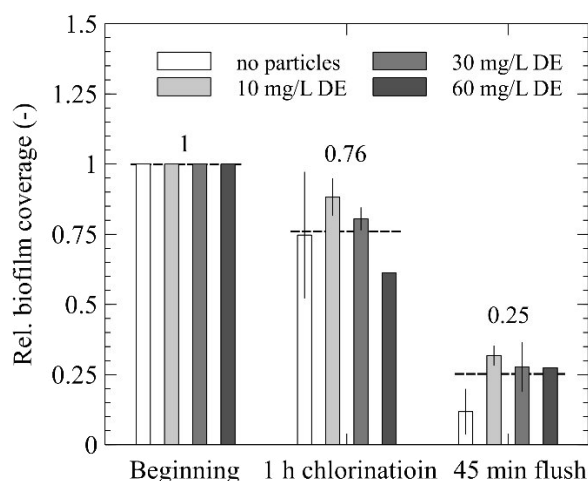
Figure 4-14. Relative biofilm detachment after the 1 h chlorine treatment and 45 min flushing. Flowrates during flushing were 15 min at 2 L/h, 15 min at 3 L/h and 15 min at 4 L/h as described in Figure 4-3. The dotted lines and the numbers above the dotted lines indicate the average values of the four DE concentrations. Error bars represent standard error of the mean (n = 2).

4.3.2 Biofilm mechanical properties

To study the biofilm mechanical properties, especially compressibility, flow cells (inner flow channel: 2 mm × 1 mm × 160 mm) were used to cultivate biofilms with 0, 10, 30, and 60 mg/L DE. Biofilm deformation under changing flowrates (shear stresses) was investigated when biofilm thickness was > 100 µm.

In shear stress induced deformation experiments, the flow velocity was increased, so that the shear stress changed from 0 Pa to 3.6 Pa in 9 steps, and then back to 0 Pa step by step. OCT images (2 mm × 2 mm × 1 mm) were acquired in each step (Blauert et al., 2015). Based on the three-dimensional datasets, the biofilm thickness and volumetric coverage were calculated. Biofilm thickness was calculated only for biofilms formed in the center the bottom flow channel (0.8 mm × 2 mm, Figure 4-7, page 53). The biofilm volumetric coverage, on the other hand, accounted for biofilm in the whole three-dimensional imaging region (2 mm × 2 mm × 1 mm).

Biofilm compressibility

Compressibility is a measure of the relative volume change of fluid or solid as a response to pressure (or mean stress). Casey (2007) proposed compression (compaction) as a mechanism contributing to the structural realignment to form a higher density, lower porosity biofilm under high shear force. In this study it was assumed that the bottom surface (area) of biofilm did not change during the shear induced experiments and only the biofilm thickness changed. Therefore the biofilm compressibility was calculated based on the change (drop) of biofilm thickness at increasing shear stresses.

For the calculation of compressibility, only regions without biofilm detachment were selected. Figure 4-15 shows the correlation between mean biofilm thickness and wall shear stress during the shear stress induced experiments when biofilms were cultivated with 0, 30, and 60 mg/L DE. There is no data for biofilms cultivated with 10 mg/L DE due to massive biofilm detachment, and no proper region could be selected for calculation of compressibility. Biofilm compressibility (1/Pa) was defined as -1 times the slope (change of biofilm thickness over shear stress) in Equation 4-4.

$$\beta = -\frac{1}{L_{f0}}\frac{dL_f}{d\tau_w} \ [1/Pa] \tag{4-4}$$

Here β is the biofilm compressibility (1/Pa), τ_w is the wall shear stress (Pa), L_f is the biofilm thickness (µm), and L_{f0} is the initial biofilm thickness (µm).

The compressibilities of biofilms cultivated with 0, 30, and 60 mg/L DE were 0.01, 0.06, and 0.08 (1/Pa), respectively. This means that biofilm thickness changed 8 % under 1 Pa of wall shear stress when biofilm was cultivated with 60 mg/L DE, while the thickness variation was only 1 % when cultivated with 0 mg/L DE. It thus suggests that biofilms formed with higher DE concentrations were more compressible than biofilms cultivated without inorganic particles.
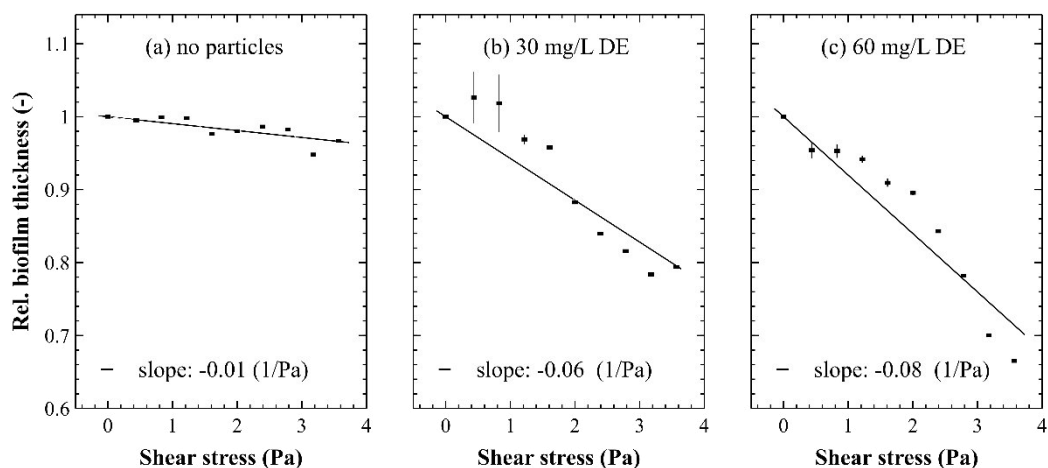
Figure 4-15. Biofilm compressibility when biofilms were cultivated with (a) no particles, (b) 30 mg/L DE, and (c) 60 mg/L DE. Error bars represent standard error of the mean (n = 2).

Comparing the biofilm compressibility in literature is difficult, since conclusive studies are missing. In 2001, Körstgens et al. performed compression experiments, but they studied the biofilm mechanical stability and viscoelastic properties instead of compressibility. Biofilm compression was further described by Paul et al. (2012). They reported that compression prevailed for the basal layers of the biofilms and detachment prevailed for the upper part. Dreszer et al. (2014), Derlon et al. (2016), and Valladares Linares et al. (2016) observed biofilm compression (compaction) during membrane filtration processes by means of OCT. Moreover, Blauert et al. (2015) visualized biofilm compression on solid surface at elevated shear stresses using OCT. But they did not give a number of the biofilm compressibility. The results above clearly show the importance of biofilm compressibility as an important parameter for the biofilm mechanical properties. The compressibility seems to better correlate with the concentration of added particles than the other measured values like growth rate, volumetric coverage or detachment.

As mentioned, biofilm compression (compaction) is a process which reduces biofilm porosity (Casey, 2007). The porosity calculated in this study was based on the binarized OCT images, e.g. in Figure 4-16. The black pixels under the bulk/biofilm interface were recognized as pores/voids in the biofilm matrix. Therefore, the porosities of the biofilms (from two-dimensional cross sections without flow) shown in Figure 4-16, were 32 % (0 mg/L DE) and 30 % (60 mg/L DE), respectively. However, the high reflection of incorporated inorganic particles does not allow qualitative determination of porosity, either during the growth or during the compression process. For instance, Figure 4-16(b) shows that the biofilm formed with 60 mg/L DE had a high reflective upper layer. The inorganic particles also hinder light penetration during the imaging process and lead to an underestimation of the biofilm formed directly beneath the particles. Nevertheless, decrease of biofilm porosities has been observed by Blauert et al. (2015) during compression process.
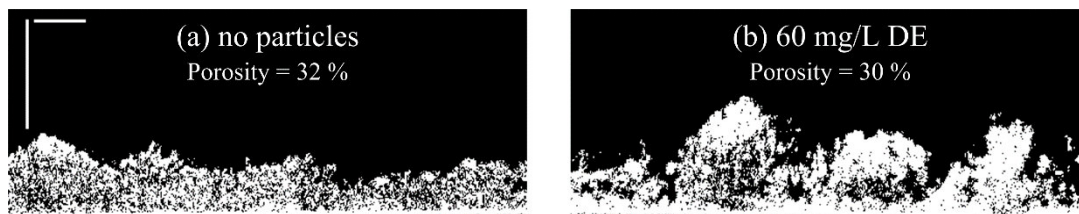
Figure 4-16. OCT images of flow cell cross-sections visualized without flow. Horizontal and vertical scale bars = 200 µm. During cultivation flow direction was from left to right.

There are several studies investigating biofilm mechanical properties with inorganic particles in the membrane filtration field. Chomiak et al. (2014) reported that diatomaceous earth at a concentration of 300 mg/L increased biofilm heterogeneity and enhanced permeate flux in the ultrafiltration. Moreover, particles have been added to the activated sludge in the membrane bioreactors to increase its filterability. The particles which have been studied are mainly activated carbon (Jamal Khan et al., 2012; Lesage et al., 2008), or colloidal particles such as latex or melamine sub-micron beads (Loulergue et al., 2014; Teychene et al., 2011). It is reported that particles increased the permeate flux and cake reversibility (less irreversible fouling). These studies reported that particles changed the biocake structure and made it less compressible (Jamal Khan et al., 2012; Lesage et al., 2008) and less resistant (Jamal Khan et al., 2012; Lesage et al., 2008; Loulergue et al., 2014). However, one need to remember that the compressibility and resistance in membrane filtration are differently defined compared to what has been studied here. In membrane research, the cake resistant is the hydraulic resistance which attributes to the overall transmembrane resistance. And the cake

compressibility is a measure to quantify the correlation of cake resistance and transmembrane pressure. Compared to biofilms formed on solid surface, the formation of biocake in membrane systems is additional due to particle deposition by viscous drag force. In this work, the biofilm shear resistance and the compressibility were investigated under wall shear stresses instead of filtration. Therefore, the conclusions from the membrane studies about compressibility and resistant are not easily comparable to this work.

Biofilm thickness variation

In Figure 4-15 (biofilm compressibility) the biofilm thickness at regions without detachment is shown. Figure 4-17 shows the overall biofilm thickness variation at the bottom of the flow cell including compression and detachment. The white markers in Figure 4-17 indicate the change of biofilm thickness when the shear stress increased and the black markers show how the biofilm relaxed when the shear stress decreased from 3.6 to 0 Pa.

It can be seen that biofilms cultivated without particles (Figure 4-17(a)) were quite stable in the shear induced deformation experiments. The biofilm thickness did not change a lot when shear stress increased, which implies that biofilms were not compressed and the detachment was low. With 10 mg/L DE in the cultivation media, the biofilm thickness remained unchanged when the wall shear stress was below 1.2 Pa. When the wall shear stress reached 1.2 Pa, the biofilm thickness decreased indicating compression as well as detachment. Later, when the shear stress reached 2.8 Pa, the biofilm thickness dropped dramatically to half of the original biofilm thickness. This sudden drop of biofilm thickness indicates detachment of large pieces of biofilms (sloughing). Compared to biofilms cultivated without particles, biofilms cultivated with 10 mg/L TSS seemed to have a tendency to detach in large pieces.
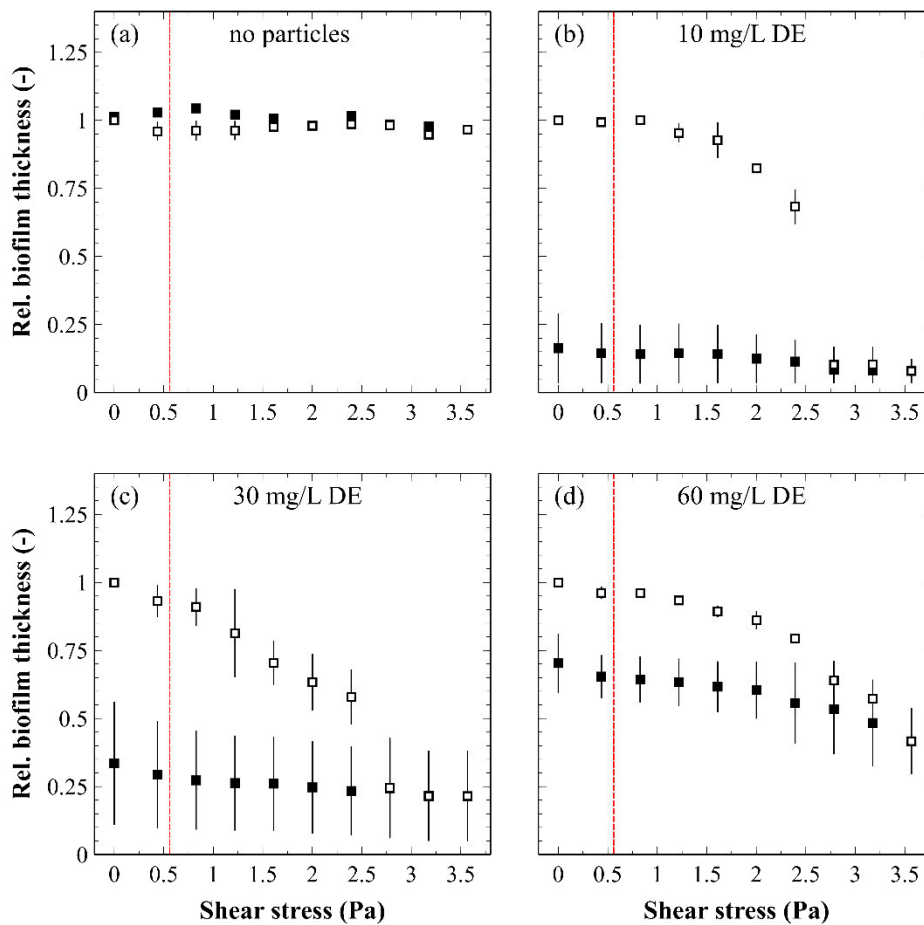
Figure 4-17. Change of relative biofilm thickness when biofilms were cultivated with (a) no particles, (b) 10 mg/L DE, (c) 30 mg/L DE, and (d) 60 mg/L DE. Error bars represent standard error of the mean (n = 2). The white markers indicate the change of biofilm thickness when the shear stress increased and the black markers show how the biofilm relaxed when the shear stress decreased from 3.6 to 0 Pa. Red dotted lines indicate the shear stress during biofilm cultivation.

For biofilms cultivated with 30 mg/L, the biofilm thickness decreased gradually. The large error bars in Figure 4-17(c) (30 mg/L DE) suggest that the biofilm thickness varied a lot between the two replicates. One replicate encountered gradual detachment/compression, and the biofilm thickness of the other replicate did not change until the shear stress was high enough to trigger a sloughing event. Lastly, for biofilms cultivated with 60 mg/L DE, the thickness decreased overall gradually with lower error bar. This indicates that the biofilm cultivated with 60 mg/L DE just encountered small detachment when the wall shear stress increased from 0 to 3.6 Pa.

Figure 4-17 also revealed that the biofilm relaxed when the shear stress decreased from 3.6 Pa to 0 Pa. Relaxation is the opposite of compression, defined as decrease in biofilm density and increase in porosity, resulting in a rise of thickness (Valladares Linares et al., 2016). It can be seen that the biofilm cultivated without particles displayed a slightly fluctuating biofilm thickness. When there was more DE particles in the cultivation media (i.e. 60 mg/L) the biofilm thickness increased by 20 % when the shear stress decreased from 3.6 Pa to 0 Pa. This results also confirm that the compressibility increased when there were more DE particles in the cultivation media.

It was discussed before that biofilms, cultivated with 60 mg/L DE, show the least detachment in the MFD flushing experiments (section 4.3.1.4, page 65 – 66). This might be explained by the biofilm compressibility. The biofilm structure is supposed to be stabilized when biofilm is compressed. The overall results imply that addition of particles affects biofilm stability in two different ways. On the one hand, addition of particles (more than 30 mg/L) made the biofilm structure unstable under normal cultivation conditions (relative low shear stresses). On the other hand, biofilm compressibility increased and biofilm structure was stabilized under increasing shear stresses. For biofilms cultivated at 60 mg/L, biofilm detachment occurred statistically during the cultivation phase. However, the biofilms (at 60 mg/L) were compacted at increasing shear stresses (flushing and shear stress induced experiments) due to the high biofilm compressibility which prevented sloughing events at high shear stresses. Moreover, biofilm cultivated with 10 mg/L DE was stable under lower shear stress during normal cultivation conditions in the MFDs, but it experienced sloughing events in both MFD flushing experiments and the shear induced deformation (compressibility) experiments. The incorporation of a small amount of inorganic particles (10 mg/L DE) seems to have a low impact on compressibility. The microorganisms grew compact with low concentration of particles and thereby form more rigid biofilm structure which might be more susceptible to sloughing.

Furthermore, the biofilm detachment between cultivation and the flushing experiments (3×15 min) are different due to the biofilm viscoelastic behavior. Stoodley et al. (2002) found that the biofilms were viscoelastic fluids which behaved like elastic solids over periods of a few seconds but like linear viscous fluids over longer times. Shaw et al. (2004) further determined that the transition time from elastic to viscoelastic deformation is approximately 18 min over a wide sample of biofilms. This means that during the flushing experiments, the biofilms behaved more like elastic solids, while during the cultivation more like viscoelastic fluid. Therefore biofilms responded differently in the cultivation and flushing experiments, which also leaded to different detachment behavior.

Biofilm detachment

The amount of biofilm detachment was calculated as the difference of biofilm volume before and after the shear stress induced experiment as shown in Equation 4-5. The volumetric coverage used here represent the biofilm coverage in the 2 mm × 2 mm × 1 mm volume.

$$detachment = \frac{Cov_{after} - Cov_{before}}{Cov_{before}} \times 100 \ [\%] \qquad (4\text{-}5)$$

Here Cov_{before} and Cov_{after} represent the biofilm volumetric coverage before and after the shear stress induced experiments.

Table 4-6 lists the amount of detached biofilm cultivated with four different TSS concentrations. It shows that cultivation without particles produced biofilms which were quite stable. The amount of detached biofilm volume was on average 10 %. When particles were integrated in the biofilm, the amount of biofilm detachment increased to 17 – 37 %. Furthermore, results shows that biofilms cultivated with 60 mg/L experienced the second lowest detachment. This result is consistent with the flushing experiments performed in the MFDs. As discussed before, the biofilm was more compressible when more DE particles were incorporated in the biofilm matrix. This makes the biofilm structure stable at higher shear stresses.

Table 4-6. Relative biofilm detachment after the stress induced experiments (n = 2).

TSS	Biofilm detachment (after 36 min experiment)
0 mg/L	10 %
10 mg/L	37 %
30 mg/L	27 %
60 mg/L	17 %

4.4   Summary

In this chapter, the influence of inorganic particles on biofilm formation in the dripper structure and the biofilm compressibility was studied. The achieved results justify the following conclusions:

- Biofilms cultivated with 30 and 60 mg/L DE encountered statistic detachment in the MFDs and ended up with a lower volumetric coverage compared to biofilms cultivated with 0 and 10 mg/L DE.

- The biofilm compressibility is higher when more DE particles are dosed in the cultivation media.

- Biofilm detachment in the flushing experiment (MFDs) and shear induced experiment (straight flow cells) revealed that biofilm detachment was the lowest when the DE concentration was 0 and 60 mg/L. The low detachment when cultivated with 60 mg/L DE was attributed to high biofilm compressibility. Biofilm compressibility proved to be a good parameter to characterize biofilm stability.

- Combination of chlorine treatment and flushing demonstrated a higher biofilm removal effect compared to flushing or chlorine treatment alone.

Chapter 5

Conclusions and outlook

Drip irrigation systems can increase water use efficiency, minimize salinity hazard to plants, improve chemical application, decrease energy requirements and improve cultural practices. Due to the small flow channel in the dripper and utilization of treated wastewater (TWW) in (semi-) arid regions, fouling occurs and drippers block. This work sets out to examine the fouling driving factors in drip irrigation systems. Experiments in both drip irrigation systems and microfluidic devices (MFDs) which mimic the inner dripper geometry were performed to study the influence of water quality, daily temperature cycle and particles on the biofilm development and occurrence of dripper blockage. Specially, biofilms were cultivated in straight flow cells and biofilm mechanical properties (stability and compressibility) when cultivated with inorganic particles were investigated. The results will be high-lighted briefly in the following.

To explore the impact of water quality on biofilm formation, real TWW and synthetic wastewater (SynWW) were utilized in both drip irrigation systems and MFD experiments. Results from both drip irrigation systems and MFD experiments proposed that better water quality (low BOD_5) can delay the occurrence of dripper blockage. Accumulation of inorganic particles, on the other side, suggests to mitigate the fouling problem in the drip irrigation systems.

The biofilm structure in the drippers was not yet visualized at the mesoscale and non-invasively. In this work 3D printed MFDs were used to mimic the inner dripper geometry and optical coherence tomography (OCT) was applied to follow biofilm formation inside the

MFDs *in-situ* and non-invasively. Three-dimensional OCT datasets unveil the biofilm distribution (e.g. initial biofilm attachment, regions favor biofilm formation) and biofilm structure (e.g. streamer formation) in the dripper geometry. Both biofilm distribution and structure were influenced by fluid dynamics.

Discharge rates of the MFDs were controlled during the cultivation period in MFDs. It is revealed that biofilm coverage in the labyrinth of up to 60 % did not reduce the discharge rate, whereas further increasing coverage to 80 % reduced the discharge rate by 50 % in this experimental setup. It therefore suggests that the amount of biomass in the drippers maybe underestimated by measuring discharge rate alone in the field.

TWW often contains inorganic particles. In order to evaluate the fouling potential of TWW in the drip irrigation systems, the influence of inorganic particles on biofilm development in dripper structure requires a thorough understanding. In this work, Diatomaceous earth (DE) and montmorillonite (MMT) were dosed in the cultivation media. Results showed that (DE/MMT) often encountered statistic detachment in the MFDs during cultivation. Therefore biofilms cultivated with high load of TSS ended up with lower biofilm volumetric coverages compared to that cultivated with 0 or 10 mg/L TSS.

Further studies of biofilm material property were performed in straight flow cells. An important finding from this work is that biofilms cultivated with a high load of inorganic particles (60 mg/L DE) showed a higher biofilm compressibility compared to biofilms cultivated without particles. The addition of particles during biofilm cultivation affected biofilm stability in two ways. On the one hand, the biofilm structure became unstable under 30 or 60 mg/L particles and experienced more detachment events during normal cultivation periods. On the other hand, biofilms became more compressible when cultivated with certain amount of particles. The biofilm structure is supposed to be stabilized when it gets compressed at increasing shear stresses. Therefore less biofilm detached during the flushing experiments (at increasing shear stresses) when cultivated with 60 mg/L DE.

Understanding the effect of a daily temperature cycle till 50 °C in arid and semi-arid regions is important when the fouling driving factors in drip irrigation systems are to be characterized. Comparing biofilm formed in ambient (20 °C) and temperature cycle, daily temperature cycle had a negative impact on biofilm formation. The biofilm formation rate was inhibited in daily temperature cycle independent of the cultivation medium used. However, fouling still occurs in arid and semi-arid regions when the drip irrigation is performed in the daily temperature cycle. Possible reason can be the accumulation of organic and inorganic particles and different types of microorganisms in the field. In this work, the

TSS concentration in the TWW was lower than 10 mg/L, while in the field, the TSS concentration in the TWW can be higher than 100 mg/L

The presented results provide extended knowledge about biofilm growth and dripper blockage which are not accessible non-invasively in drip irrigation systems. OCT datasets imply that biofilm formation is governed by the hydrodynamic conditions. High shear stress in the labyrinth compartment can provide microorganisms a thinner concentration boundary layer and thus a better substrate availability. But it doesn't assist the initial bacterial attachment (longer lag phase probable) and can cause more biofilm detachment. Further simulation studies concerning the hydrodynamic conditions in the MFD with OCT datasets as biofilm structure template will help to better understand the biofilm formation in the MFD.

Furthermore, bacteria also attach to particles in the bulk medium. Inorganic particles were spiked in the cultivation medium in several experiments in this work. The settlement of particle-associated bacteria in the flow cell depends on the physical properties of the particles (e.g. size and density). CFD simulation can provide better understanding and prediction of biofilm formation in the MFDs when particles are present in the cultivation medium.

Moreover, this work has mainly focused on the effect of DE ($dp_{0.5} = 37$ µm) on biofilm development. The effect of different particle sizes and particle types on the biofilm development and detachment was not fully investigated yet and can be incorporated in future studies. To study the biofilm detachment when cultivated with inorganic particles, the size distribution of the detached biomass and detachment rates during steady state and shear conditions are also of research interest.

Biofilm material properties may in future be linked to biofilm detachment. Understanding the biofilm material property with respect to elasticity, compressibility and brittleness will bring the knowledge of biofilm to a new level. More effort on studying the biofilm mechanical properties is necessary and the use of OCT provides the necessary tool for that.

Appendix

Supplementary information to Chapter 2

S 2-1. Temperature conditions in pilot-scale Exp. B

The temperature condition during the experimental period is illustrated in Figure S 2-1 (WeatherSpark). It was warm in 2015 in Karlsruhe and the high temperature in July and August was often above 30 °C. The temperature from 4th November to 21st November was also warmer than average temperatures, including 2 days with a high temperature above 20 °C.
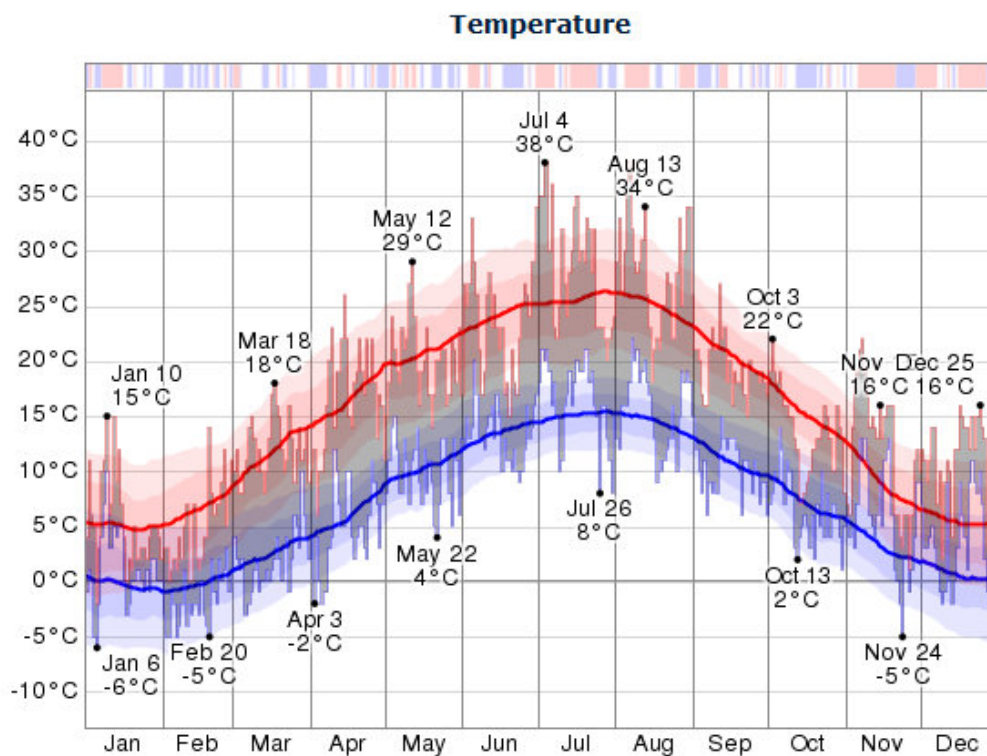
Figure S 2-1. Temperature in Karlsruhe-Baden Baden in 2015. The daily low (blue) and high (red) temperature during 2015 with the area between them shaded gray and superimposed over the corresponding averages (thick lines), and with percentile bands (inner band from 25th to 75th percentile, outer band from 10th to 90th percentile). The bar at the top of the graph is red where both the daily high and low are above average, blue where they are both below average, and white otherwise.

S 2-2. Comparison of the SynWW used in Exp. A and Israeli TWW.

Table S 2-1. Comparison of the SynWW and Israeli TWW

Parameter	Israel TWW (mg/L)	Karlsruhe SynWW (Exp. A) (mg/L)	Karlsruhe Drinking water (mg/L)
COD	58	12	-
BOD$_5$	10.5	12	-
NO$_3^-$-N	5.2	8.2	3.6
NH$_4^+$-N	3.6	4.6	<0.01
P-soluble	2.2	2.16	-
P-total	3.8	2.16	0.01
SO$_4^{2-}$	37	66	56
Na$^+$	180	174	11
Cl$^-$	260	257	14
K-soluble	27	29	2
Ca^{2+}	70	112	112
Mg^{2+}	24	10	10

References

Adin, A., Elimelech, M., 1989. Particle Filtration for Wastewater Irrigation. J. Irrig. Drain. Eng. 115, 474–487.

Adin, A., Sacks, M., 1991. Dripper-clogging factors in wasterwater irrigation. J. Irrig. Drain. Eng. 117, 813–826.

Al-Muhammad, J., Tomas, S., Anselmet, F., 2016. Modeling a weak turbulent flow in a narrow and wavy channel: case of micro-irrigation. Irrig. Sci. 34, 361–377.

Al-Nakshabandi, G.A., Saqqar, M.M., Shatanawi, M.R., Fayyad, M., Al-Horani, H., 1997. Some environmental problems associated with the use of treated wastewater for irrigation in Jordan. Agric. Water Manag. 34, 81–94.

Alimova, A., Roberts, M., Katz, A., Rudolph, E., Steiner, J.C., Alfano, R.R., Gottlieb, P., 2007. Effects of smectite clay on biofilm formation by microorganisms. Biofilms 3, 47–54.

Allison, D.G., Evans, D.J., Brown, M.R.W., Gilbert, P., 1990. Possible involvement of the divison cycle in Dispersal of Escherichia coli from biofilms. J. Bacteriol. 172, 1667–1669.

Armon, R., Gold, D., Brodsky, M., Oron, G., 2002. Surface and subsurface irrigation with effluents of different qualities and presence of Cryptosporidium oocysts in soil and on crops. Water Sci. Technol. 46, 115–122.

Bar-Yosef, B., 1999. Advances in fertigation. Adv. Agron. 65, 1–77.

Becker, N. (Ed.), 2013. Water policy in Israel: context, issues and options. Springer Science & Business Media, Dordrecht, Heidelbeg, New York, London.

Besemer, K., Hödl, I., Singer, G., Battin, T.J., 2009. Architectural differentiation reflects bacterial community structure in stream biofilms. ISME J. 3, 1318–1324.

Bielefeldt, A.R., Stensel, H.D., 1999. Evaluation of biodegradation kinetic testing methods and longterm variability in biokinetics for BTEX metabolism. Water Res. 33, 733–740.

Blauert, F., Horn, H., Wagner, M., 2015. Time-resolved biofilm deformation measurements using optical coherence tomography. Biotechnol. Bioeng. 112, 1893–1905.

Boppart, S.A., Tearney, G.J., Bouma, B.E., Southern, J.F., Brezinski, M.E., Fujimoto, J.G., 1997. Noninvasive assessment of the developing Xenopus cardiovascular system using

References

optical coherence tomography. Proc. Natl .Acad. Sci. USA 94, 4256–4261.

Boppart, S., Bouma, B., Pitris, C., Southern, J., Brezinski, M., Fujimoto, J., 1998. In vivo cellular optical coherence tomography imaging. Nat. Med. 4, 861–865.

Bouma, B.E., Tearney, G.J. (Eds.), 2001. Handbook of optical coherence tomography. CRC Press.

Boyle, J.D., Lappin-Scott, H., 2006. Quantification of the effect of flowrate on the rates of arrival and attachment to glass of Pseudomonas aeruginosa. Biofouling 22, 117–23.

Boyle, J.D., Lappin-Scott, H., 2007. The effect of flow direction and magnitude on the initial distribution of Pseudomonas aeruginosa cells attached to glass. Biofouling 23, 139–150.

Brenner, A., Shandalov, S., Messalem, R., 2000. Wastewater Reclamation for Agricultural Reuse in Israel : Trends and Experimental Results. Water. Air. Soil Pollut. 123, 167–182.

Bucks, D.A., Nakayama, F.S., Gilbert, R.G., 1979. Trickle irrigation water quality and preventive maintenance. Agric. Water Manag. 2, 149–162.

Capra, A., Scicolone, B., 2005. Assessing dripper clogging and filtering performance using municipal wastewater. Irrig. Drain. 54, 71–79.

Casey, E., 2007. Tracer measurements reveal experimental evidence of biofilm consolidation. Biotechnol. Bioeng. 98, 913–918.

Characklis, G.W., 1990. Microbial biofouling, in: Characklis, G.W., Marshall, K.C. (Eds.), Biofilms. Wiley, New York, pp. 523–584.

Chomiak, A., Sinnet, B., Derlon, N., Morgenroth, E., 2014. Inorganic particles increase biofilm heterogeneity and enhance permeate flux. Water Res. 64, 177–86.

Christensen, B.E., Trønnes, H.N., Vollan, K., Smidsrød, O., Bakke, R., 1990. Biofilm removal by low concentrations of hydrogen peroxide. Biofouling 2, 165–175.

Cochran, W.L., McFeters, G.A., Stewart, P.S., 2000. Reduced susceptibility of thin Pseudomonas aeruginosa biofilms to hydrogen peroxide and monochloramine. J. Appl. Microbiol. 88, 22–30.

Coufort, C., Derlon, N., Ochoa-Chaves, J., Liné, A., Paul, E., 2007. Cohesion and detachment in biofilm systems for different electron acceptor and donors. Water Sci. Technol. 55, 421–428.

References

Dasberg, S., Or, D., 1999. Drip irrigation. Springer-Verlag Berlin Heidelberg 1999, p. 172.

de Beer, D., Srinivasan, R., Stewart, P.S., 1994. Direct Measurement of Chlorine Penetration into Biofilms during Disinfection. Appl. Environ. Microbiol. 60, 4339–4344.

de Kreuk, M.K., Kishida, N., Tsuneda, S., van Loosdrecht, M.C.M., 2010. Behavior of polymeric substrates in an aerobic granular sludge system. Water Res. 44, 5929–5938.

Decamp, O., Warren, a, 2000. Investigation of Escherichia coli removal in various designs of subsurface flow wetlands used for wastewater treatment. Ecol. Eng. 14, 293–299.

Derlon, N., Grütter, A., Brandenberger, F., Sutter, A., Kuhlicke, U., Neu, T.R., Morgenroth, E., 2016. The composition and compression of biofilms developed on ultrafiltration membranes determine hydraulic biofilm resistance. Water Res. 102, 63–72.

Derlon, N., Masse, A., Escudie, R., Bernet, N., Paul, E., 2008. Stratification in the cohesion of biofilms grown under various environmental conditions. Water Res. 42, 2102–2110.

Derlon, N., Peter-Varbanets, M., Scheidegger, A., Pronk, W., Morgenroth, E., 2012. Predation influences the structure of biofilm developed on ultrafiltration membranes. Water Res. 46, 3323–3333.

DIN 38414, 1985. DIN 38414 part 2 - German Standard Methods for the Examination of Water, Waste Water and Sludge - sludge and sediments (Group S) - Determination of the moisture content and the dry residue respectively the dry solid substance (S 2). Beuth Verlag GmbH, Berlin.

Dosoretz, C., Tarchitzky, J., Katz, I., Kenig, E., Chen, Y., 2011. Development and effects of a fouling layer in distribution and irrigation systems applying treated wastewater effluents., in: Levy, G., Fine, P., Bar-Tal, A. (Eds.), Use of Treated Sewage Water in Agriculture: Impacts on Crops and Soil Environment. Blackwell Publishing, Oxford, pp. 328–350.

Dreszer, C., Vrouwenvelder, J.S., Paulitsch-Fuchs, A.H., Zwijnenburg, A., Kruithof, J.C., Flemming, H.C., 2013. Hydraulic resistance of biofilms. J. Memb. Sci. 429, 436–447.

Dreszer, C., Wexler, A.D., Drusova, S., Overdijk, T., Zwijnenburg, A., Flemming, H.C., Kruithof, J.C., Vrouwenvelder, J.S., 2014. In-situ biofilm characterization in membrane systems using Optical Coherence Tomography: Formation, structure, detachment and impact of flux change. Water Res. 67, 243–254.

Duran-Ros, M., Puig-Bargués, J., Arbat, G., Barragán, J., Ramírez de Cartagena, F., 2009.

Effect of filter , emitter and location on clogging when using effluents. Agric. Water Manag. 96, 67–79.

Epstein, N., 1982. Fundamentals of heat transfer surface fouling: With special emphasis on laminar flow., in: Kakac, S., Shah, R.K., Bergles, A.E. (Eds.), Low Reynolds Number Flow Heat Exchangers. Hemisphere, Washington, DC, pp. 951–964.

Esteban, R.I., 2009. Water reuse in spain: Data overview and costs estimation of suitable treatment trains, in: INNOVA-MED CONFERENCE "Water Reclamation and Reuse."

Everitt, B.S., 1988. The Cambridge dictionary of statistics. Cambridge University Press, Cambridge,UK, New York.

Farhat, N.M., Vrouwenvelder, J.S., Van Loosdrecht, M.C.M., Bucs, S.S., Staal, M., 2016. Effect of water temperature on biofouling development in reverse osmosis membrane systems. Water Res. 103, 149–159.

Feigin, A., Ravina, I., Shalhevet, J., 1991. Irrigation with treated sewage effluent: management for environmental protection. Springer-Verlag, Berlin, Heidelberg, New York, London, Paris, Tokyo, Hong kong, Barcelona.

Flemming, H.C., 2002. Biofouling in water systems - Cases, causes and countermeasures. Appl. Microbiol. Biotechnol. 59, 629–640.

Food and Agriculture Organization of the United Nations (FAO), 2016. FAO AQUASTAT website. Food and Agriculture Organization of the United Nations (FAO). http://www.fao.org/nr/water/aquastat/didyouknow/index2.stm (accessed 12.9.16).

Forslund, A., Ensink, J.. . . J., Markussen, B., Battilani, A., Psarras, G., Gola, S., Sandei, L., Fletcher, T., Dalsgaard, A., 2012. Escherichia coli contamination and health aspects of soil and tomatoes (Solanum lycopersicum L.) subsurface drip irrigated with on-site treated domestic wastewater. Water Res. 46, 5917–5934.

Gärdenäs, A.I., Hopmans, J.W., Hanson, B.R., Šimůnek, J., 2005. Two-dimensional modeling of nitrate leaching for various fertigation scenarios under micro-irrigation. Agric. Water Manag. 74, 219–242.

Gerardi, M., 2006. Wastewater bacteria, 1st ed. Wiley-Interscience, New Jersey, USA, p. 272.

Haisch, C., Niessner, R., 2007. Visualisation of transient processes in biofilms by optical coherence tomography. Water Res. 41, 2467–2472.

Hebbar, S.S., Ramachandrappa, B.K., Nanjappa, H. V., Prabhakar, M., 2004. Studies on NPK

drip fertigation in field grown tomato (Lycopersicon esculentum Mill.). Eur. J. Agron. 21, 117–127.

Hills, D.J., Brenes, M.J., 2001. Microirrigation of wastewater effluent using drip tape. Appl. Eng. Agric. 17, 303–308.

Huang, D., Swanson, E.A., Lin, C.P., Schuman, J.S., Stinson, W.G., Chang, W., Hee, M.R., Flotte, T., Gregory, K., Puliafito, C.A., Fujimoto, J.G., 1991. Optical Coherence Tomography. Science. 254, 1178–1181.

Huang, L.-K., Wang, M., 1995. Image Thresholding By Minimizing the Measure Of Fuzzyness. Pattern Recognit. 28, 41–51.

Ingraham, J.L., 1958. Growth of Psychrophilic Bacteria. J. Bacteriol. 76, 75–80.

ISO, 2014. ISO 9261:2004 - Agricultural irrigation equipment -- Emitters and emitting pipe -- Specification and test methods.

Jamal Khan, S., Visvanathan, C., Jegatheesan, V., 2012. Bioresource technology effect of powdered activated carbon (PAC) and cationic polymer on biofouling mitigation in hybrid MBRs. Bioresour. Technol. 113, 165–168.

Katz, S., Dosoretz, C., Chen, Y., Tarchitzky, J., 2014. Fouling formation and chemical control in drip irrigation systems using treated wastewater. Irrig. Sci. 32, 459–469.

Keller, W.D., 1982. Applications of scanning electron microscopy to clays and other fine-grained minerals, in: Hagni, R.D. (Ed.), Proceedings Process Mineralogy II. Asm Intl, pp. 245–261.

Körstgens, V., Flemming, H.-C., Wingender, J., Borchard, W., 2001. Uniaxial compression measurement device for investigation of the mechanical stability of biofilms. J. Microbiol. Methods 46, 9–17.

Lawrence, J., Neu, T., 1999. Confocal laser scanning microscopy for analysis of microbial biofilms. Methods Enzymol. 310, 131–142.

Lesage, N., Sperandio, M., Cabassud, C., 2008. Study of a hybrid process: Adsorption on activated carbon/membrane bioreactor for the treatment of an industrial wastewater. Chem. Eng. Process. Process Intensif. 47, 303–307.

Li, C., Felz, S., Wagner, M., Lackner, S., Horn, H., 2016. Investigating biofilm structure developing on carriers from lab-scale moving bed biofilm reactors based on light microscopy and optical coherence tomography. Bioresour. Technol. 200, 128–136.

References

Li, C., Wagner, M., Lackner, S., Horn, H., 2015. Assessing the influence of biofilm surface roughness on mass transfer by combining optical coherence tomography and two-dimensional modeling. Biotechnol. Bioeng. 113, 989–1000.

Li, G.B., Li, Y.K., Xu, T.W., Liu, Y.Z., Jin, H., Yang, P.L., Yan, D.Z., Ren, S.M., Tian, Z.F., 2011. Effects of average velocity on the growth and surface topography of biofilms attached to the reclaimed wastewater drip irrigation system laterals. Irrig. Sci. 30, 103–113.

Li, J., Chen, L., Li, Y., 2009. Comparison of clogging in drip emitters during application of sewage effluent and groundwater. Trans. ASABE 52, 1203–1211.

Li, Y., Yang, P., Ren, S., Xu, T., 2006. Hydraulic characterizations of tortuous flow in path drip irrigation emitter. J. Hydrodyn. Ser. B 18, 449–457.

Liu, H., Huang, G., 2009. Laboratory experiment on drip emitter clogging with fresh water and treated sewage effluent. Agric. Water Manag. 96, 745–756.

Loulergue, P., Weckert, M., Reboul, B., Cabassud, C., Uhl, W., Guigui, C., 2014. Mechanisms of action of particles used for fouling mitigation in membrane bioreactors. Water Res. 66, 40–52.

Lubello, C., Gori, R., Nicese, F.P., Ferrini, F., 2004. Municipal-treated wastewater reuse for plant nurseries irrigation. Water Res. 38, 2939–2947.

Mah, T.-F.C., O'Toole, G. a, 2001. Mechanisms of biofilm resistance to antimicrobial agents. Trends Microbiol. 9, 34–39.

Malik, R.S., Kumar, K., Bhandari, A.R., 1994. Effect of urea application through drip irrigation system on nitrate distribution in loamy sand Soils and pea yield. J. Indian Soc. Soil Sci. 42, 6–10.

Mathieu, L., Bertrand, I., Abe, Y., Angel, E., Block, J.C., Skali-lami, S., Francius, G., Lorraine, D., 2014. Drinking water biofilm cohesiveness changes under chlorination or hydrodynamic stress. Water Res. 55, 175–184.

Maurer, M.A., Davies, F.S., Box, P.O., Box, P.O., 1995. Reclaimed wastewater irrigation and fertilization of mature " redblush " grapefruit trees on spodosols in Florida. J. Am. Soc. Hortic. Sci. 120, 394–402.

Metcalf & Eddy Inc, 2003. Wastewater engineering: treatment and reuse, 4th ed, McGraw-Hill Science/Engineering/Math; 4th edition, New York, p. 1848.

MFA, 2016. Water recycling technologies in Israel. Isr. Minist. Foreign Aff. URL http://mfa.gov.il/mfa/innovativeisrael/greenisrael (accessed 5.12.16).

Mohammad, M.J., Ayadi, M., 2004. Forage Yield and Nutrient Uptake as Influenced by Secondary Treated Wastewater. J. Plant Nutr. 27, 351–365.

Monod, J., 1949. The Growth of Bacterial Cultures. Annu. Rev. Microbiol. 3, 371–394.

Morgenroth, E., Milferstedt, K., 2009. Biofilm engineering: Linking biofilm development at different length and time scales. Rev. Environ. Sci. Biotechnol. 8, 203–208.

Nakayama, F.S., Boman, B.J., Pitts, D.J., 2007. Maintenance, in: Lamm, F.R., Ayars, J.E., Nakayama, F.S. (Eds.), Microirrigation for Crop Production. Design,operation, and Management. Elsevier, Amsterdam, the Netherlands, pp. 389–430.

Nakayama, F.S., Bucks, D.A., 1991. Water quality in drip / trickle irrigation : A review. Irrig. Sci. 12, 187–192.

Neilsen, G.H., Stevenson, D.S., Fitzpatrick, J.J., Brownlee, C.H., 1989. Nutrition and yield of young apple trees irrigated with municipal waste water. J. Am. Soc. Hortic. Sci. 114, 377–383.

Nywening, J.P., Zhou, H., 2009. Influence of filtration conditions on membrane fouling and scouring aeration effectiveness in submerged membrane bioreactors to treat municipal wastewater. Water Res. 43, 3548–3558.

Oliver, M.M.H., Hewa, G. a., Pezzaniti, D., 2014. Bio-fouling of subsurface type drip emitters applying reclaimed water under medium soil thermal variation. Agric. Water Manag. 133, 12–23.

Paris, T., Skali-Lami, S., Block, J.C., 2009. Probing young drinking water biofilms with hard and soft particles. Water Res. 43, 117–126.

Paul, E., Ochoa, J.C., Pechaud, Y., Liu, Y., Line, A., 2012. Effect of shear stress and growth conditions on detachment and physical properties of biofilms. Water Res. 46, 5499–5508.

Pirt, S.J., 1985. Principles of microbe and cell cultivation. Blackwell scientific publications, Oxford London Edinburgh, p. 274.

Pollice, A., Lopez, A., Laera, G., Rubino, P., Lonigro, A., 2004. Tertiary filtered municipal wastewater as alternative water source in agriculture: A field investigation in Southern Italy. Sci. Total Environ. 324, 201–210.

References

Puig-Bargués, J., Arbat, G., Barragán, J., Ramírez de Cartagena, F., 2005. Effluent particle removal by microirrigation system filters. Spanish J. Agric. Res. 3, 182.

Puig-Bargués, J., Arbat, G., Elbana, M., Duran-Ros, M., Barragán, J., de Cartagena, F.R., Lamm, F.R., 2010. Effect of flushing frequency on emitter clogging in microirrigation with effluents. Agric. Water Manag. 97, 883–891.

Qin, Z., Berliner, P.R., Karnieli, A., 2005. Ground temperature measurement and emissivity determination to understand the thermal anomaly and its significance on the development of an arid environmental ecosystem in the sand dunes across the Israel-Egypt border. J. Arid Environ. 60, 27–52.

Qingsong, W., Gang, L., Jie, L., Yusheng, S., Wenchu, D., Shuhuai, H., 2008. Evaluations of emitter clogging in drip irrigation by two-phase flow simulations and laboratory experiments. Comput. Electron. Agric. 63, 294–303.

Raso, J., 2013. Update of the final report on wastewater reuse in the European Union.

Ravina, I., Paz, E., Sofer, Z., Marcu, A., Schischa, A., Sagi, G., Yechialy, Z., Lev, Y., 1997. Control of clogging in drip irrigation with stored treated municipal sewage effluent. Agric. Water Manag. 33, 127–137.

Ravina, I., Paz, E., Sofer, Z., Marcu, A., Shisha, A., Sagi, G., 1992. Control of emitter clogging in drip irrigation with reclaimed wastewater. Irrig. Sci. 13, 129–139.

Remy, M., Potier, V., Temmink, H., Rulkens, W., 2010. Why low powdered activated carbon addition reduces membrane fouling in MBRs. Water Res. 44, 861–867.

Rickert, D.A., Hunter, J. V., 1971. General nature of soluble and particulate organics in sewage and secondary effluent. Water Res. 5, 421–436.

Rogers, J., Dennis, P.J., Lee, J. V, Keevil, C.W., 1994. Influence of temperature and plumbing material selection on biofilm formation and growth of Legionella pneumophila in a model potable water system containing complex microbial Influence of Temperature and Plumbing Material Selection on Biofilm Formation a. Appl. Environ. Microbiol. 60, 1585–1592.

Rusconi, R., Lecuyer, S., Autrusson, N., Guglielmini, L., Stone, H. a, 2011. Secondary flow as a mechanism for the formation of biofilm streamers. Biophys. J. 100, 1392–1399.

Saravanan, P., Nancharaiah, Y.V., Venugopalan, V.P., Rao, T.S., Jayachandran, S., 2006. Biofilm formation by Pseudoalteromonas ruthenica and its removal by chlorine.

Biofouling 22, 371–381.

Schacht, K., Chen, Y., Tarchitzky, J., Marschner, B., 2016. Chapter 18 The use of treated wastewater for irrigation as a component of integrated water resources management: reducing environmental implications on soil and groundwater by evaluating site-specific soil sensitivities, in: Borchardt, D, Bogardi, JJ, Ibische, RB. Integrated Water Resources Management. Springer, Switzerland, p. 768.

Schindelin, J., Arganda-Carreras, I., Frise, E., Kaynig, V., Longair, M., Pietzsch, T., Preibisch, S., Rueden, C., Saalfeld, S., Schmid, B., Tinevez, J.-Y.J.-Y., White, D.J., Hartenstein, V., Eliceiri, K., Tomancak, P., Cardona, A., Liceiri, K., Tomancak, P., A., C., 2012. Fiji: an open source platform for biological image analysis. Nat. Methods 9, 676–682.

Schlosser, C., Strzepek, K., Gao, X., Gueneau, A., Fant, C., Sergey, P., Rasheed, B., Smith-Greico, T., Blanc, E., Jacoby, H.D., Reilly, J.M., 2014. The future of global water stress: an integrated assessment. MIT Jt. Progr. Sci. Policy Glob. Chang.

Shaw, T., Winston, M., Rupp, C.J., Klapper, I., Stoodley, P., 2004. Commonality of elastic relaxation times in biofilms. Phys. Rev. Lett. 93.

Shen, Y., Monroy, G.L., Derlon, N., Janjaroen, D., Huang, C., Morgenroth, E., Boppart, S.A., Ashbolt, N.J., Liu, W.T., Nguyen, T.H., 2015. Role of biofilm roughness and hydrodynamic conditions in legionella pneumophila adhesion to and detachment from simulated drinking water biofilms. Environ. Sci. Technol. 49, 4274–4282.

Song, I., Stine, S.W., Choi, C.Y., Gerba, C.P., 2006. Comparison of Crop Contamination by Microorganisms during Subsurface Drip and Furrow Irrigation. J. Environ. Eng. 132, 1243–1248.

Sousa, G., Fangueiro, D., Duarte, E., Vasconcelos, E., 2011. Reuse of treated wastewater and sewage sludge for fertilization and irrigation. Water Sci. Technol. 64, 871–879.

Srinivasan, R., Stewart, P.S., Griebe, T., Chen, C.I., Xu, X., 1995. Biofilm parameters influencing biocide efficacy. Biotechnol. Bioeng. 46, 553–560.

Staudt, C., Horn, H., Hempel, D.C., Neu, T.R., 2004. Volumetric measurements of bacterial cells and extracellular polymeric substance glycoconjugates in biofilms. Biotechnol. Bioeng. 88, 585–592.

Stewart, P.S., 2012. Mini-review: Convection around biofilms. Biofouling 28, 187–198.

Stoodley, P., Cargo, R., Rupp, C.J., Wilson, S., Klapper, I., 2002. Biofilm material properties as related to shear-induced deformation and detachment phenomena. J. Ind. Microbiol. Biotechnol. 29, 361–367.

SWRCB, DWR, 2009. Results, challenges, and future approaches to California's municipal wastewater recycling survey. Sacramento, California, State Water Resources Control Board (SWRCB) and Department of Water Resources (DWR). California, USA.

Taherzadeh, D., Picioreanu, C., Horn, H., 2012. Mass transfer enhancement in moving biofilm structures. Biophys. J. 102, 1483–1492.

Tarchitzky, J., Rimon, a., Kenig, E., Dosoretz, C.G., Chen, Y., 2013. Biological and chemical fouling in drip irrigation systems utilizing treated wastewater. Irrig. Sci. 31, 1277–1288.

Tearney, G.J., Brezinski, M.E., Bouma, B.E., Boppart, S.A., Pitris, C., Southern, J.F., Fujimoto, J.G., 1997. In vivo endoscopic optical biopsy with optical coherence tomography. Science (80-.). 276, 2037–2039.

Teychene, B., Guigui, C., Cabassud, C., 2011. Engineering of an MBR supernatant fouling layer by fine particles addition : A possible way to control cake compressibility. Water Res. 45, 2060–2072.

Trinci, A.P.J., 1969. A kinetic study of the growth of Aspergillus nidulans and other fugi. J. Gen. Microbiol. 57, 11–24.

Tsuda, A., Henry, F.S., Butler, J.P., 2013. Particle transport and deposition: Basic physics of particle kinetics. Compr. Physiol. 3, 1437–1471.

UNEP, 2005. Guidelines for municipal water reuse in the mediterranean region, United Nations Environment Programme.

United Nations Development Programme (UNDP), 2006. Human Development Report 2006 - Beyond scarcity: Power, poverty and the global water crisis, Journal of Government Information.

US EPA, 2012. Guidelines for Water Reuse. EPA/625/R-04/108, Epa/625/R-04/108.

Valladares Linares, R., Wexler, A.D., Bucs, S.S., Dreszer, C., Zwijnenburg, A., Flemming, H.-C., Kruithof, J.C., Vrouwenvelder, J.S., 2016. Compaction and relaxation of biofilms. Desalin. Water Treat. 57, 12902–12904.

Verheye, W., 2007. Land use, land cover and soil sciences, Soils of Arid and Semi-Arid

References

Areas. UNESCO - Encyclopedia of life support system, p. 248.

Wagner, M., Taherzadeh, D., Haisch, C., Horn, H., 2010. Investigation of the mesoscale structure and volumetric features of biofilms using optical coherence tomography. Biotechnol. Bioeng. 107, 844–853.

Walter, M., Safari, A., Ivankovic, A., Casey, E., 2013. Detachment characteristics of a mixed culture biofilm using particle size analysis. Chem. Eng. J. 228, 1140–1147.

Walters, E., Graml, M., Behle, C., Müller, E., Horn, H., 2013. Influence of particle association and suspended solids on UV inactivation of fecal indicator bacteria in an urban river. Water, Air, Soil Pollut. 225, 1822.

Watanabe, I., Okada, S., 1967. Effect of temperature on growth rate of cultured mammalian cells (L5178Y). J. Cell Biol. 32, 309–323.

WeatherSpark, n.d. Historical weather for 2015 in Baden Baden - Karlsruhe. Cedar Lake Ventur. Inc. URL https://weatherspark.com/history/28657/2015/Baden-Baden-Karlsruhe-Baden-Wurttemberg-Germany (accessed 9.24.16).

Wei, Q., Shi, Y., Dong, W., Lu, G., Huang, S., 2006. Study on hydraulic performance of drip emitters by computational fluid dynamics. Agric. Water Manag. 84, 130–136.

West, S., Wagner, M., Engelke, C., Horn, H., 2016. Optical coherence tomography for the in situ three-dimensional visualization and quantification of feed spacer channel fouling in reverse osmosis membrane modules. J. Memb. Sci. 498, 345–352.

Wiesner, M.R., Tarabara, V., Cortalezzi, M., 2005. Processes of particle deposition in membrane operation and fabrication. Water Sci. Technol. 51, 345–348.

World Health Organization (WHO), 1989. Health guidelines for the use of wastewater in agriculture and aquaculture. World Heal. Organ. - Tech. Rep. Ser.

Wright, D.A., Killham, K., Glover, L.A., Prosser, J.I., 1995. Role of Pore Size Location in Determining Bacterial Activity during Predation by Protozoa in Soil. Appl. Environ. Microbiol. 61, 3537–3543.

Wu, X., Conkle, J.L., Ernst, F., Gan, J., 2014. Treated wastewater irrigation: Uptake of pharmaceutical and personal care products by common vegetables under field conditions. Environ. Sci. Technol. 48, 11286–11293.

Xi, C., Marks, D., Schlachter, S., Luo, W., Boppart, S. a, 2006. High-resolution three-dimensional imaging of biofilm development using optical coherence tomography. J.

Biomed. Opt. 11, 34001.

Yan, D., Bai, Z., Rowan, M., Gu, L., Shumei, R., Yang, P., 2009. Biofilm structure and its influence on clogging in drip irrigation emitters distributing reclaimed wastewater. J. Environ. Sci. 21, 834–841.

Yan, D., Yang, P., Rowan, M., Ren, S., Pitts, D., 2010. Biofilm accumulation and structure in the flow path of drip emitters using reclaimed wastewater. Trans. ASABE 53, 751–758.

Zhou, B., Li, Y., Liu, Y., Pei, Y., Jiang, Y., Liu, H., 2014. Effects of flow path depth on emitter clogging and surface topographical characteristics of biofilms. Irrig. Drain. 63, 46–58.

Zhou, B., Li, Y., Liu, Y., Xu, F., Pei, Y., Wang, Z., 2015. Effect of drip irrigation frequency on emitter clogging using reclaimed water. Irrig. Sci. 33, 221–234.

Zhou, B., Li, Y., Song, P., Xu, Z., Bralts, V., 2016. A kinetic model for biofilm growth inside non-PC emitters under reclaimed water drip irrigation. Agric. Water Manag. 168, 23–34.

Publications

Peer-reviewed publications

Qian, J., Walters, E., Rutschmann, P., Wagner, M., Horn, H., 2016. Modeling the influence of total suspended solids on *E.coli* removal in river water. Water Science Technology, 73, 6, 1320-1332.

Qian, J., Horn, H., Tarchitzky, J., Chen, Y., Katz, S., Wagner, M. Water quality and daily temperature cycle affect biofilm formation in drip irrigation devices revealed by optical coherence tomography. Biofouling, Biofouling, 2017, 33(3), 211-221.

Conference contributions

Qian, J., Wagner, M., Horn, H., 2015. Effect of the daily temperature cycle on the biofilm formation, structure and composition in micro-fluidic devices mimicking drip irrigation systems. 7th ASM Conference on Biofilms, 24-29 Sep. 2015, in Chicago, USA.

Qian, J., Wagner, M., Horn, H., 2016. Revealing the effect of water quality and daily temperature cycle on the biofilm formation inside drip irrigation devices by means of optical coherence tomography. Biofilms7, 26-28 June 2016, in Porto, Portugal.

Qian, J., Sultan, Z., Wagner, M., Horn, H., 2016. Influence of inorganic particles on biofilm development in microfluidic devices monitored non-invasively by optical coherence tomography. MEWE and Biofilms IWA Specialist Conference, 4-7 Sep. 2016, in Copenhagen, Denmark.

Qian, J., Ateş, A., Sultan, Z., Wagner, M., Horn, H., 2017 Influence of inorganic particles on biofilm development and mechanical property in drip irrigation devices monitored non-invasively using optical coherence tomography. 10th International Conference on Biofilm Reactors, 9-12 May. 2017, in Dublin, Ireland.

Non-peer-reviewed publication

Wagner, M., **Qian, J.,** Horn, H., 2016. Biofilm formation in drip irrigation systems. WaterSolutions (GWF-Wasser), 1, 30-34.

Schriftenreihe des Lehrstuhls für Wasserchemie und Wassertechnologie und
der DVGW-Forschungsstelle am Engler-Bunte-Institut
des Karlsruher Instituts für Technologie (KIT)

Band 35: Symposium on Refractory Organic Substances in the Environment – ROSE, 1997, 248 S., 12,80 €.

Band 36: Symposium on Refractory Organic Substances in the Environment – ROSE II, 2000, 265 S., 12,80 €.

Band 37: Thomas Brinkmann: Alkalischer und solarinduzierter Abbau von natürlicher organischer Materie, 2003, 212 S., 15,00 €.

Band 38: Andreas Gorenflo: Rückhalt und Fouling von natürlichen organischen Substanzen bei der Nano- und Ultrafiltration, 2003, 219 S., 18,00 €.

Band 39: Philip Hörsch: Einfluss der chemischen Oxidation auf das toxische Potenzial und das biologische Abbauverhalten von Industrieabwässern, 2004, 210 S., 20,00 €.

Band 40: Margit B. Müller: Bewertung von Anreicherungs- und Fraktionierungsverfahren für die strukturelle Charakterisierung der gelösten organischen Substanz in Gewässern, 2004, 185 S., 18,00 €.

Band 41: Fritz H. Frimmel, Gudrun Abbt-Braun: Praktikum Allgemeine Chemie und Chemie in wässrigen Lösungen – Qualitative und quantitative Bestimmungen, 2004, 158 S., 18,00 €.

Band 42: Tusnelda E. Doll: Photochemischer und photokatalytischer Abbau von Carbamazepin, Clofibrinsäure, Iomeprol und Iopromid, 2004, 158 S., 18,00 €.

Band 43: Ayşe B. Değer: Entfernung von organischen Schadstoffen aus Wasser mit Hilfe von Poly(ε-caprolacton), 2005, 205 S., 18,00 €.

Band 44: Fritz H. Frimmel, Gudrun Abbt-Braun: Wassertechnologisches und wasserchemisches Praktikum, 2005, 201 S., 20,00 €.

Band 45-I, 45-II: Fritz H. Frimmel, Gudrun Abbt-Braun (Eds.): Humic Substances – Linking Structure to Functions. Proceedings of the 13th Meeting of the International Humic Substances Society, July 30 to August 4, 2006, Universität Karlsruhe, 2006, 492 S. (45-I), 623 S. (45-II), 50,00 €.

Band 46: Fritz H. Frimmel, Gudrun Abbt-Braun: Praktikum Allgemeine Chemie und Chemie in wässrigen Lösungen – Qualitative und quantitative Bestimmungen II, 2. verbesserte und ergänzte Neuauflage 2007, 139 S., 20,00 €.

Band 47: Thomas Glauner: Aufbereitung von Schwimmbeckenwasser – Bildung und Nachweis von Desinfektionsnebenprodukten und ihre Minimierung mit Membran- und Oxidationsverfahren, 2007, 233 S., 20,00 €.

Band 48: George Metreveli: Kolloidale Wechselwirkungen und kolloidgetragener Transport von Metall(oid)en in porösen Medien, 2008, 215 S., 20,00 €.

Band 49: Florencia Saravia: Entfernung von organischen Spurenstoffen und Untersuchung von Foulingprozessen in getauchten Membranen und Hybridverfahren, 2009, 213 S., 20,00 €.

Band 50: Markus Delay: Dynamische versus statische Elutionsversuche – Ein Beitrag zur Beurteilung der Wiederverwertbarkeit von Abfallmaterialien, 2010, 206 S., 20,00 €.

Band 51: Luis A. Tercero Espinoza: Heterogeneous photocatalysis with titanium dioxide suspensions containing bromide and dissolved organic matter, 2010, 172 S., 20,00 €.

Band 52: Ulrich-M. Metzger: Extrazelluläre polymere Substanzen aus Biofilmen – Aufklärung von Strukturen und ihr Einfluss auf die Foulingbildung in Membranbioreaktoren, 2011, 211 S., 20,00 €.

Band 53: Fritz H. Frimmel, Gudrun Abbt-Braun: Praktikum Allgemeine Chemie und Chemie in wässrigen Lösungen – Qualitative und quantitative Bestimmungen, 3. überarbeitete Neuauflage 2011, 139 S., 20,00 €.

Band 54: Markus Ziegmann: Beurteilung von Cyanobakterienblüten und Untersuchung geeigneter Verfahrenskombinationen zur Elimination cyanobakterieller Zellen und Toxine, 2011, 191 S., 20,00 €.

Band 55: Fritz H. Frimmel, Gudrun Abbt-Braun: Praktikum Allgemeine Chemie und Chemie in wässrigen Lösungen – Qualitative und quantitative Bestimmungen, 4. ergänzte Neuauflage 2012, 137 S., 20,00 €.

Band 56: Angela Klüpfel: Nanofiltration bei der Aufbereitung von Trink- und Schwimm-beckenwasser – Foulingmechanismen und Rückhalt anthropogener Kontaminanten, 2012, 259 S., 20,00 €.

Band 57: Christina Schmalz: Bildung, Phasentransfer und Toxizität halogenierter Desinfektionsnebenprodukte im Aufbereitungszyklus von Schwimmbeckenwasser – Schwerpunkt stickstoffhaltige Verbindungen, 2012, 195 S., 20,00 €.

Band 58: Fritz H. Frimmel, Gudrun Abbt-Braun, Harald Horn: Praktikum Allgemeine Chemie und Chemie in wässrigen Lösungen – Qualitative und quantitative Bestimmungen, 5. ergänzte Neuauflage 2013, 120 S., 20,00 €.

Band 59: Heiko Schwegmann: Wechselwirkungen zwischen anorganischen Nanopartikeln und Mikroorganismen – Nutzungs- und Gefährdungspotentiale, 2013, 149 S., 20,00 €.

Band 60: Fritz H. Frimmel, Gudrun Abbt-Braun, Harald Horn: Praktikum Allgemeine Chemie und Chemie in wässrigen Lösungen – Qualitative und quantitative Bestimmungen, 6. Überarbeitete Neuauflage 2014, 129 S., 20,00 €.

Band 61: Carsten Jobelius: Anaerobe Metabolite organischer Schadstoffe im Grundwasser - Analytik, Bildung und Nutzung als Indikatoren, 2014, 247 S., 20,00 €.

Band 62: Eva M. Gilbert: Partielle Nitritation / Anammox bei niedrigen Temperaturen, 2014, 115 S., 20,00 €.

Band 63: Aleksandr O. Kondrakov: Heterogeneous photocatalysis and sensitized photolysis for enhanced degradation of bisphenol A and its analogues, 2015, 155 S., 20,00 €.

Band 64: Meijie Ren: TiO_2: application in photocatalysis for the degradation of organic pollutants and aggregation behavior in aquatic systems, 2015, 121 S., 20,00 €.

Band 65: Fritz H. Frimmel, Gudrun Abbt-Braun, Harald Horn: Praktikum Allgemeine Chemie und Chemie in wässrigen Lösungen – Qualitative und quantitative Bestimmungen, 7. überarbeitete Neuauflage 2016, 126 S., 20,00 €.

Band 66: Chunyan Li: Using optical coherence tomography to quantify biofilm structure and mass transfer in combination with mathematical modeling, 2016, 121 S., 20,00 €.

Band 67: Maria Pia Herrling: Nanoparticles in biofilm systems – assessment of their interactions by magnetic susceptibility balance and magnetic resonance imaging, 2016, 132 S., 20,00 €.

Band 68: Elham Fatoorehchi: Sludge disintegration techniques – assessment of their impacts on solubilization of organic carbon and methane production, 2016, 116 S., 20,00 €.

Band 69: Norman Hack: Refraktäre organische Substanzen im Kapillarsaum: ihre Dynamik, Gradienten und Reaktionen, 2016, 152 S., 20,00 €.

Band 70: Di Peng: Disinfection by-products and the application potential of nanofiltration in swimming pool water treatment, 2016, 112 S., 20,00 €.

Band 71: Jueying Qian: Investigation of the fouling driving factors in drip irrigation systems, 2017, 112 S., 20,00 €.

Preise verstehen sich zzgl. der gesetzlichen Mehrwertsteuer und Versandkosten.

Bestellungen über:

Lehrstuhl für Wasserchemie und Wassertechnologie und DVGW-Forschungsstelle

am Engler-Bunte-Institut des Karlsruher Instituts für Technologie (KIT)

Engler-Bunte-Ring 9

D-76131 Karlsruhe

Tel.: +49-(0)721-608-42581

Fax: +49-(0)721-608-46497

E-mail: ebi-sekretariat-wasserchemie@kit.edu